Design and Control of Anthropomorphic Hands with Multimodal Sensing and Semi-Autonomous Grasping Abilities

Zur Erlangung des akademischen Grades eines

Doktors der Ingenieurwissenschaften

von der KIT-Fakultät für Informatik
des Karlsruher Instituts für Technologie (KIT)

genehmigte
Dissertation

von

Pascal Weiner

Tag der mündlichen Prüfung: 14. Februar 2023

1. Referent: Prof. Dr.-Ing. Tamim Asfour
2. Referent: Prof. Dr. Gordon Cheng

Deutsche Zusammenfassung

Menschen verfügen über außergewöhnliche Greif- und Manipulationsfähigkeiten, welche durch ein komplexes Zusammenspiel von Kinematik, Muskeln, Sensorsignalen, reflexbasierten Reglern und Kognition auf semantischer Ebene ermöglicht werden. Die menschliche Hand verfügt über 21 Freiheitsgrade die über 38 Muskelstränge aktuiert werden und erlaubt durch ca. 18.000 Sensoren die Wahrnehmung diverser Stimuli wie statische und dynamische Deformation der Haut, Vibration, Temperatur, Schmerz Gelenkkonfigurationen und aufgebrachte Muskelkraft. Es ist daher nicht verwunderlich, dass ein überproportional großer Teil des Motor- und somatosensorischen Cortex des Gehirns der Steuerung und Sensorik der Hand zugeordnet ist. Um die Steuerung dieses komplexen Systems zu ermöglichen unterteilen Menschen den Greifvorgang unterbewusst in mehrere Aktions-Phasen welche Sensorstimuli mit kontextspezifischen Regelzielen verbinden. Der Greifvorgang wird darüber hinaus stark durch erlerntes Vorwissen über die Aufgabe und die involvierten Objekte beeinflusst.

Myoelektrischen Handprothesen und humanoiden Robotern fehlen viele dieser Fähigkeiten des Menschen. Das Greifen bei humanoiden Robotern und Prothesen basiert primär auf der visuellen Wahrnehmung der Szene durch den Roboter oder Prothesenträger. Zwar kann ein Prothesenträger basierend auf visueller Wahrnehmung und Vorwissen detailliert planen wie das Objekt zu greifen ist, allerdings ist bei Prothesen die Bandbreite der Schnittstelle zur Steuerung zwischen Mensch und Prothese stark limitiert. Jede einzelne Bewegung der Finger und des Handgelenks muss durch eine Sequenz an Kontrollsignalen manuell gesteuert werden. Auch Aspekte des Greifens wie die richtige Griffkraft, das Rutschen von Objekten aus dem Griff und und Deformation der gegriffenen Objekte muss über visuelle Information gesteuert werden. Die hohe kognitive Last, die durch die manuelle Steuerung aller Aspekte des Greifens erzeugt wird, ist einer der Gründe aus dem fast die Hälfte der Prothesenträger nach ein bis zwei Jahren ihre Prothese gar nicht mehr oder nur passiv nutzen. Bei Humanoiden Robotern ist die Abhängigkeit von visuellen Informationen ebenfalls eine gravierende Einschränkung, da das semantische Verständnis der Szene, der

Aufgabe und der involvierten Objekte ebenso fehlt wie die jahrelange Erfahrung im Greifen von Objekten.

Ziel dieser Arbeit ist es, in anthropomorphe Hände integrierte haptische Sensoren und Sensoren Wahrnehmung der Umgebung zu nutzen um semi-autonome und autonome Steuerungen zu entwickeln, die das Greifen mit Prothesen und Roboterhänden vereinfachen. Um diese Steuerungen zu ermöglichen werden multi-modale Sensoren und ein leistungsstarkes eingebettetes System in Hände und frei skalierbare Finger integriert. Speziell für Prothesenhände stellt diese Arbeit ein semi-autonomes Kontrollschema vor, welches basierend auf nur zwei Nutzereingaben die Auswahl und Regelung des richtigen Griffs sowie der Drehung des Handgelenks steuert. Für das Greifen, Anheben, Halten und Abstellen von Objekten stellt diese Arbeit einen voll-autonomen Ansatz basierend auf der Erkennung von Kontakten, Interaktionskräften und Ereignissen vor. Der Ansatz ist durch Erkenntnisse über die Steuerung des Greifens bei Menschen inspiriert. Im Folgenden werden die drei zentralen Beiträge der Arbeit vorgestellt:

Anthropomorphe Hände mit Integriertem Multimodalem Sensorsystem: Der erste Beitrag der Arbeit ist die Entwicklung und Integration eines multimodalen Sensorsystems sowie eines eingebetteten Systems in anthropomorphe Hände. Das Sensorsystem besteht aus Druck- und Scherkraftsensoren, Gelenkwinkelencodern, Beschleunigungssensoren und Temperatursensoren zur haptischen Wahrnehmung sowie Distanzsensoren, inertialen Messeinheiten und einer Kamera zur Wahrnehmung der Umgebung. Das Sensorsystem erweitert den Stand der Technik im Hinblick auf die Menge an verschiedemen integrierten Sensormodalitäten und dem Grad der Integration. Im Gegensatz zu vorhergehenden Arbeiten ist das mechanische Modell der Finger inklusive aller haptischen Sensoren ist mechanisch frei skalierbar in Abhängigkeit von nur sieben Parametern. Um diese Skalierbarkeit auf elektrischer Ebene zu ermöglichen ist das Sensorsystem in einzelne Module aufgeteilt die frei kombiniert werden können um die gesamte verfügbare Oberfläche des skalierten Fingers auszunutzen. Zur Verarbeitung, der Sensordaten und Steuerung der Hand werden eingebettete Systeme entwickelt welche die Ausführung rechenintensiver Aufgaben wie neuronaler Netze erlauben und direkt in der Hand verbaut sind. Darüber hinaus leistet diese Arbeit einen Beitrag zum mechanischen Design anthropomorpher Hände, unter anderem durch die Konzeption eines miniaturisierten und Reibungsarmen unteraktuierten Mechanismus.

Semi-Autonomes Greifen: Mithilfe des Sensorsystems und des eingebetteten Systems wird eine neuartige semi-autonome Steuerung für Prothesenhände entwickelt, welche einige Aspekte des Greifens autonom steuert. Die Steuerung nutzt visuelle Information des zu greifenden Objekts, um dem Nutzer automatisch einen passenden Griff vorzuschlagen. Ebenso wird mithilfe der inertialen Messeinheit die Handorientierung erfasst und basierend darauf ein Griff von der Seite oder von Oben vorgeschlagen. Nach Bestätigung der Vorschläge durch den Nutzer wird das Handgelenk automatisch orientiert und die Finger formen den, für das Objekt passenden, Griff. Die Hand schließt automatisch sobald sich das Objekt in Reichweite befindet. Im Gegensatz zu verwandten Arbeiten erfolgt die Ausfürhrung der semi-autonomen Steuerung vollständig auf dem eingebetteten System der Prothese und nutzt ausschließlich Sensoren welche in der Hand selbst verbaut sind. Über den Stand der Technik hinausgehend werden alle Freiheitsgrade der Prothese simultan gesteuert. Die Steuerung wurde in einer Nutzerstudie evaluiert um die Reduktion der kognitiven und körperlichen Belastung des Prothesennutzers im Vergleich zur Nutzung einer klassischen, manuellen Prothesensteuerung zu ermitteln.

Vom Menschen Inspirierte Greifphasensteuerung: Der dritte Beitrag der Arbeit ist die Entwicklung einer, vom Menschen inspirierten, Greifphasensteuerung für fünffingrige anthropomorphe Hände. wie neurowissenschaftliche Studien zeigen, unterteilt der Mensch den Greifprozess unterbewusst in einzelne Aktionsphasen, jede gestartet durch ein bestimmtes Ereignis in den haptischen Sensordaten und jede mit einen eigenen Steuerungsziel. Die Greifphasensteuerung in dieser Arbeit adaptiert diese Strategie um automatisch die Finger der Hand mit dem Objekt in Kontakt zu bringen, Normalkräfte auszuüben, das Objekt zu heben, abzustellen und loszulassen. Jede Phase dieser Steuerung nutzt einen eigenen Regler mit einem korrespondierenden Regelziel, welches für diese Phase spezifisch ist. Übergänge zwischen Phasen werden durch charakteristische Ereignisse in den haptischen Sensordaten ausgelöst. Jeder Motor in der multiartikulierten Hand führt seine eigene Reglerinstanz aus, basierend auf den Sensordaten aus den Fingern die von diesem Motor angetrieben werden. Wärend verwandte Arbeiten Greifphasensteuerungen entweder auf einem Backengreifer demonstrieren oder die Finger teilweise manuell gesteuert werden müssen, werden in dieser Arbeit alle Finger einer fünf-fingrigen hand in allen Phasen autonom gesteuert. Für Fälle in denen die Hand das Object an nicht mit Sensoren ausgestatteten Flächen berührt, ist die GreifphasenSteuerung explizit in der Lage anhand von unvollständigen Sensordaten zu regeln, wärend die Kon-

takflächen in Verwandten Arbeiten üblicherweise auf sensorisierte Flächen der Hand beschränkt werden. Die Greifphasensteuerung wurde in Greifversuchen mit diversen Haushaltsgegenständen und Lebensmitteln getestet.

Acknowledgment

The research presented in this thesis is the result of my research work at the High Performance Humanoid Technologies Lab (H^2T) at the Karlsruhe Institute of Technology (KIT).

This thesis would not have been possible without Prof. Tamim Asfour, who gave me the opportunity to pursue studies in the fascinating field of humanoid robotics and contribute to many inspiring projects. His ambitious vision of the future of humanoid robotics and his unwavering drive to pursue this vision have been a great inspiration. I am especially thankful for his continuous support and guidance throughout my research as well as for trusting me with the development of several humanoid robots. I would also like to extend my gratitude to Prof. Gordon Cheng who kindly co-supervised my thesis.

The team at H^2T consists of talented and passionate roboticists whom I proudly call my colleagues and friends. I am truly grateful to all present and past members of the team for all the fruitful discussions, scientific insights and collective work, but also for all the great time spent during lunch breaks, conferences, project meetings, late night shifts, after hours activities and vacations. The deep trust and understanding between all members of H^2T makes this working environment truly unique. In particular I would like to thank Lukas Kaul for introducing me to the H^2T lab, mentoring me throughout my time as a student assistant as well as early PhD student and, last but not least, for introducing me to climbing. Samuel Rader and Julia Starke for sharing an office and so many memorable moments with me. Julia Starke for the great collaboration and joint research in the INOPRO project as well as for all the enjoyable gaming nights. Felix Hundhausen for being the better half of our two men electronics development team and taking the time to repair innumerable electronic boards with me, but also for many completely ill-advised yet great outdoor adventures. I also would like to thank Lukas Kaul, Samuel Rader, Julia Starke, Felix Hundhausen, Stefan Reither, Cornelius Klas, Dmitriy Shingarey and many talented student assistants for the countless yet truly enjoyable hours designing and building humanoid robots and hands. Simon Ottenhaus and Mirko Wächter for all the

constructive discussions and valuable input on my topic and PhD student life in general. Throughout my thesis I had the pleasure to supervise multiple student projects, who's contribution to this thesis I gratefully acknowledge: Florian von Bertrab, Markus Crell, Catarina Neef, Felix Hundhausen, Lena Kopnarski, Philippe Spoden and Yvonne Ahring.

I want to thank my girlfriend Valerie for her patience, support and for reminding me of the important things in life. Finally, I want to wholeheartedly thank my parents Monika and Klaus-Peter for their encouragement and unconditional support.

Karlsruhe, February 2023 *Pascal Weiner*

Contents

1. Introduction

Humans exhibit exceptional grasping and manipulation skills which originate from a complex interplay of kinematics and actuation, sensory stimuli, neuromorphic control and higher level cognition. The human hand is endowed with 21 degrees of freedom and actuated by 38 muscle strains (Jones and Lederman, 2006), resulting in extraordinary dexterity of fingers, thumb and wrist. Each square centimeter of hand skin tissue is innervated by hundreds of tactile and proprioceptive afferents, conveying diverse sensory information about static and dynamic skin deformation, vibration, tension, joint configurations and muscle states (Johansson and Vallbo, 1979). It is hence not surprising that a disproportionally large part of the sensory and motor cortex inside the brain is allocated to sensing and control of both hands (Ehrsson et al., 2000). To enable control of such a complex system, the brain subconsciously breaks down the task into several action-phases that link sensory stimuli to context-specific control goals (Johansson and Flanagan, 2009a). The grasping or manipulation process is heavily informed by prior knowledge about the task and properties of the involved objects.

In comparison, humanoid robotic and prosthetic grasping and manipulation capabilities in every-day environments are blatantly lacking (Negrello et al., 2020). Both humanoid robots and prosthesis users mainly utilize visual information to control grasping tasks. In case of myoelectric prostheses (driven by electric motors and controlled through voluntary muscle contractions), the bandwidth of the interface from user to the prosthesis is usually severely limited and feedback from prosthesis to the user is typically not implemented. This lack of bandwidth leads to a high cognitive burden while grasping, as every aspect of the grasp like hand orientation, preshape and grasping force needs to be deliberately controlled based on visual cues observed by the user. For myoelectric prostheses, lack of a suitable control interface is identified as one of the main disadvantages by user studies (Cordella et al., 2016), contributing to 44 % of prosthesis users abandoning their prosthesis (Salminger et al., 2020). For an autonomous robot the problem of having only visual cues is amplified by the lack of both general understanding of the visual input and lack of prior knowledge compared to

a human. While the benefits of multimodal haptic feedback and closed loop control algorithms are evident in both cases, the inherent complexity of such an approach, as observed in the human role model, makes progress in this field challenging.

The thesis investigates how haptic and environmental sensing integrated into prosthetic and humanoid robotic hands can be utilized to develop autonomous behaviors that aid grasping and manipulation with prostheses and humanoid robot hands. To enable these semi-autonomous and autonomous behaviors, a multimodal sensor suit and a corresponding processing system are integrated into anthropomorphic hands and freely scalable fingers. Specifically for prostheses, the thesis presents a semi-autonomous control scheme that automates parts of the pre-grasping process, i. e. forming a preshape, rotating and stabilizing the wrist and choosing an appropriate grasping force. Additionally, a human-inspired grasp phases controller based on detection of contacts, interaction forces and transient events is developed to enhance the grasping capabilities of the hands.

To tackle the problems posed in the thesis, transfer and adaptation of the physiology as well as control strategies employed in human grasping to robotic systems has great potential to contribute to dexterous grasping and manipulation capabilities. Learning from the proven human approach to grasping allows to divide the inherently complex problem of dexterous grasping and manipulation into more clearly defined subproblems. Such transfer lends itself especially to the fields of humanoid robotic hands as well as prosthesis since the kinematics and appearance of such hands is already close to the human role model.

We first introduce the central research questions posed in the thesis and present contributions made towards solving these questions. Afterwards an overview of the structure of the thesis is given.

1.1. Problem Statement

The thesis contributes to answering the question on how prostheses and humanoid robotic hands can aid their users in grasping and manipulation tasks through intelligent systems and control. The problem of enabling dexterous grasping and manipulation is approached by transferring and adapting concepts and techniques observed in humans to prosthetic and humanoid robotic hands. To this end, an embedded multimodal perception system is developed and subsequently utilized for semi-autonomous pre-shaping and autonomous

Figure 1.1.: Overview of the contributions in the thesis. Sensors perceive the state of the hand, robot/user as well as interactions with the environment. Based on the provided sensor information a semi-autonomous pre-grasp control scheme controls hand preshape and wrist orientation prior to grasping known objects. During the actual grasp, an automatic grasp-phases controller generates suitable finger motions and contact forces to grasp, hold and replace unknown objects.

force-controlled grasping for arbitrary objects. While the contributions in the thesis are primarily developed in the context of prosthetics, the majority of the presented work is readily applicable to robotic grasping. An overview of the contributions in this thesis is given in Figure 1.1. The thesis is structured around three central research questions:

1. **How to perceive the environment as well as capture the prosthesis user state and intention to implement helpful autonomous behavior?**
   Multimodal sensing is key to robust closed-loop control of grasping and manipulation tasks. This includes both sensor data about the local environment of the hand through tactile and distance sensing as well as vision data but also information about the intent of the user. All sensor data streams

should be ideally processed locally so that no external devices are needed for control and cabling is minimized. As prostheses need to adapt to the user's size and dimensions, the developed solution must to be adaptable to different hand sizes and especially different finger dimensions.

2. **How to choose a hand preshape and wrist orientation prior to prehension?**
   With classical Electromyography (EMG) based control, a prosthesis user has to manually control both hand aperture and wrist rotation to correctly approach an object prior to grasping. A semi-autonomous control scheme can partly automate and thereby simplify this process by automatically or interactively choosing both preshape and wrist rotation, ideally leading to a reduction in cognitive burden. The first research aspect is hence how to interpret the available multimodal sensor data and then act appropriately according to the estimated user's intent. The second aspect is to implement such a control scheme on resource-constraint hardware directly embedded into the hand itself.
3. **How to grasp safely with the right amount of force?**
   Most humanoid robotic hands and prostheses do not provide feedback about the amount of grasping force to the user. Hence, both robots and prostheses users have to estimate the amount of applied grasping force based on only visual clues which can lead to dropping or unintendedly squishing objects. Additionally, the coordination between thumb and fingers is usually difficult to achieve for a prosthesis user, as at least two degrees of freedom have to be controlled simultaneously. One possible solution is to automatically control the movement of fingers and thumb as well as the grasping force based on tactile data. The main challenge for such an controller is to adapt to unknown objects with different weights, surface properties, shape, size and softness. Furthermore, not only holding an object is important in grasping, but also closing the fingers around the object and placing the object back down.

1.2. Contributions

This thesis contributes to three areas of research: multimodal sensor systems for prosthetic and humanoid robotic hands, semi-autonomous control of prostheses and autonomous force control of the complete grasping process. With the integration of a novel multimodal sensor system for haptic and environmental

sensing and an embedded system into scalable fingers and the palm of the hands, the groundwork for intelligent behavior is laid. Sensors and embedded system are then used to implement a semi-autonomous control scheme for prosthesis, that allows to choose grasp type and approach direction as well as to execute the grasp using only two user inputs. Lastly the haptic sensor system is utilized to implement an autonomous grasp force controller based on human-inspired segmentation of the grasping process into distinct phases.

Athropomorphic Hands with a Multimodal Sensor System: The first contribution of this thesis is the development and integration of a *multimodal tactile and environmental sensor system* as well as an *embedded system* into an anthropomorphic hand. The sensor system comprises pressure and force sensors, joint angle encoders, accelerometers as well as distance and temperature sensors. These sensors are distributed throughout the mechanical structure of the fingers, extending related work in terms of multimodality and level of integration. Further sensors, including an Inertial Measurement Unit (IMU) and a camera are embedded into the palm. For processing of the multimodal data, embedded systems are designed that allow for sensor based control and allow to run compute-intensive tasks like convolution neural networks. In contrast to related work, the mechanical model of the fingers is *automatically scalable* by seven parameters to allow deriving different finger sizes from a single model. The *sensor system is modularized* and adapts to the size of the fingers by combining individual modules to match the size of the finger. Further, the thesis contributes to the mechanical design of the hand, among other things in terms of a novel underactuated mechanism design.

Semi-Autonomous Grasping: Using the multimodal sensor system developed in the first part, the thesis presents a novel semi-autonomous control scheme that controls several aspects of the grasp automatically. The control scheme utilizes object information extracted from camera images to suggest a corresponding preshape. Based on the hand orientation, the control scheme chooses an approach direction to the object and actuates fingers, thumb as well as wrist accordingly upon approval by the user. During approach, the wrist orientation is continuously monitored and adjusted to compensate for arm rotation. The hand closes automatically as soon as it is close enough to the object. In contrast to related work, the control scheme *relies solely on sensors and processing resources available in the prosthetic hand itself*. Unlike previous methods, the control scheme *controls all degrees of freedom of the hand simultaneously*. The scheme is

evaluated in a user study to access cognitive and physical workload reduction in comparison to classical EMG-based control.

Human-inspired Grasp Phases Control: The third contribution of the thesis is a *human-inspired grasp phases controller for five-fingered hands*. As studies in neuroscience show, humans subconsciously divide the process of grasping into distinct action phases, each triggered by a characteristic event and with its own individual control goal. The grasp phases controller in the thesis adapts this control strategy to wrap the fingers around an object, apply normal force to the object, lift it, place it back down and unload the object. Each phase of grasping employs its own sub-controller with a control goal specific to this phase. Transitions between these phases are detected based on distinct haptic events. Each motor in the hand is independently controlled by its own sub-controller instance based on the haptic sensor data provided by the controlled fingers. While related works demonstrate controllers either on parallel grippers or manually select fingers for the grasp, the proposed grasp-phases controller *controls all fingers of a five-fingered hand fully autonomously*. The controller explicitly *deals with incomplete sensor data* arising from the object contacting non-sensorized surfaces of the hand or fingers missing the object. The controller is evaluated in grasping trials with household and food items.

1.3. Structure of the Thesis

The reminder of this thesis is structured into five parts. Chapter 2 introduces relevant works in the areas of hardware design and control of prosthetic hands. The following chapters describe the main contributions of this thesis. Chapter 3 describes the developed prosthetic hands with their multimodal sensor system and embedded system. In Chapter 4, the implementation of the semi-autonomous control scheme for grasp selection is presented. The human-inspired grasp phases controller is detailed in Chapter 5. The thesis concludes with a discussion of the contributions in Chapter 6.

2. Related Work

The goal of the thesis is the conception and implementation of a system that supports grasping and manipulation with prosthetic and humanoid robotic hands by transferring sensing abilities and strategies observed in humans. This chapter introduces and discusses the state of the art in different fields relevant to this goal.

First, Section 2.1 introduces different haptic sensor technologies suitable for use in humanoid robotic hands, with a focus of readily available systems. Furthermore, the integration of sensor systems and embedded electronics into fingers and hands is detailed. Next, different approaches for semi-autonomous control of prostheses is discussed in Section 2.2. Section 2.3 then details related work in control in grasping and manipulation tasks with a focus on methods that consider the whole grasping process beginning with closing the fingers around an object, lifting, holding, replacing and releasing the object.

2.1. Multimodal Sensor-Systems

Humans rely heavily on haptic and visual perception to plan and execute grasps for arbitrary objects. To be able to utilize grasping strategies similar to those in humans, prostheses and humanoid robotic hands hence have to embed a multitude of different sensors into their mechanical structure. Yet, anthropomorphic hands and especially fingers are already complex mechanical systems where installation space is heavily constrained. Sensor candidates for integration must hence be carefully selected based on size, ease of integration and quality of the signals they provide. Therefore, Subsection 2.1.1 first introduces human haptic perception, followed by an introduction to potentially suitable sensing technologies in Subsection 2.1.2. Subsection 2.1.3 then discusses the selection of a multimodal sensor system from these technologies. We then present related work regarding the integration of both sensors and embedded systems into humanoid hands in Subsection 2.1.4.

2.1.1. Human Hand Haptic Perception

Understanding the physiology of human tactile perception provides valuable insights on how robotic sensory systems can be designed on hardware level and is a necessary prerequisite to understanding human grasp control. The glabrous (hair-free) skin on the palmar side of the hand is innervated by mechanoreceptive units consisting of afferent fibers and endings. The mechanoreceptive afferents (nerves carrying spike trains generated by receptors) are distinguished into categories based on their receptive field and reaction to static and dynamic stimuli (Knibestöl and Vallbo, 1970; Johansson and Åke B. Vallbo, 1983). Two categories can be distinguished by analyzing the response to static and ramped indentation. While one category (around 44 % of afferents), the *slowy adapting* afferents (SA), respond with a sustained discharge to static indentation, *fast adapting* (FA) afferents encode transient events without a lasting static response. Each of these two categories can be further divided into *type I* afferents with a small and well defined receptive field and *type II* afferents with a larger receptive field with diffuse borders.

Figure 2.1 illustrates the receptive field and neural response to indentations of the skin next to the receptor. Type I afferents show a well-defined and confined spatial response. The sensitivity decreases rapidly as the distance from the receptors increases by a few millimeters. This can be seen in the almost exponential increase in indentation depth for each step in the height map of both type I afferents. Both contain multiple areas of highest sensitivity attributed to multiple receptors connected to the afferent fiber. Especially the SA type I afferents are very sensitive to edge contours of objects indenting the skin (Johansson et al., 1982b). Fast adapting type I afferents are excited by mechanical oscillations in the range of 5 Hz to 40 Hz. This magnitude of response is dependent on the specific function of the oscillation. While a sinusoidal mechanical indentation may elicit only a minor response, ”fluttery” or ”stuttering” oscillations cause a strong response (Johansson et al., 1982a).

Type II afferents show a far less localized response to tactile stimuli. They exhibit a single region of maximum sensitivity that gradually fades over comparatively large distances. In contrast to the type I afferents, the decrease in sensitivity is more linear. Fast adapting type II afferents are exquisitely sensitive to mechanical transients and mechanical oscillations between 100 Hz to 300 Hz (Johansson et al., 1982a). The afferents respond to stimuli over large areas, for example a whole finger or good portion of the palm (Johansson and Åke B. Vallbo, 1983). Slow adapting type II afferents mainly respond to remote static skin stretch. The

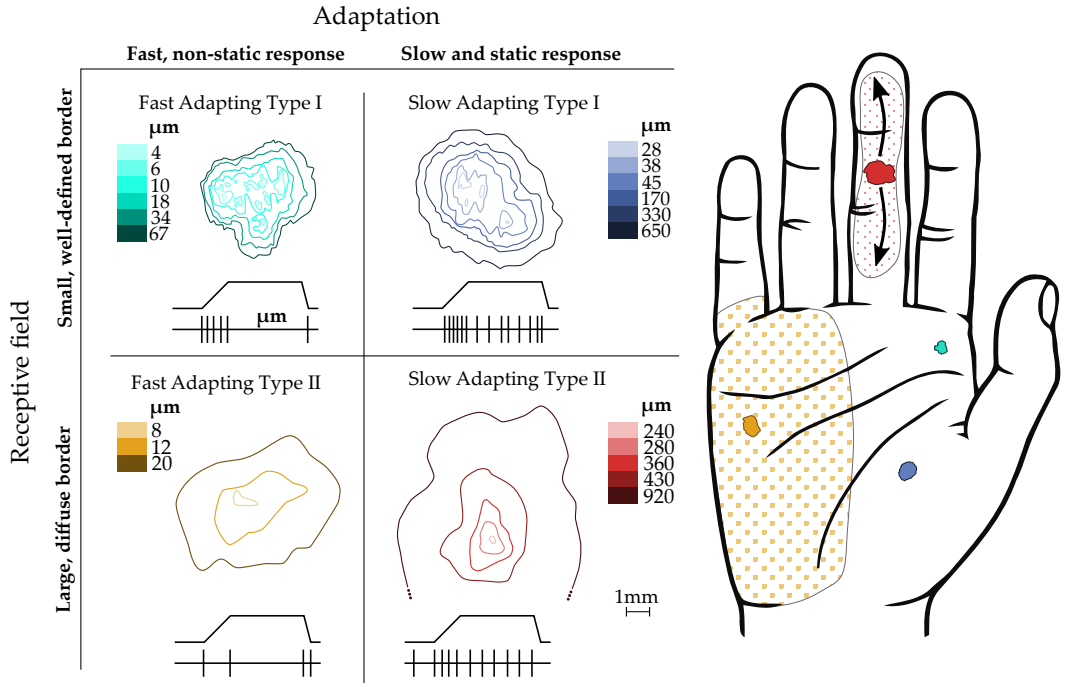

Figure 2.1.: Receptive fields and stimuli response of mechanoreceptive afferents. The left shows a detailed view of the high-sensitivity receptive field of each afferent. The receptive field is displayed as a height map, indicating at which indentation depth in micrometers with a round 0.4 mm probe the afferent is exited depending on the position of the stimulus. Below the receptive field, an exemplary spike train response of the afferent to an indentation is displayed. The indentation is first increased as a constant rate and then held constant before dropping rapidly. On the right, the high-sensitivity receptive field is exemplarily embedded into a human hand for scale comparison and to highlight the complete sensing range of the type II afferents. The fast adapting type II afferent shows a large receptive field given a sufficiently large stimulus. The slow adapting type II afferent shows a larger receptive field when subjected to shear forces. (Graphs based on figures and data in (Johansson and Åke B. Vallbo, 1983), hand sketch based on OpenClipart illustration)

direction of stretch significantly influences the response of individual afferents. Some are mainly sensitive to skin stretches in single directions, while others are exited by skin stretch in two opposite directions.

As observed in (Johansson and Vallbo, 1979), the density of mechanoreceptive units is highest in the fingertip and decreases towards the wrist. This density gradient is not uniform but exhibits sudden changes. A sharp step down in density is observed between the very tip of the distal phalanx and the Distal Interpha-

langeal (DIP) joint. Another step down in unit density is apparent between the finger and palm. The maximum density of FA I and SA I units is 140 units/cm^2 and 70 units/cm^2 respectively. In the palm these values decrease to 25 units/cm^2 and 10 units/cm^2. FA II and SA II units are allocated significantly more sparsely in the glabrous skin. While FA II units follow the density gradient between finger and palm with densities of 22 units/cm^2 and 10 units/cm^2 respectively, SA II units exhibit an opposite trend with 10 units cm^{-2} in the fingertip and 18 units cm^{-2} for the palm. The total number of mechanoreceptors in the glabrous skin of the hand is estimated to be around 17.000 units at the age between 20 and 30.

2.1.2. Tactile Sensors

The sophisticated sense of touch exhibited by humans has inspired a broad range of research into antropomorphic haptic sensors and artificial skins in material science, mechanical and electrical engineering as well as robotics. A large variety of measurement principles has been employed to develop such sensors, including optical and visual, resistive, capacitive sensing, strain gauges, magnetic flux, vibrations, Micro-ElectroMechanical Systems (MEMS) and the piezo resistive effect. Each approach exhibits different advantages and disadvantages regarding resolution, range, hysteresis, spatial resolution, linearity, noise, physical dimensions, accuracy, robustness and ease of production. In contrast to other sensing modalities like sound and vision, very few haptic sensors are readily available. This makes it necessary to pick the right technology for the application from scientific literature, recreate the sensor and adapt the design. This section hence highlights different design methods for tactile sensors in the literature and discusses advantages and disadvantages relevant to the application in anthropomorphic fingers and hands. the selection of the proper technology is key because the sensors serve as the basis for all other parts of this work, hence special attention is given to evaluate all available options.

A general overview of recent developments of haptic sensors is presented in (Park et al., 2018) in terms of sensing devices and in (Zou et al., 2017) with a focus on signal processing. Robotics-focused surveys can be found in (Saudabayev and Varol, 2015) for sensors integrated into robotic hands and (Wang et al., 2018) specifically for soft robots, in (Kappassov et al., 2015; Yousef et al., 2011) grouped by sensing principle and in (Dahiya et al., 2010) grouped by miniaturization technique.

The application of haptic sensors to humanoid robotic hands presents a set of requirements that makes this use case especially challenging. As these sensors are physically interacting with the environment and a mechanical stress is hence unavoidable, haptic sensors should be easy to fabricate and replace or are able to self-heal. Jet, in many cases, current tactile sensor and skin technologies require dedicated laboratories or sophisticated machinery for production. The tightly constrained and irregularly shaped space inside the palm and the fingers of humanoid robotic hands makes miniaturization of the sensors as well as the corresponding signal processing electronics necessary. Due to the above reasons the related work presented in the following will focus on sensors and systems that are potentially robust, readily available, easy to manufacture/integrate and do not require sophisticated external signal processing. While there is also strong interest in tactile sensing for whole-body robotic skin, the application differs in that spatial density of sensors in the hand is substantially higher and sensing is far less distributed. The related work in this area will hence focus on technologies allowing high spatial density and exclude sensors geared towards a more area-wide applications. Potential technologies for inclusion in the sensor system are the following:

- Hall effect-based tactile sensors
- Barometer based tactile sensors
- Capacitive tactile sensors
- Resistive tactile sensors
- Optical tactile sensors
- Visuotactile sensors

In the following, each technology is introduced with its advantages and disadvantages.

Parts of this sections have been reprinted from (Weiner et al., 2019) with changes (CC BY 4.0).

Hall Effect-Based Tactile Sensors

(Kyberd and Chappell, 1993) first describe the basic principle of using a hall effect sensor together with a moveable magnet in soft material for force sensing. A variant using a hallow dome of soft material is reported in (Torres-Jara et al., 2006). (Tomo et al., 2016a,b) and (Wang et al., 2016) utilize commercially available digital 3-axis hall effect sensors in combination with a magnet embedded into

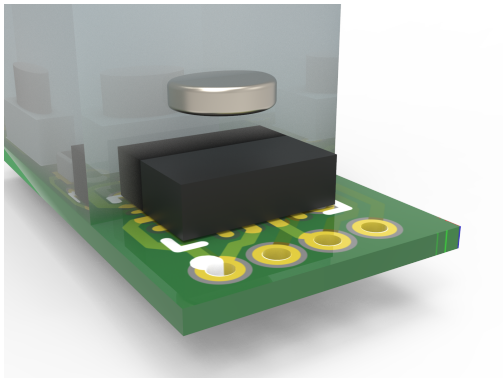

Figure 2.2.: Schematic structure of magnetic shear force sensors with Printed Circuit Board (PCB) (green), a mounted Hall effect sensor (black), a cylindrical magnet (silver) and silicone (cut at sensor center line for visualization)

flexible material above the sensor to measure normal and shear forces through the displacement of the magnet. Arrays of these sensors were integrated into the Allegro hand in (Tomo et al., 2017; Mohammadi et al., 2019; Funabashi et al., 2019) and the iCub hands and fingers in (Tomo et al., 2018) and (Holgado et al., 2019b). An interesting variation of the barometer-based sensing method is presented in (Votta et al., 2019), where a single sensor is used to measure elastic deformation of the finger structure induced by applied forces. By combining the permanent magnet with an electromagnet, (Holgado et al., 2018) present a method for dynamic change of the resolution of the sensor based on the current through the electromagnet. Iterative improvements have since been made to the mechanical structure and experimental characterization of the sensor in(Holgado et al., 2019a, 2020a). Additionally, a version of the above sensor has been presented in (Holgado et al., 2020b) that incorporates a capacitive proximity sensor into the mechanical structure.

The clear advantage of utilizing 3D Hall effect sensors as the base of tactile sensors is the ability to sense applied forces in all three dimensions. This makes them especially interesting for grasp force control and friction coefficient estimation, despite a number of considerable disadvantages. Resolution of the normal force direction is notably smaller than the resolution of both shear force directions as only a small amount of soft material sits between the sensor and magnet which is completely compressed easily. Small variations in the position of the magnet above the sensor during manufacturing lead to large offsets that are different for each sensor, making a per-sensor offset calibration necessary. Shape and strength of the magnetic field of the magnet is highly nonlinear so

that an linear change in the sensor value does not correspond to a linear change in magnet position. The change in magnet position is additionally dependent on the mechanical properties of the surrounding soft material, which again shows nonlinear deformation behavior and introduces hysteresis into the measurement. Because the magnetic flux is only measured in three dimensions, the position of the magnet can not be reconstructed as the floating magnet has six degrees of freedom inside the soft material. The magnetic field is symmetrical around the axis between the magnetic poles, eliminating the rotational degree of freedom around the normal force axis, but tilt around both shear force axes induces unwanted measurement errors. A possible solution would be to suspend the magnet in the middle between three sensors and compare the measured flux values to an analytical model (lookup table) to obtain a precise estimate of the magnets pose and thereby displacement. This approach has not been studied in literature to the best of the authors knowledge.

(Hellebrekers et al., 2019) substitute the magnet above the sensor with magnetic particles mixed into silicone. The mixture is then cured under an external magnetic field to align the particles. This way the magnetic field can deform together with the silicone, allowing the sensor to sense stimuli on a large area that would not be feasible to cover with a classical magnet. Since the particles form a complex magnetic field that is not easily analytically described, the correspondence between stimulus and sensor signal has to be determined using a regression method. (Hellebrekers et al., 2020) employ a neural network for this regression task, which later is enhanced by a self-supervised learning scheme to adapt to unseen sensor modules as described in (Bhirangi et al., 2021). The adaptation to new sensor modules takes around 400 interactions with the sensor.

Barometer Based Tactile Sensors

(Tenzer et al., 2014) utilize MEMS barometers to design tactile normal force sensors. The sensors are completely covered and filled with polyurethane, which acts as the force transmitting medium. When a force is exerted on the soft material, it is transmitted to the sensor and measured as a change in the pressure reading. An overview of the original sensors is depicted in Figure 2.3. These sensors have been integrated into the three fingers of the *iHY Hand* (Odhner et al., 2014) and subsequently sensor arrays have been made commercially available by RightHand Robotics Inc.[1]. A robotic fingertip with similar sensor and an

[1] https://www.labs.righthandrobotics.com/takkstrip

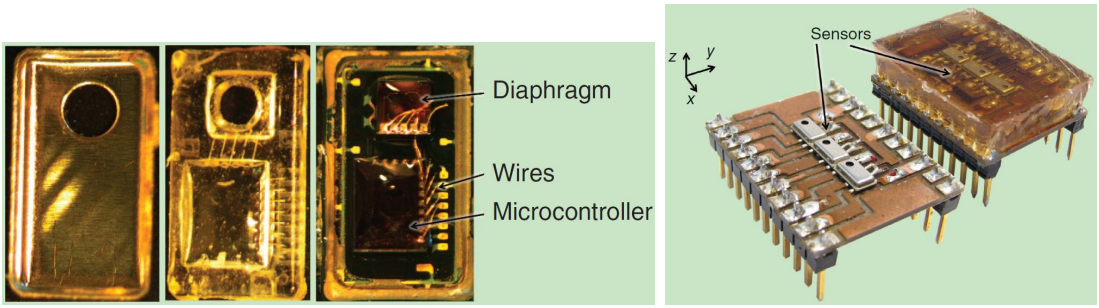

(a) (b)

Figure 2.3.: a) Inside view of the MEMS barometers originally used in (Tenzer et al., 2014); b) Sensor array cast into polyurethne rubber; Reprinted from: Tenzer et al. , "The Feel of MEMS Barometers", Transactions on Neural Systems & Rehabilitation Engineering, V. 30, ©2014 IEEE.

additional distance sensor is available from SparkFun Electronics[2]. The sensors have also be integrated into a three finger tripper (Pelliccia et al., 2018). Recently, this measurement principle has been adapted in (Kõiva et al., 2018) to sense interactions of an artificial fingernail mounted on a custom sensorized fingertip of a shadow hand in (Kõiva et al., 2013) with the environment. Barometers have also been applied to the shadow hand as a skin, covering the palm of the hand using a matrix of sensors in (Koiva et al., 2020). (Piacenza et al., 2018) incorporate multiple barometer sensors into a tactile dome and regression based mapping of the raw sensor signals to force intensity and position of contact on the dome.

MEMS barometer based normal force sensors exhibit a very high sensitivity, making them well suited for detection of initial contact between hand and the environment. Since the barometers measure absolute pressure, only the sensor range from 1 Bar (ambient pressure) to the maximum pressure readable by the sensor can be used for force measurement. As the sensors are meant for measuring ambient pressure, the upper sensing limit oftentimes is at about 2.1 Bar, meaning close to half of the sensing range of the sensor is not usable during operation. Depending on the stiffness of the soft material, this can lead to saturation of the barometer signal. As with 3D Hall effect-based shear force sensors, the barometer based sensors are covered by soft material, resulting in a compliant and high-friction surface well suited to physical interaction.

The original sensor implementation used comparatively large barometers covered by a lid with a large venting hole. When these sensors are casted into soft material, the hole allows the mixture to flow into the casing and directly cover

[2] https://www.sparkfun.com/products/14687

the sensors. Casting becomes far more difficult with miniaturized sensors where the venting hole measures in the range of 0.1 mm to 0.4 mm as the mixture will not flow into the sensor. This can be mitigated by casting small soft covers for the sensors including a pressure chamber (Weiner et al., 2018a; Ma et al., 2021) or by removing the covers, drilling lager holes and gluing the lid back on as done in (Koiva et al., 2020). Alternatively, sensors for medical applications can be used where the sensing element is covered by elastic gel ((Weiner et al., 2021), see subsection 3.2.1), requiring no customization of the sensor. A pressure chamber is used in (George Thuruthel et al., 2021) in combination with an self-healing elastomer to realize detection and localization of damage through sensing of abrupt pressure loss.

Capacitive Tactile Sensors

For the humanoid robot iCub, capacitive tactile sensors were developed in (Schmitz et al., 2010) and integrated into the hand. One plate of the capacitor is formed by a flexible PCB, the other by a deformable conductor. Both are separated by silicone foam. The sensor signal is digitalized using a commercially available capacitance-to-digital converter. In an extension of the work, the production process is optimized in order to make the sensors easier to manufacture and more robust (Jamali et al., 2015), the resulting sensors are shown in Figure 2.4. The capacitive sensing principle is also used as the basis for robotic skin, spanning larger parts of the iCub robot (Schmitz et al., 2011; Maiolino et al., 2013). Capacitive sensor arrays have been commercialized for force distribution measurement for product design and engineering[3], demonstrating practicality of the principle.

The principle of capacitive tactile sensors is expanded in (Göger et al., 2013) by incorporating capacitance-based distance sensing and demonstrating the application of the sensor to an anthropomorphic hand. The system is improved in (Alagi et al., 2016), depicted in Figure 2.4, allowing for individual sensor cells to be joined or split to dynamically change sensor sensitivity and spatial resolution.

Due to their simple structure, capacitive sensors can be easily adapted to different geometries inside hands and fingers, provided that the geometry can be unfolded into a planar surface for the fabrication of a flexible PCB. While the electronics for capacitance measurement is relatively simple, the extension to

[3] https://pressureprofile.com/sensor-systems/sensors

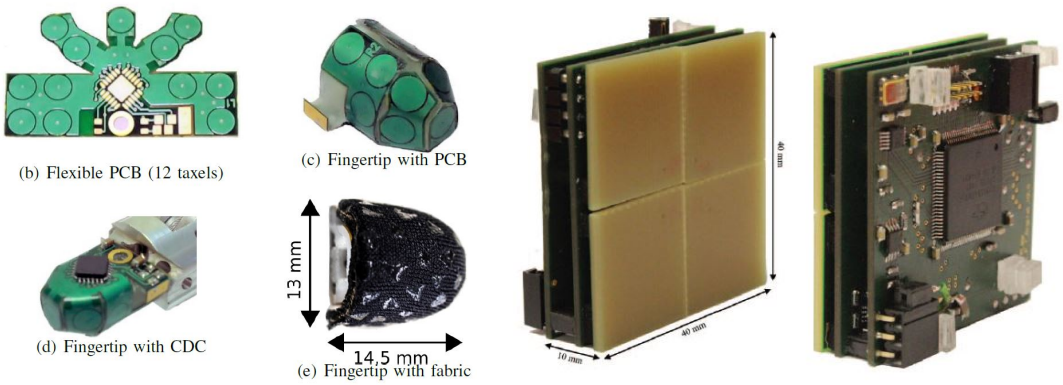

(a) (b)

Figure 2.4.: a) Capacitive normal force sensors of iCub in (Jamali et al., 2015); b) Capacitive Sensing Module in (Alagi et al., 2016); Reprinted from: Jamali et al. , "A new design of a fingertip for the iCub hand", IROS 2015, ©2015 IEEE and Alagi et al. ; "A Versatile and Modular Capacitive Tactile Proximity Sensor", HAPTICS 2016, ©2016 IEEE.

proximity sensing requires more sophisticated electronics and hence more space. It is also important to note that the magnitude of the proximity signal and to some degree also the tactile reading depend on the material of the sensed object. In an effort to reduce the amount of wiring needed for sensors with multiple taxels, (Sonar et al., 2018) develop a readout scheme for a single large taxel based on measurement of the capacity at different frequencies to localize the area of contact on the sensor.

Resistive Tactile Sensors

Traditional Force Sensing Resistors (FSRs) made of resistive ink between two conductive traces or plates have seen little use in tactile sensors since these sensors usually exhibit poor sensitivity and linearity. Hence most research in this area is focused on creating sensors with improved characteristics, for example by varying the resistive material. In (Weiss and Wörn, 2005), a resistive sensing method is introduced, using conductive foam and interlaced traces on rigid PCBs. When the foam is compressed onto the traces, resistance between the traces is changed, allowing for an estimation of the force acting on the foam based on the change in resistance. A tactile fingertip based on this measurement method using a Three-Dimensional Molded Interconnect Device (3D-MID) as the fingertip structure for the Shadow hand is implemented in (Kõiva et al., 2013). The fingertip structure is manufactured using injection-molding of special thermoplastic which, in a second step, can be selectively metallized using a

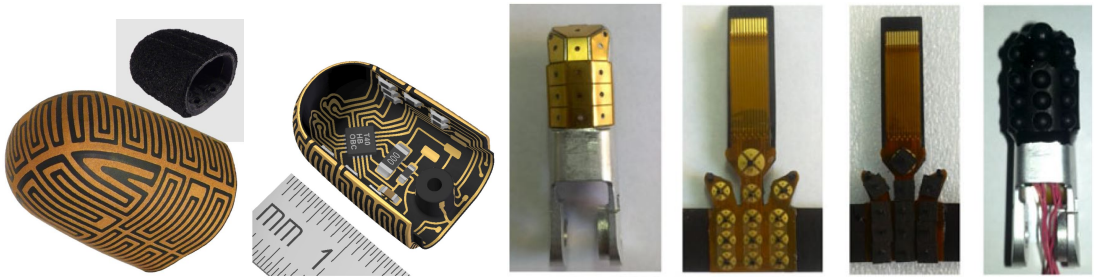

(a) (b)

Figure 2.5.: a) Resistive sensing fingertip in (Kõiva et al., 2013); b) Resistive 3D force sensing in (Zhang et al., 2015); Reprinted from: Kõiva et al. , "A highly sensitive 3D-shaped tactile sensor", International Conference on Advanced Intelligent Mechatronics 2013, ©2013 IEEE; Zhang et al. , "Fingertip Three-Axis Tactile Sensor for Multifingered Grasping", Transactions on Mechatronics V. 20 I. 4, ©2015 IEEE.

laser, forming electric traces on the surface. Using this method, the resistive measurement principle can be applied and tailored to the 3D-geometry of a finger without the need for more fragile flexible PCBs. The tactile fingertip is depicted in Figure 2.5. Since injection-molding requires an expensive mold, this approach is less suited for a scalable finger design.

The authors in (Suzuki, 2017) construct curved tactile fingertips using a flexible PCB and conductive rubber instead of foam. By layering two sensors above one another, shear forces can be estimated by comparing the difference in position of the pressure distribution on upper and lower sensor. Another approach for measuring shear forces is presented in (Zhang et al., 2015), who arrange four sensing elements in a cross configuration covered by a soft dome, shown in Figure 2.5. Shear forces can hence be estimated by taking the difference between opposite sensing elements, similar to the strain gauge based TrackPoint technology pioneered by IBM in (Berstis and Zimmerman, 2000). Utilizing conductive fabric, (Wade et al., 2017) construct tactile skin for curved surfaces. Above the force sensors, a layer of thermistors is utilized for active thermal sensing of contacting objects. A customizable and low-cost variant of a resistive tactile matrix is presented in (Fiedler et al., 2021) by cutting all conductive traces out of aluminum foil using a cutting plotter, allowing for arbitrary shapes. A conducting foil is then placed between two aluminum layers to form the sensor. As the four works above make use of analog sensors, a large amount of wires is needed to connect the sensors to the readout electronics for higher spatial resolutions. All presented sensor foils need to be custom-made for the application.

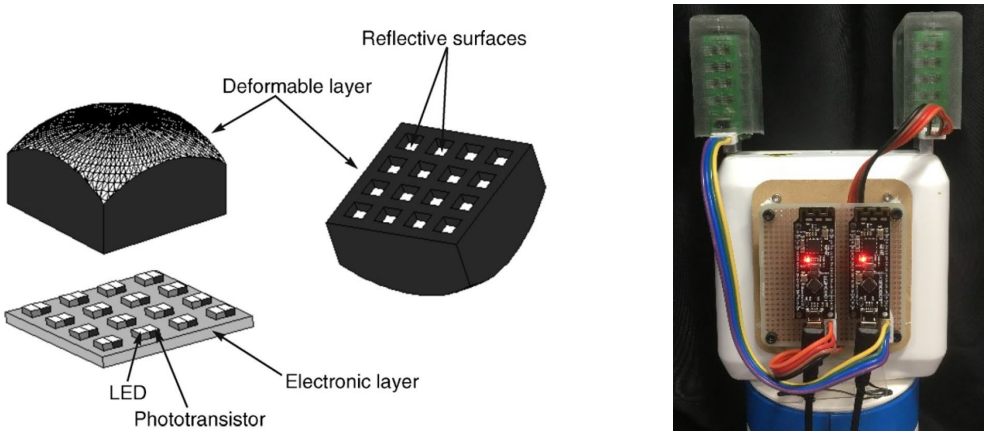

(a) (b)

Figure 2.6.: a) Optical normal force sensor array in (De Maria et al., 2015); b) Proximity sensor based force sensors on the yaws of a parallel gripper in (Yamaguchi et al., 2018); Reprinted from: Sensors and Actuators A: Physical, V. 175, De Maria et al. , "Force/tactile sensor for robotic applications", ©2012, with permission from Elsevier; Yamaguchi et al. , "A Gripper for Object Search and Grasp through Proximity Sensing", IROS 2018, ©2018 IEEE.

Optical Tactile Sensors

Sensors based on an array of Light Emitting Diodes (LEDs) and phototransistors covered by light scattering foam are presented and characterized in (De Maria et al., 2012). When the foam is deformed, the intensity of reflected light changes for each pair of LED and sensor, allowing to estimate normal and shear forces acting on the foam. Sensors of this type have been included into the *Sandia Hand* (Quigley et al., 2014) and *PRISMA Hand II* (Liu et al., 2019). A related principle has been proposed in (Torres-Jara et al., 2006) using a dome of soft material over multiple pairs of LEDs and sensors. The sensing principle is similar to the later developed *OptoForce* sensors, 3-axis force sensors which have been commercially available until 2020.

Three tactile systems using commercially available digital proximity sensors have recently been introduced in (Patel et al., 2018; Yamaguchi et al., 2018) and (Lancaster et al., 2019). The sensors are covered by a layer of a translucent elastomer, allowing the sensor to measure the intensity of reflected light through the material before an object comes in contact with the sensor. When an object comes into contact with the elastic layer it is compressed causing even more light to be reflected to the sensor. The measured light intensity can then be translated into a force measurement as the material properties of the elastomer

are known. The design hence combines both pre-touch distance information and normal force in a single system with miniaturized sensors integrating signal processing and digital bus interfaces. Due to the sensing principle, optical tactile sensors are naturally resistant to electromagnetic interference. The downside of this method is that the measurement is dependent on the optical properties of the objects in proximity as well as stray light from external light sources.

Visuotactile Sensors

Vision based tactile sensors, named visuotactile sensors, convert tactile stimuli into images. They consist of a camera directed at the backside of a transparent and flexible material which is often covered by a opaque coating at front side. The material is supported by a sheet of glass or plastic at the back side so that pressure exerted on the soft material is not transmitted to the camera. When an object comes in contact with the front side of the flexible material it is indented, which creates a visual representation that is recorded by the camera.

The underlying principle has already been exploited for robotics in the 1960's as detailed in the survey paper in (Abad and Ranasinghe, 2020b), but recent developments in both miniature cameras and artificial intelligence based image processing have sped up the development considerably. A visuotactile sensor called *GelForce*, presented in (Sato et al., 2008, 2010), places a camera inside a transparent half-dome with opaque paint at the surface. Colored markers on the inside of the half-domes surface are visually tracked to sense deformation of the dome and calculate contact position and the force vector. In a later version, the half-dome is painted with thermo-sensitive pigments such that the domes color indicated the temperature of contacted objects. The authors in (Chorley et al., 2009) and (Winstone et al., 2012) also employ a half-dome, but here the markers are located at the tips of pegs that point inwards into the half-dome. The pegs amplify the movement of the markers when the half-dome is deformed, resulting in an increased sensitivity of the sensor. Multiple cameras are employed in (Yamaguchi and Atkeson, 2016) on two gripper yaws covered by a flat layer of transparent material with markers at the surface. The markers allow calculation of forces and torque in normal direction and the transparent material allows to capture images of the object in contact or close vicinity.

Another class of visuotactile sensors, called *GelSight* aims to capture the local surface geometry at the area of contact. *GelSight* sensors are also composed of a camera with transparent soft material on top. The outer geometry of the soft material is flat and the outer surface is covered in reflective coating. A red,

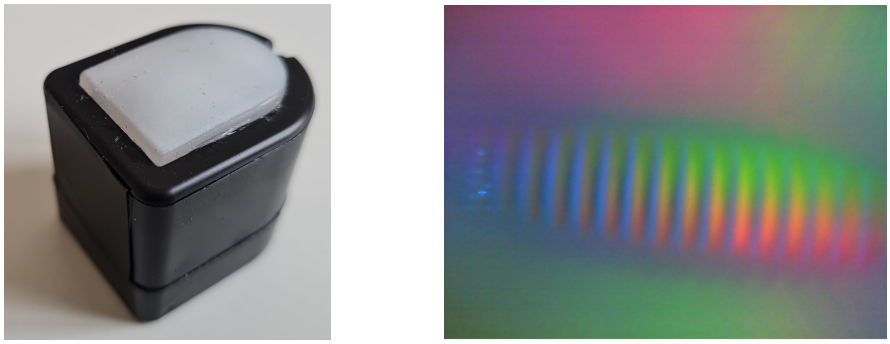

(a) (b)

Figure 2.7.: a) The commercially available Gelsight sensor; b) Image generated by a Gelsight sensor with a screw pressed against the sensor's surface

green and blue LED is directed from the sides inward with an rotational offset of 0°, 120° and 240° respectively. An object that indents the soft material will hence not only create a visible imprint, the slopes of this imprint will also be colored according to the color of the diode they are sloped towards. This allows a reconstruction of the 3D contact geometry.

A first demonstrator for surface reconstruction was presented in (Johnson and Adelson, 2009) and (Johnson et al., 2011). The application to robotic grippers was first demonstrated in (Li et al., 2014) and improved in (Dong et al., 2017). Later, (Donlon et al., 2018) published a simplified design called *Digit* including Computer Aided Design (CAD) data, a python framework and simulation environment for machine learning with the goal to make the technology available to a broader community. The sensor technology has also been commercialized[4] in a sensor package suitable for use with the Allegro multi-finger hand, depicted in Figure 2.7. To be able to capture the tactile imprint and forces simultaneously, (Yuan et al., 2015, 2017) combine the design with colored markers as similar to the *GelForce* sensors.

An alternate approach for simultaneous contact geometry and force measurement is presented in (Li et al., 2018) who design polymer beams whose compression can be seen on the same image as tactile data. Since the markers interfere with the 3D contact geometry reconstruction, (Abad and Ranasinghe, 2020a) use ultraviolet (UV) markers that are only visible to the camera if illuminated by a UV LED. Similar to the *GelForce* sensors, (Abad et al., 2021b) introduce thermo-sensitive pigments to the sensors. In their latest work, (Abad et al.,

[4]https://digit.ml/

2021a) integrate both UV markers and thermo-sensitive pigments to a sensor that can sense contact geometry, forces and temperature.

While visuotactile sensors are able to provide rich information on contact geometry, location and in some cases forces and temperature, there are three main disadvantages of such sensors, namely size, shape and required processing recourses. The cameras need to be mounted at a distance from the opaque coating that corresponds to their minimum focal length, which is in the range of centimeters for the cameras usually used in the these sensors. To reduce the resulting thickness of the sensor (Donlon et al., 2018), (Ma et al., 2019) and (Wang et al., 2021) introduce a mirror that reflects the tactile image to the side, which allows to mount the camera perpendicular to the tactile surface. This reduces the thickness of such sensors at the cost of sensor length. Secondly, the shape of the *GelSight* sensor surface is flat, hence reliable sensor signals can only be gathered if the contact between finger and sensor is roughly normal to the sensing surface. While (Romero et al., 2020) presents the design of a fingertip-shaped sensor, it offers reduced tactile resolution while increasing manufacturing complexity. The third disadvantage is the need for high bandwidth connections and extensive computing resources for transmission and processing of the image data. Lastly, the reflective coating abrades over time as it is applied to the outside of the soft material and is directly in contact with the manipulated objects.

2.1.3. Selection of Tactile Sensing Technologies

Although development of the sensor system is an important part of this work, the focus lies on the integration of a sensor systems into humanoid robotic hands and not on the development of sensor technologies themselves. Hence, readily available sensors and technologies are preferred over involved fabrication techniques at the potential cost of sensitivity and resolution. From this technical point of view, this work has been inspired by the successful *CellulARSkin*, a large scale robot skin made out of modules that makes heavy use of readily available sensors and fabricating processes (Cheng et al., 2019). Another consideration is the compatibility of the sensing technologies selected for inclusion in the sensor system. Optimally, all sensor modalities should share a continuous mechanical interface to the environment which should preferably be soft to increase friction and compliance. As described in subsection 2.1.2, there is a range of possible candidates for the realization of a human-inspired tactile sensor system. On the other hand it becomes clear that no single sensing technology can substitute all four kinds of mechanoreceptors in humans simultaneously. Hence, multiple

sensing technologies are combined in this work to build a more complete system inspired from the human tactile sense.

In this context the technical realization of the sensing abilities of slow adapting type II afferents proves especially challenging. Only few of the considered tactile sensing technologies are able to sense shear forces. While *visuotactile sensors* with visual markers offer the ability to track shear forces and are able to detect object geometry similar to SA type I afferents their inherent size does not allow for integration into human-sized fingers. The compute-intensive evaluation of the resulting video stream presents an additional hurdle. *Capacitive, resistive* and *optical tactile sensors* allow to estimate shear forces when used in an array configuration of at least four sensors, but the resulting amount of analog signals is strongly disadvantageous. *Hall effec-based tactile sensors* are not as sensitive as *visuotactile sensors* and offer lower spatial resolution as *optical tactile* or *capacitive sensor* arrays. Yet, they offer small-scale housing, are cast into compliant soft material and offer a digital interface for sensor readout minimizing external electronics and cables. For these reasons they are chosen as the basis for SA type I afferents in the anthropomorphic fingers in this work. As 3D Hall effect sensors offer sample rates into the kHz range, they can also serve to sense mechanical transients corresponding to the capabilities of FA type I afferents and to an extend FA type II afferents. Due to the poor normal force resolution of *Hall effect-based tactile sensors*, an additional sensor modality is needed to represent the function of SA type I afferents.

For normal force sensing inspired by SA type I afferents, a larger selection of sensing technologies is available. *Capacitive sensors* allow adaptation to arbitrary shapes since the sensing elements are flexible and can be cut into any shape. Yet, they offer a comparably poor sensitivity depending on the sensor size and are prone to interference when the grasped object is conductive. The sensors need additional read out electronics, namely an Capacitance to Digital Converter (CDC), that requires additional cabling and space in proximity of the sensor. *Resistive sensors* can also be arranged relatively freely with respect to the geometry of humanoid fingers and are less prone to interference due to the material of grasped objects. But to make use of this potential, more complex fabrication techniques like 3D-MID are necessary. *Resistive sensors* share the disadvantage of requiring additional circuitry and hence space in the form of Analog to Digital Converters (ADCs) for signal readout with *capacitive sensors*. Proximity sensor based *optical tactile sensors* offer both pre-touch and normal force sensing combined with integrated signal processing and a digital interface in a single readily available sensor package. For these sensors to work optimally,

the finger needs to be transparent and its surface should be flat to allow optimal transmission of light from the inside of the finger material. The sensitivity to normal force depends on the reflective properties of the grasped object and the thickness of the transparent material.

Barometer based tactile sensors show exquisite sensitivity combined with a integrated signal processing electronics in miniature packages. While they are not as adaptable to the finger's geometry as *capacitive* or *resistive sensors*, their small size of just 2 mm by 2 mm still allows to utilize multiple sensors even in small spaces. Fabrication of *barometer based tactile sensors* is very simple as the barometers only need to be cast into silicone to create normal force sensors. Due to their integrated signal processing, easy fabrication and exceptional sensitivity, *barometer based tactile sensors* are chosen as the main modality for normal force sensing in this work. Similar to *Hall effect-based tactile sensors* the sample rate of up to 200 Hz allows to incorporate to an extend the functionality of FA type I afferents. Since *optical tactile sensors* offer valuable pre-touch information in combination with integrated signal processing, they will be used sparingly to provide supplementary information.

To mimic the functionality of FA type II afferents, an MEMS accelerometer will be integrated into the finger to sense more global mechanical transients. The tactile sensor system discussed above hence represents the functions of all four mechanoreceptive units. As all selected sensors are readily available in standard packages, the complete sensor system can be mounted on standard PCBs. Fabrication of the PCBs and soldering of the components are standard processes with very little variance. The working principle of *hall-effect based tactile sensors*, *barometer based tactile sensors* and *optical tactile sensors* is dependent on a soft material as mechanical interface. Therefore, these sensors can be cast into the same soft material, easing the manufacturing process.

2.1.4. Sensorized Hands and Fingers

Providing meaningful sensory feedback for closed-loop control of grasping and manipulation tasks requires not only measurement of normal forces and contact locations. Like the human role model, anthropomorphic hands benefit from further sensing modalities including temperature and vibrations sensors, joint angle encoders, internal forces/torques and even pain receptors. Anthropomorphic hands further offer the possibility to include sensing modalities not present in the human role model like distance sensing or cameras, which

can further support the grasping process. All these sensors as well as their corresponding cables need to be embedded into the heavily constrained space of human-sized fingers, which is considered a major challenge in robotics as detailed in (Saudabayev and Varol, 2015). Especially for prosthetic applications, anthropomorphic appearance and dimensions are required for a prosthesis to be accepted by most users (Cordella et al., 2016). This not only implies that each finger needs to be sized individually, e. g. the middle finger should be larger than the little finger, but also that the hand and finger sizes of the prosthesis should match the size of the able hand.

This section highlights works that aim to solve different aspects of the issues raised above while focusing on anthropomorphic hands and fingers, as these present unique challenges compared to robotic grippers. Hands with extrinsic actuation, for example by compressed air, are not included since the focus lies explicitly on fully integrated hands akin to classical prostheses and humanoid robotic hands. A broader overview of prosthetic and robotic hands can be found in (Piazza et al., 2019), an overview of the (mechanical) capabilities of commercial prosthesis is provided in (Belter and Dollar, 2013). The thesis makes use of the nomenclature for human hand bones and joints, described for reference in appendix A. In the following the integration of haptic and environmental sensors into fingers and complete anthropomorphic hands is described.

Humanoid Robotic Fingers

Parts of the following discussion on related work have been reprinted from (Weiner et al., 2019) with changes (CC BY 4.0).

In (Wang et al., 2011), the authors present tendon-actuated fingers integrating an potentiometer-based joint angle encoder in each joint and an FSR-based tactile sensor at each phalanx. The routing of the cables through the finger as well as measures against cable break are not documented.

For the Shadow hand[5], an anthropomorphic five-fingered robotic hand, multiple sensing systems where integrated. A fingertip with an resistive sensing array consisting of 12 taxels is presented in (Kõiva et al., 2013). The mechanical structure of the fingertip is realized as an 3D-MID, with electrodes at the outside of the fingertip shape. A Computer Numerical Control (CNC) milled conductive foam is placed around the fingertip. At the inside of the fingertip, the ADC and other electronic components can be directly soldered to the fingertip. The ADC

[5]https://www.shadowrobot.com/dexterous-hand-series/

is connected to the finger internal Serial Peripheral Interface (SPI) bus provided by the shadow hand. In addition, dynamic events can be measured using a 3-axis accelerometer. The fingertip was later extended with an mechatronic fingernail (Kõiva et al., 2018). The fingernail sits on top of a soft nail bed which includes both an barometer based normal force sensor and a Hall effect-based shear force sensor. In addition, an accelerometer attached to the nail allows to pick up mechanical transients, exemplarily shown for detecting the end of tape on a tape roll. Recently, the palm of the hand was also sensorized using an array of 60 barometer based normal force sensors mounted on a flexible PCB.

The tendon-actuated fingers of the three-fingered *iHY Hand* in (Odhner et al., 2014) embed an array of barometer based tactile sensors on both the distal and proximal phalanx. The Intermediate phalanx is fused into the distal phalanx, resulting in two Degree of Freedom (DoF). Instead of a classical rotational joint, the Proximal Interphalangeal (PIP) joint is constructed from a bar of flexible material which elastically deforms as the finger is actuated. Four optical fibers are running through the neutral phase of the bar with a light source at the distal and two phototransistors at the proximal end. Hence, for each finger eight analog signals need to be digitalized by corresponding signal processing electronics. The resulting signals are used to estimate flexion, torsion and shear of the joint using a model based approach. Signal transmission through the joints is realized by free-moving cables with service loops at the joints.

The multimodal BioTac tactile fingertip from SynTouch[6] incorporates 19 electrodes embedded into a fluid-filled soft fingertip. When pressure is applied to the fingertip, the distribution of the liquid inside the finger changes and the impedance between the different electrodes changes with it. A pressure sensor measures high frequency vibrations through the liquid and additional temperature sensors in combination with heating elements enable temperature flux measurements. The structure and working principle of the sensor is described in (Wettels et al., 2014). The fingertip fuses the distal and intermediate phalanx. A proximal phalanx or an PIP joint are not included. The intermediate phalanx houses the signal processing electronics and pressure sensor while the distal phalanx is covered by the electrodes. As the fingertip is not perfectly sealed, the fluid needs to be refilled periodically[7].

A finger specifically designed for use in prostheses is presented in (Ming Cheng et al., 2017). The linkage-actuated finger includes all three finger joints and embeds an unspecified tactile sensor in the fingertip as well as joint angle

[6]https://www.syntouchinc.com/en/sensor-technology/
[7]https://www.syntouchinc.com/wp-content/uploads/2018/08/BioTac-Manual-V.21.pdf

measurement in metacarpophalangeal (MCP) and PIP joint. All sensors are connected to a signal processing PCB located inside the distal phalanx. The routing of the cables through the finger as well as measures against cable break are not documented.

The authors in (Segil et al., 2019) present the design of a prosthetic fingertip for the Bebionic hand with integrated normal force and proximity sensing. The finger is 3D-printed with a cavity at the tip for a PCB with sensors. On this PCB a single barometric pressure sensor and a distance sensor is placed. The remainder of the cavity is then cast into silicone.

Humanoid Robotic Hands

Published works on sensorized humanoid hands are classified into three categories in this work. the first category puts special emphasis on actuation either by means of novel underactuation mechanisms or in the contrary on a high number of active DoF. While the sensor system is in most cases a side aspect in these category of works, especially the strategies to integrate sensors into the highly actuated structure are of high relevance.

The second category is highly focused on manufacturing aspects of sensorized humanoid hands. This includes novel manufacturing techniques for the mechanical structure and embedding of sensors as well as integration of sensors using for example 3D-printing techniques. Additionally works are included that emphasize an especially robust or cost-aware design.

The third category is concerned with the sensor system itself as the primary contribution. Works in this category for example explore new sensor principles to be included in hands, present multimodal sensor systems or aim at advanced control of grasping force or automatic control of parts of the grasping tasks.

Exemplary works are depicted in Figure 2.8. Parts of the following discussion on related work have been reprinted from (Weiner et al., 2018a), “The KIT prosthetic hand: Design and control”, IROS 2018, ©2018 IEEE.

Focus on Actuation

- The hands of the humanoid robot ARMAR-4 presented in (Asfour et al., 2013) are pneumatically actuated five-fingered hands with human proportions. The hand is shown in Figure 2.8c. Each finger is actuated by two fluidic actuators, the thumb can additionally be actuated in circumvention

direction. Actuation of both ring and little fingers are coupled, resulting in nine DoF controllable over a valve system in the hand's palm. Each finger is equipped with joint angle encoders and pressure sensors for model based contact force estimation. All electronics needed for valve control and sensor signal processing are embedded into the back of the hand.

- The fingers of the *UT Hand I* described in (Peerdeman et al., 2014) utilize flexure sensor based joint angle encoders and barometer based tactile sensors inside the flexible fingertip. The thumb can either also embed barometer-based tactile sensors or can be equipped with a *BioTac* fingertip at the cost of the distal joint. Transmission of the sensor signals through the finger is not discussed. The fingers are actuated by a single motor through an underactuated mechanism. Additional solenoids allow to lock individual fingers to realize different grasping patterns.
- The *SSSA-MyHand*, presented in (Controzzi et al., 2017) and shown in Figure 2.8a, primarily focuses on dexterous and fast movement. The two DoFs in each finger are actuated by a rigid four bar linkage system. Each finger is sized individually. The authors state that they plan to embed FSR sensors into the fingertips in the future, although, to the best of my knowledge, this has not been reported until now. In contrast to most other research prostheses, the control of the prosthesis is mostly realized on the embedded system inside the palm of the hand. The microcontroller runs a finite state machine based on information from Electromyography (EMG) sensors and external input over a serial interface.
- In (Jeong et al., 2017) a prosthetic hand is presented that is driven twisting a pair of tendons, thereby shortening the tendons. A custom tension sensor embedded into the internal structure of each finger. The sensor consists of a LED and phototransistor pair where the light of the LED can be partially blocked by a pin. The part holding the pin deforms elastically upon tension, altering the amount of light transmitted from the LED to the phototransistor. Analog sensor signals are transmitted through the finger using individual loose wires.

Focus on Manufacturing

- The *Vanderbilt Hand* described in (Dalley et al., 2010; Wiste et al., 2011) and (Varol et al., 2014) does not include sensors inside the fingers, instead the finger forces are calculated from the motor positions and currents. This

is archived through a model of the series elastic elements in the tendon force transmission. A distinguishing aspect of this hand is the consistent and holistic use of additive manufacturing for the mechanical parts of the hand. Both the palm of the hand as well as all three phalanges are fabricated using a Stereolithography (SLA) process using thermoplastic that is afterwards coated with nickel. The design is further developed as the *Vanderbilt Hand 2*, depicted in Figure 2.8b, in (Bennett et al., 2015). As with the first version, the hand structure is completely 3D-printed, including the soft exterior of the fingers. Each finger is individually sized, according to the 35^{th} percentile male hand dimensions. The hand includes an embedded system based on a 50 MHz microcontroller for motor control. The embedded system features a CAN port for higher level control using an external device. Later, (Wiste and Goldfarb, 2017) presented the *SCCA Hand*, a minimalist design focused on actuation following the philosophy of the first *Vanderbilt Hand* without including sensors or an embedded system.

- The *SoftBionic Hand* presented in (Tavakoli et al., 2017) is equipped with soft fingers with integrated soft capacitive sensors. Each finger consists of a 3D-printed endoskeleton covered by soft silicone. The endoskeleton is printed as a single piece including two joints using an Selective Laser Sintering (SLS) process. Meandering spring structures are printed as the joint, while the phalanges are printed as solid pieces as described in (Tavakoli et al., 2017). A flexible capacitive sensor is embedded in the fingertip, made from two layers of silicone mixed with carbon nanoparticles separated by a non-conductive silicone layer. The sensor allows to sense conducting materials before touching the finger and for non-conducting materials to measure the change in capacitance induced by force exerted on the fingertip. Small copper wires cast into the finger's soft material connect the sensors to corresponding readout electronics.
- The fingers of the *PRISMA Hand II* introduced in (Liu et al., 2019) are specifically designed to increase robustness. Each finger is made of three phalanges connected by elastic ligaments. The joint motion is accomplished by rolling contacts between the phalanges, actuated by tendons. The finger base is also actuated in adduction/abduction direction. Each fingertip houses four optical tactile sensors and corresponding signal processing electronics aimed at normal and shear force detection as described in detail in (Canbay et al., 2021). Routing of the electrical connection from the fingertip through the finger is not documented.

- Recently, the *Galileo Hand* has been introduced in (Fajardo et al., 2020). The hand development's primary objective to keep material cost low and provide open source access to the relevant design data. Inside the palm a microcontroller-based embedded system is placed including an Inertial Measurement Unit (IMU) on the PCB. Additionally, a display is embedded into the dorsal side of the palm to provide feedback to the user and enable interactive IMU-based control over a menu.
- In (Ntagios et al., 2020) the authors present a 3D-printing technique to print the complete hand from layers of ABS and TPU plastics. Rigid sections of the hand are printed from ABS while the joints are made from a layer of TPU only. The fingertips include a hollow where the readout electronics for capacitive finger tip sensors are placed, connected to the actual pads by printed conductive traces. The capacitive sensors themselves are also printed from layers of ABS, TPU and conductive ink, sealed by poured rubber.

Focus on Sensorization

- The *Manus Hand Prosthesis*, depicted in Figure 2.8d in (Pons et al., 2004) is one of the earliest works to include tactile sensing in a prosthesis. Goal of the development was a prosthesis suitable for dexterous manipulation and autonomous grasp force control. It includes Hall effect-based tactile sensors in the fingertips of index and middle finger as well as the thumb. These three fingers also include Hall effect-based joint angle encoders. The cables are loosely routed along the fingers to a hierarchical embedded system. A *host controller*, connected to the user interface coordinates three *local controllers*, which are connected to the motors and sensors of the index finger, middle finger and thumb respectively. On the host controller a force controller is implemented. The ring and little fingers are not actuated.
- The goal of the development of the *HIT/DLR Hand* in (Huang et al., 2006) was a lightweight, yet easily controllable hand prosthesis. Thumb and index are driven by one motor each, middle, ring and little finger are driven by a third motor. The sensor system, as detailed in (Gao et al., 2003), includes three joint angle encoders, three strain gauge based joint torque sensors, two temperature sensors and a custom-made digital 6D-force/torque sensor in each fingertip. All fingers have identical dimensions. The sensor signals are transmitted via a flexible PCB inside the finger that also carries an ADC to digitalize the signals of the joint torque sensors

and a Field Programmable Gate Array (FPGA), aggregating all sensor signals. Each finger FPGA is connected to a larger FPGA in the palm that further aggregates the five finger sensor streams and makes them externally available via an USB interface. Opening and closing of the hand can be controlled by voice commands.

- The *CyberHand* hand prosthesis in (Carrozza et al., 2006; Edin et al., 2008) is specifically designed to mimic the neurophysiological sensor modalities of the human role model. Each of the identical fingers contains three joint angle encoders as well as tendon tension sensors. The phalanges of each finger are covered in a matrix of contact switches, further the finger tip contains both a custom-made 3D force sensor in the internal structure as well as another custom-made 3D force sensor embedded in soft material at the fingertip. All sensors inside each finger are connected via a flexible PCB to two external PCs.

- For the humanoid robot iCub, 12 capacitive taxels where integrated on the fingertip of each finger (Schmitz et al., 2010; Jamali et al., 2015). The innermost layer of the sensor is constructed from a flexible PCB and contains the electrodes for the capacitors and a CDC for all twelve electrodes. Above that a protective plastic interface is mounted and on top a three-layer fabric with the ground electrode is placed. The palm contains a microcontroller that samples all CDCs. The cables connecting the microcontroller to the converters are guided at the outside of the finger next to the neutral phase of the joints. Recently, a variant of the iCub fingers with two Hall effect-based tactile sensors was developed (Holgado et al., 2019a). The sensors are embedded into a fingertip adapter that is placed on top of the actual fingertip and is connected with flying cables to a controller at the forearm, and from there to an external PC.

- The *SmartHand* prosthetic hand introduced in (Cipriani et al., 2010, 2011) is, from a design standpoint, based on the *CyberHand*. the hand is shown in Figure 2.8e. Joint angle encoders are included in each of the three finger joints in addition to motor relative encoders. Each finger contains a tendon tension sensor and both index and thumb include optical tactile sensors in intermediate and proximal phalanx. Mechanically, the fingers are very similar to the ones of the *CyberHand*. The palm of the hand includes an embedded system that digitalizes the sensor data streams, makes them available to external devises and provides motor control electronics.

- The four-fingered *Sandia hand* presented in (Quigley et al., 2014) utilize two antagonistic steel tendons in the fingers for both actuation and digital signal transmission for sensors embedded into the fingertip and phalanges. The two tendons supply Direct Current (DC) power to the sensors while the sensor communication is modulated on top as Alternating Current (AC) signals. While this approach eliminates all cables, it comes at the expense of additional signal processing electronics at both ends of the tendon, to modulate and demodulate the sensor signals. Further care must be take to isolate the tendons from other metallic parts like the motor shafts or pulleys, to not short the electrical connection. Each finger includes an array of optical force sensors on a flexible PCB at the tip, two accelerometers at the tip and the base of the finger and a strain gauge at the PIP joint. the finger is covered by soft foam. The palm of the four-fingered hand includes a camera and a structured light projector for image and depth sensing. Additionally, two PCBs are included, one based on a microcontroller for motor control and sensor signal interfacing to USB/Ethernet and one FPGA-based PCB for in-hand camera interfacing over Ethernet.
- In (Zhang et al., 2018) the design of a hand prosthesis with a custom made shear force sensor array in each fingertip is presented. Each finger is driven by a motor directly embedded into the proximal phalanx of the finger, leaving the fused intermediate/distal phalanx for sensorization. The shear force sensor array is constructed from two flexible PCBs with multiple electrodes, connected by a individual cells of quantum tunneling composite material. This material changes its resistance in accordance with applied pressure. Shear forces are calculated from differences in the output of neighboring electrodes as detailed in (Zhang et al., 2015). All sensors are connected to three PCBs in the fingertip where the signals are digitalized and aggregated by a microcontroller. Each finger is connected to a central processing system in the palm by Flat Flex Cables (FFCs). The embedded system in the palm consists of a FPGA connected to a microcontroller.
- For the purpose of reactive grasping, the *KIT Finger-Vision Soft Hand* described in (Hundhausen et al., 2020) embeds cameras into the fingertips of soft robotic fingers. Each finger is constructed from a PET-plastic strip acting as a leaf spring. 3D-printed bones are mounted on the spring to define the phalanges, the spaces between the bones define the joints. A high resolution camera is mounted at the finger tip and connected to a FFC glued to the leaf spring and hence close to the neutral phase during bending. The whole finger assembly is then cast into silicone to form the

fingers shape. All five cameras from the fingers are connected to an hybrid embedded system with FPGA and microcontroller inside the palm of the hand. The FPGA is used to accelerate individual layers of Convolutional Neural Networks (CNNs) evaluating the captured images in real time as detailed in (Hundhausen et al., 2021).

2.1.5. Discussion

The preceding sections presented related work in sensorized fingers and hands with respect to utilized sensors, their integration into the mechanical structure and connection to readout electronics. These aspects are discussed in detail in the following.

Sensor Modalities

Although a large variety of sensing technologies for robotic tactile perception exist, their integration into anthropomorphic hands and fingers is often limited to a few sensors of a single modality. This is for example the case in the *iCub* hand (Jamali et al., 2015), *UT Hand I* (Peerdeman et al., 2014), *SoftBionic Hand* (Tavakoli et al., 2017) and *PRISMA Hand II* (Liu et al., 2019). While some hands adopt multiple sensing technologies like the *Sandia Hand* (Quigley et al., 2014) or the *SmartHand* (Cipriani et al., 2010, 2011), these hands still lack the ability to sense either shear forces, vibrations or localized contact. Tactile systems embedded into prosthetic hands trying to represent all mechanoreceptive units present in humans are rare, to the best of the author's knowledge, the only approach towards this goal is the one described in (Edin et al., 2008) for the *CyberHand* hand prosthesis. Yet, in the *CyberHand*, the perception akin to SA type II afferents is limited to two 3D shear force sensors at the finger tip while the remainder of the fingers surface area is covered in tactile switches capable only of indicating binary contact.

Especially for prostheses, not only tactile data is of interest, but also data on the state of the hand, the grasp and ideally intention of the user. As (Friedl and Roa, 2021) have shown in a comparative study with different tactile and proprioceptive sensor setups, a combination of IMU, proximity sensor and Hall effect-based sensors performs best in sensor-based grasping tasks. Multimodal sensor data is especially critical in the case of automating grasping and is thereby essential to the second contribution of this work. Sensors that can provide such data are for example IMUs, cameras, distance sensors, joint angle encoders,

motor encoders or temperature sensors. Although some of these sensors are easy to integrate, for example an IMU, few hands make use of these sensors as can be seen in Table 2.1. The table gives an overview of the sensorization, embedded systems and mechanical properties of both commercial and research prostheses.

In summary, a hand design embedding a multi-modal sensor system for haptic and environmental persception into an athropomorphic hand is not demonstrated in related work.

Integration of Sensors

Another important aspect is the integration of an embedded system for processing of sensor information into the hand. This is primarily of interest for prostheses, as the user otherwise has to carry an external device to use intelligent functions of the hand if the controller is not directly embedded. For robotic applications an embedded system directly integrated into the hand is also beneficial to pre-process and aggregate data to not overload the robot bus system. With a few exceptions like (Hundhausen et al., 2020) or (Fajardo et al., 2020), the embedded system in the discussed hands is either completely missing or primarily aimed at motor control. Sensor data acquired by the embedded systems in literature is usually not processed but directly transmitted to an external computer.

Lastly, the anthropomorphic appearance and morphology is a decisive factor for acceptance of prostheses (Cordella et al., 2016; Salminger et al., 2020). None of the presented finger and hand designs considers adaptation or scalability of dimensions or proportions of the prosthesis to the prosthesis user. The majority of the works utilizes a single finger size for all four fingers, so even for one given hand size, the dimensions of the individual fingers are not anthropomorphic. Commercial prostheses are typically available in two to four sizes which allows only limited adaptation to the specific morphology of the prosthesis user.

Contribuitons of the Thesis

The tactile sensor system in this work includes different physical sensors for different tactile stimuli, thereby taking inspiration from the functionality of all four human mechanoreceptive units. The sensors are namely barometer based normal force sensors, Hall effect base shear force sensors, proximity sensor based optical sensors and accelerometers. Multiple sensors with different technologies

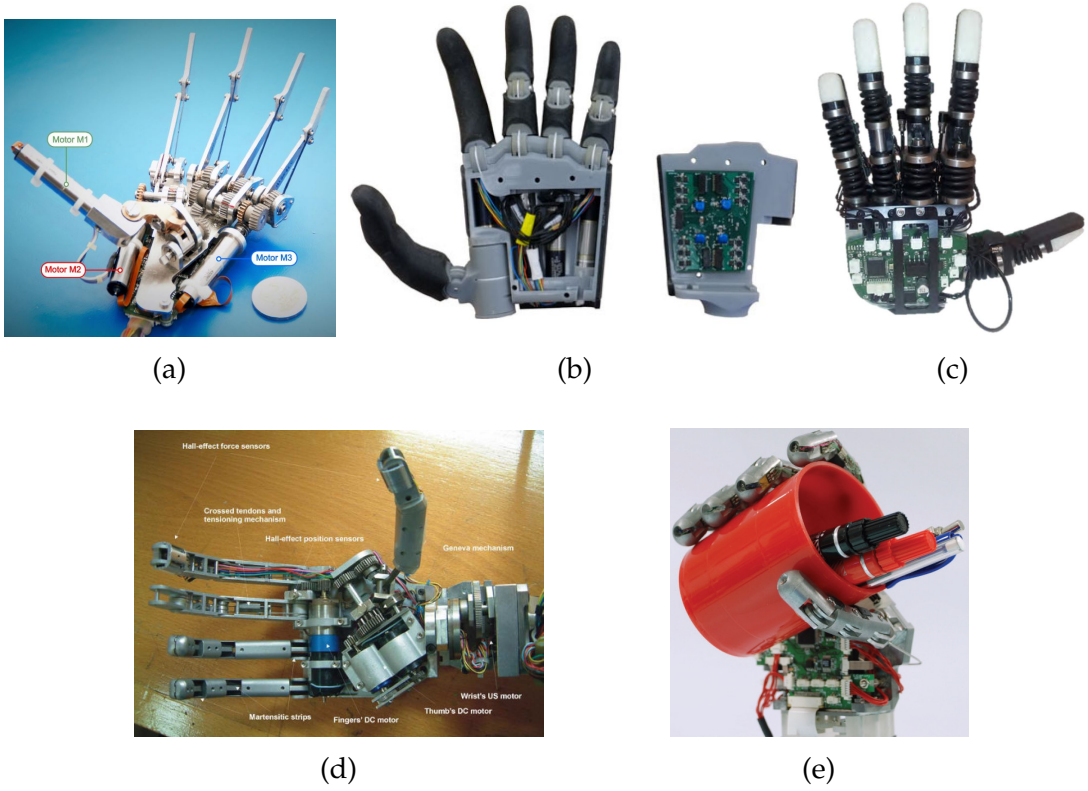

(a) (b) (c)

(d) (e)

Figure 2.8.: a) SSSA-MyHand without cosmetic cover in (Controzzi et al., 2017); b) Vanderbilt Hand 2 in (Bennett et al., 2015) with palm cover removed, showing motors and embedded system; c) Hand of the humanoid ARMAR-IV in (Asfour et al., 2013); d) The MANUS hand prosthesis in (Pons et al., 2004); e) The SmartHand hand prosthesis in (Cipriani et al., 2011); Reprinted from: a) Controzzi et al. , "The SSSA-MyHand: A Dexterous Lightweight Myoelectric Hand Prosthesis", Transactions on Neural Systems & Rehabilitation Engineering V. 25 I. 5, ©2018 IEEE; b) Bennett et al. , "A Multigrasp Hand Prosthesis for Providing Precision and Conformal Grasps", Transactions on Mechatronics V. 20 I. 4, ©2015 IEEE; c) Asfour et al. , "ARMAR-4: A 63 DOF torque controlled humanoid robot", Humanoids 2013, ©2013 IEEE; d) by permission from Springer: Autonomous Robots "The MANUS-HAND Dextrous Robotics Upper Limb Prosthesis: Mechanical and Manipulation Aspects", J.L. Pons, E. Rocon, R. Ceres, D. Reynaerts, B. Saro, S. Levin, W. Van Moorleghem, ©2004; e) Cipriani et al. "The SmartHand transradial prosthesis", Journal of NeuroEngineering and Rehabilitation V. 8, (CC BY 2.0)

Table 2.1.: Overview of commercial and research prostheses. [A]Adaptive underactuation of multiple fingers, S for spring-based mechanism, T for tendon-based mechanism and W for whippletree-based mechanism; [B]Embedded system integrated; [C]● in case of joint angle encoders, ◐ for motor relative encoders; [D]Dimensions in mm, l = length, w = width, h = height; [E]Measured weight in Gramm; [F]Measured force in Newton, PG = Power Grasp, FF = Finger Forces, P = Pinch; [G]Including wrist and socket; [H]Including hand adapter; Reprinted from (Starke, Weiner et al., 2022) with changes (CC BY 4.0)

Prosthesis	Actuation				Sensors					Mechanical Characteristics		
	DoF	DoA	Adap. Un.[A]	Emb. Sys.[B]	Position[C]	Force	Orientation	Vision	Distance	Size[D]	Weight[E]	Force[F]
SensorHand (SensorHand (2020))	2	1	○	●	n.a.	●	○	○	○	178-210 l	460	100 PG
iLimb Pulse (Belter and Dollar (2013))	11	5	○	●	n.a.	○	○	○	○	180-182 l x 75-80 w x 35-45 h	460-465	6.2-11.8 FF
Bebionic (Belter and Dollar (2013))	11	5	○	●	n.a.	○	○	○	○	190-200 l x 84-92 w x 50 h	495-539	12.3-16.1 FF
Michelangelo (Belter and Dollar (2013))	6	2	○	●	n.a.	n.a.	○	○	○	180 l	420	70 P
Vincent Hand (Belter and Dollar (2013))	11	6	○	●	n.a.	n.a.	○	○	○	145-180 l x 65-85 w	386 (XS)	4.8-8.4 FF
Taska Hand (Taska (2020))	10	6	○	●	n.a.	n.a.	○	○	○	179-181 l x 81-88 w	556-671	6.7-22 FF
MANUS-Hand (Pons et al. (2004))	10	3	○	●	●	●	○	○	○	1.2*50th percentile male	1200[G]	60 PG
HIT/DLR Prosthetic Hand (Huang et al. (2006))	13	3	S	●	●	●	○	○	○	n.a.	n.a.	n.a.
CyberHand (Carrozza et al. (2006))	16	6	○	○	●	●	○	○	○	n.a.	360	70 PG
SmartHand (Cipriani et al. (2011)	16	4	S	●	●	●	○	○	○	50th percentile male	520	16-36 PG
Vanderbilt (Wiste et al. (2011))	16	4	S	○	◖	○	○	○	○	n.a.	320	10-34 FF
UT Hand I (Peerdeman et al. (2014))	15	3	W	○	●	●	○	○	○	185 l x 82 x w x 26 h	n.a.	n.a.
Vanderbilt 2 (Bennett et al. (2015))	9	4	S	●	◖	○	○	○	○	200 l x 89 w	546	15-30 FF
SoftHand Pro-D (Piazza et al. (2016))	19	1	T	●	○	○	○	○	○	235 l x 230 w x 40 h	n.a.	20 PG
SSSA-MyHand (Controzzi et al. (2017))	10	3	○	●	●	○	○	○	○	200 l x 84 w x 56 h	478	9.4-14.6 FF
Jeong 2017 (Jeong et al. (2017))	11	6	○	○	○	●	○	○	○	Average Male	380	15.7-48.2 FF
SCCA Hand (Wiste and Goldfarb (2017))	11	5	S	○	◖	○	○	○	○	n.a.	437	146 PG
SoftBionic Hand (Tavakoli et al. (2017))	10	2	T	●	◖	●	○	○	●	200 l x 91 w x 40 h	285	n.a.
Zhang 2018 (Zhang et al. (2018))	11	6	T	●	◖	●	○	○	○	171 l x 80.2 w x 27.4 h	450	8-12 FF
PRISMA Hand II (Liu et al. (2019))	19	3	S	○	◖	●	○	○	○	210 l x 80 w	n.a.	n.a.
Galileo Hand (Fajardo et al. (2020))	15	6	○	●	◖	○	●	○	○	162 l x 69.6 w x 25 h	350	50 PG

are distributed along the surface of the finger. Having different sensors does not only provide different aspects of tactile feedback, but allows to mutually verify sensor signals as the different sensor technologies provide overlapping information. Additionally, a camera, distance sensors and an IMU provide environmental information.

In contrast to related works, this work considers scalability of both mechanical parts and electrical systems of the fingers from the ground up. The developed fingers are modelled to be automatically scalable according to a few numerical parameters like phalanx lengths and joint heights. The multimodal sensor system scales together with the mechanical model, so larger fingers will include more sensors than smaller fingers.

While the sensor information in most research hands is transmitted to a PC or other external device, the thesis introduces embedded systems that allow reading of all sensor modalities and control locally in the hand. This includes computational resources to evaluate camera images and parallel read-out of close to 100 sensor streams from the fingers in real time.

In recent years, soft anthropomorphic hand designs and their sensorization have been studied to increase robustness and safety of grasping while exploiting natural interaction with the objects and passive compliance and/or active regulation of grasping forces, for example (She et al., 2015; Deimel and Brock, 2016; Zhao et al., 2016; Fras and Althoefer, 2018; Wall and Brock, 2019). To understand the potential for prosthetic applications, this thesis introduces a soft variant of the sensorized fingers based on the mechanical design in (Hundhausen et al., 2020). These soft fingers embed the same multimodal sensor system and are also fully scalable.

In conclusion, the sensor system and fingers developed in this work address several shortcomings in the state of the art. The developed sensor system does not only allow to measure diverse tactile stimuli akin to human perception but also captures information about the state of the hand and its user needed for semi-autonomous control. The multiple sensor signals can be directly processed on the embedded system inside of the prosthesis. The finger's mechanics and its electronics are freely scalable to the dimensions of any human finger, which to the authors' knowledge, is the first solution to address this problem in literature. In addition, the thesis presents a novel mechanical implementation of an underactuated mechanism on the basis of the TUAT/Karlsruhe (Fukaya et al., 2000, 2013) mechanism as well as novel fabrication techniques for barometer based pressure sensors.

2.2. Semi-Autonomous Control of Prosthetic Hands

Recent advances in prosthetics and humanoid robotics have led to anthropomorphic hands with improved dexterity and grasping abilities (Belter et al., 2013; Piazza et al., 2019). Therefore, simple yet reliable control strategies are needed to enable user to exploit the hand's dexterous grasping abilities to their full extent (Cordella et al., 2016; Dhillon and Horch, 2005). Such easy-to-use control aims at reducing the amount of attention a prosthesis user has to pay during the execution of a grasp. Traditionally, electrically actuated prostheses are controlled with signals captured by two EMG electrodes attached in the socket on the user's arm. Through contraction of the muscles in the forearm the user can then sequentially control all degrees of freedom of the prosthesis. While prosthetic hands get increasingly versatile, control of these added degrees of freedom is difficult with the limited expressiveness provided by the EMG interface. Hence, long control signal sequences are needed to control prostheses with a multitude of functions. Besides the need for a long training time, the direct control of more than two DoF with only two EMG electrodes results in a high cognitive load for the user while controlling their device (Amsuess et al., 2014). Therefore, a simplification of the prosthetic control strategy for the user is desirable in order to reduce the user's workload while operating their device. The following description of related work has been published in (Starke et al., 2022) without changes (CC BY 4.0).

An active field of research is the classification of *electromyography* (EMG) and *mechanomyography* (MMG) signals from multiple sensors to improve upon the muscle activation control strategies currently applied in commercial prostheses, as for example proposed in (Ortiz-Catalan et al., 2014; Hahne et al., 2014; Wilson and Vaidyanathan, 2017; Piazza et al., 2016; Zhuang et al., 2019; George et al., 2020; Paskett et al., 2021). A comprehensive survey of these techniques can be found in (Ciancio et al., 2016). However, acquiring fine-granular, continuous and robust signals is challenging due to imperfect fitting of the socket and changing skin surface conditions, such as sweat and temperature (Chadwell et al., 2016). Therefore, the emerging field of semi-autonomous control concentrates on reducing the amount of commands sent by the user to execute an action by incorporating environmental information extracted from additional sensor modalities and predicting the user's intention. These are especially interesting where the user's stump condition does not permit to capture feature-rich EMG signals. For this specific user group, a prosthetic control should require as little

direct EMG commands as possible to mitigate the proneness to errors caused by wrong or missing muscular signal detection.

2.2.1. Semi-Autonomous Control Schemes

The idea of partially automating prosthetic control has a long history. For an early version of the Southampton Hand, (Swain and Nightingale, 1980) utilize predefined grasps adapted based on information from a gyroscope, force sensors and slip detection supporting the user during grasping.

To assess the performance of different levels of autonomy in prosthetic control regarding grasp success, subjective complexity and satisfaction, (Cipriani et al., 2008) applied several control schemes to the *CyberHand* hand prosthesis. The evaluation shows that less complex control schemes perform notably better in terms of perceived satisfaction, required attention and difficulty. The authors also noted that a full, individual control over all functionalities offered by the prosthesis was seldom used by the subjects. The study thereby supports the general merit of semi-autonomous control techniques.

Vision-Based Systems

the semi-autonomous control scheme described in (Došen et al., 2010) is based on a cognitive vision system for prosthetic grasping. With a camera and a distance sensor mounted externally on the dorsal side of a prosthetic hand looking over the fingers, the object is detected and its distance can be measured. Here, the user directly controls the wrist rotation, while grasp type and hand aperture are determined based on visual and distance information and a set of if-then rules of a decision making system. While offering nine different grasp types and apertures, the system achieved an accuracy of 84 %. Grasping failures were attributed to errors of the visual object detection. The work was extended in (Došen and Popović, 2011) to include the wrist rotation into the semi-autonomous control scheme, leaving the user only responsible for triggering the grasping action.

Another approach using electrooculography and four sensors placed around the eye to determine grasp affordances was presented in (Hao et al., 2013). The user has to scan the object's borders with the eyes and trigger the closing movement by EMG signals as soon as the desired preshape is obtained. While grasping in a defined setup shows an object recognition rate of 86.2 %, the robustness regarding different object-eye distances remains to be assessed.

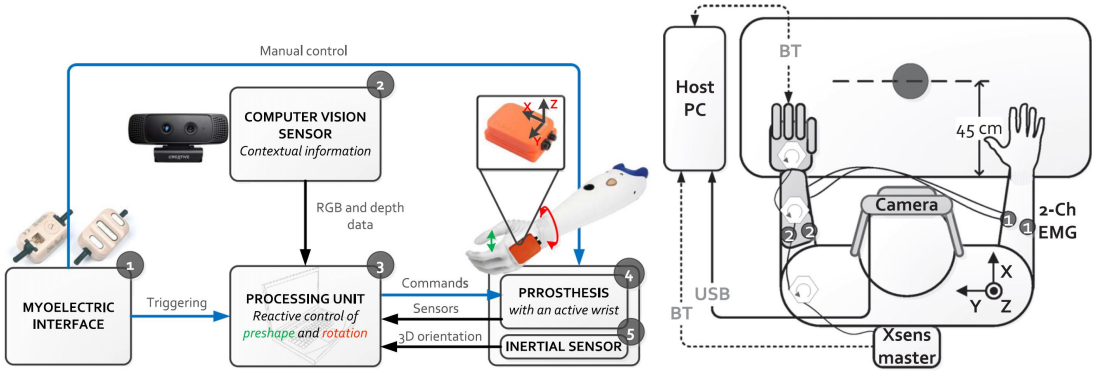

Figure 2.9.: a) The system architecture employed in (Markovic et al., 2015) for their semi-autonomous control scheme; b) The experimental setup for the user trails; Reprinted from: Marko Markovic et al. , "Sensor fusion and computer vision for context-aware control of a multi degree-of-freedom prosthesis", 04.11.2015, Journal of Neural Engineering, V. 12, I. 06, 10.1088/1741-2560/12/6/066022; ©IOP Publishing. Reproduced with permission. All rights reserved.

In (Markovic et al., 2014) the authors present a semi-autonomous control architecture that is based on augmented reality glasses. In contrast to the approaches described above, the user stays in control of the fine-tuning of the grasp. While a first preshape is adopted based on the visual information of the stereo camera system integrated in the glasses, the user is still able to adjust the grasp aperture by a proportional myoelectric controller according to the transmitted feedback. In their following work, (Markovic et al., 2015) use an IMU on the dorsal side of the palm and combine it with a stereo camera system mounted in the room as well as position and force sensors embedded into the prosthetic hand. Based on this multi-modal sensor information, the wrist rotation and grasp preshape of a prosthesis are controlled autonomously. The architectural overview and the setup for user trials are depicted in Figure 2.9.

The semi-autonomous control was compared to three manual control schemes with increasing difficulty. Compared to a manual control of grasp type, wrist orientation and finger closing, the grasp execution was faster with the semi-autonomous control.

Proximity and Tactile Based Systems

The grasp type selection scheme desribed in (Tavakoli et al., 2017) is based on capacitive proximity and tactile sensors embedded into the fingers and palm

of a custom-build prosthetic hand. If the object to be grasped is conductive and is sensed by all sensors a power grasp is chosen, while a precision grasp is chosen if only the thumb and index finger detect the object. If the object is non-conductive, a power, precision or intermediate grasp is chosen if the object first contacts the palm, index finger or both index finger and thumb respectively. The proposed grasp type selection scheme remains to be evaluated in a user trial.

A semi-autonomous control scheme with a multi-electrode user interface is shown on the TASKA hand (Hansen et al., 2021). Using combined force and proximity sensing at the fingertips, the finger closing motion and the grasp force applied to the object are controlled autonomously. The fingers close as soon as an object is detected by the proximity sensor until contact with the object is detected, at which point the motors are switched to a position hold mode. The user controls the grasping motion similar to a pure multi-electrode manual control and the autonomous control system is activated based on a threshold set on the decoded muscle signals. This shared semi-autonomous control is shown to increase the grasp precision and decrease the workload for the user in tasks where fragile objects are to be grasped and placed.

A number of recently published object recognition systems make use of neural networks and propose grasps based on the recognized known objects (Degol et al., 2016; Ghazaei et al., 2017; Hundhausen et al., 2019).

2.2.2. Discussion

Semi-autonomous control schemes make use of environmental and haptic data to automate parts of the grasping process normally controlled manually by the user. *Vison based* semi-autonomous control schemes like the ones introduced in (Cipriani et al., 2008; Došen and Popović, 2011; Markovic et al., 2015) and (Gonzalez-Vargas et al., 2015) show clear benefits of semi-autonomous control in terms of reducing the cognitive load of prosthesis users. To achieve these results, the presented semi-autonomous control algorithms rely on sensory information not directly provided by the prosthesis. Instead they require external sensors, attached to the human body or installed in the environment. Sensor modalities used in prosthetic control range from IMU data (Markovic et al., 2015) over stereo vision (Markovic et al., 2015; Cipriani et al., 2008) to distance sensors (Došen et al., 2010; Hansen et al., 2021). Processing of and control based on sensor data is performed by an external device or computer. Hence, while clearly showing

the potential advantages of semi-autonomous control schemes for the user, the presented control schemes are stationary, or at least need additional devices attached to the user. In contrast, the control scheme presented in thesis uses the sensor system and embedded system integrated into the prosthesis to extract relevant object information, select an appropriate grasp and recognize the user's intention. No additional sensors attached to the human body or mounted in the environment or additional external processing systems are needed. Feedback to the user regarding automatically suggested grasps is provided via a color display which is also embedded into the prosthesis at the dorsal side.

In the presented semi-autonomous control schemes, the distinct degrees of freedom of the prosthetic hand are generally actuated in succession starting with wrist and thumb positioning followed by the final hand closure. This leads to a slower grasp execution compared to simultaneous actuation of all degrees of freedom of the prosthesis. The semi-autonomous control in the thesis hence controls all three DoFs, namely the thumb, fingers and wrist simultaneously and in a reactive manner.

Proximity and tactile based semi-autonomous control schemes provide assistance through detection of the object through proximity. In case of (Tavakoli et al., 2017), while a power grasp or pinch grasp can be automatically chosen for conductive objects, the grasp type for non-conductive objects has to be chosen by the user through the first area of contact with the hand. Yet, choosing a grasp type by bringing a specific part of the hand in contact with the object first provides a novel control interface for augmenting EMG. In (Hansen et al., 2021), while providing autonomous closing behavior for the fingers, the authors describe no mechanism to automatically choose the grasp type based on sensor data. While both methods are not as powerful in choosing the grasp type automatically as vision-based systems, they provide more fine-grained control and assistance as for the actual grasping motion. The thesis expands on these proximity and tactile based schemes by implementing autonomous behaviors for the complete grasping process starting with closing the fingers around to the object to placing the object back down.

2.3. Autonomous Grasp-Phases Control

Humans posses dexterous grasping and manipulation capabilities unparalleled in technical systems. These capabilities emerge as a result of over a decade of

continuous learning during childhood (Forssberg et al., 1991, 1992). Neuroscientific studies show that human grasping is divided into individual phases, namely *reach, load, lift, hold, replace* and *unload* (Johansson and Flanagan, 2009a). Each phase has with its own control subgoal and a distinct sensory event that triggers the next phase. For example, the subgoal for the reach phase is to close the fingers while establishing contact between fingers and object is the sensory event that triggers the next phase: load. As the approach in the thesis is based on the human grasping strategy, we will discuss related work based on the division into phases.

In Robotics, robust grasping of unknown objects with varying shape, weight, stiffness, fragility, material properties and changing center of mass remains a challenging problem (Billard and Kragic, 2019), yet fundamental to truly endow both humanoid robots and prosthetic hands with the abilities they need to perform dexterous grasping and manipulation tasks. Solving this problem requires the development of intelligent controllers able to interpret multimodal sensory data and to adapt to different objects and tasks. A key requirement on such controllers is the ability to continuously estimate and update grasping forces applied on an object during the execution of grasping and manipulation tasks to ensure safety and stability of the grasp. Yet, a grasping task needs not only a controller for grasp force control but also strategies to close the hand around an object, place objects back on a support surface and release the grasped object. While a majority of works in this area focus on stably holding an object (phases load, lift and hold), there exists works that employ a more holistic approach to grasping, spanning most of the phases observed in human grasping.

To implement force adaptation strategies, tactile feedback at the contact points between hand and object is crucial to describe their interactions in the different phases of a grasp, i.e. to detect initial contact, and adapt the applied forces to establish a stable grasp, to lift, hold and replace the object. An overview on the use of tactile information in grasping and manipulation tasks is presented in (Li et al., 2020). In the following, we first introduce controllers aimed at stabilizing a grasp in Subsection 2.3.1 and then focus on more holistic works in Subsection 2.3.2, taking into account multiple phases with different behaviors for the different phases in grasping observed in human grasping.

The following parts up to the discussion are reprinted from (Weiner et al., 2021), "Detecting grasp phases and adaption of object-hand interaction forces of a soft humanoid hand based on tactile feedback", IROS 2021, ©2021 IEEE;

2.3.1. Controllers for Loading, Lifting and Hold

Numerous control strategies for grasping and holding of unknown objects introduced in the literature share the common goal of estimating and controlling the friction condition at the contact points between hand and object. This is either achieved through measurement of shear and normal forces, slip detection and prevention, or a combination of both. If both is not possible, some works try to estimate the applicable normal force through the object's stiffness. The estimation of the required normal force based on these methods can then be used as input for a normal force controller or other control law to securely hold the object, even in the case of external disturbances.

Friction Coefficient Estimation

(Wettels et al., 2009) explicitly formulate the control target in terms of the friction coefficient based on normal and shear forces estimated from raw sensor data using machine learning. If the friction coefficient is out of the acceptable range, the hand opens/closes by a fixed amount. A similar formulation has been used in (Zhang et al., 2015) on the basis of 3D force sensors. (De Maria et al., 2015) use a optoelectronic sensor array and machine learning for determining normal and shear forces for friction coefficient based control. Additionally, objects are explored to estimate the friction coefficient and the noise in the shear force signal is used for slip detection. The normal force acting on the object is adapted by opening/closing the gripper by a fixed amount. (Su et al., 2015) expand on this work by implementing an online estimation of the friction coefficient. A similar approach for the online estimation of the friction coefficient at each contact point for the manipulation of heavy deformable objects based on *OptoForce* sensor data is described in (Kaboli et al., 2016). Again a fixed position increment for opening/closing is used to control the normal force. Grasp force adaption based on normal, shear and torques measured at the contact points is shown in (Ajoudani et al., 2016). Linear and rotational slip is in this work detected if a fixed friction coefficient is lower than the measured friction coefficient. The slip information is then used to either control the motor current or the stiffness of the hands.

Slip Detection

A different approach for normal force control is to explicitly deal with the problem of slip detection. (Takahashi et al., 2008) employ a hybrid position/force controller for grasping in which the controller target values are adapted based on slip signals. The controller operates in position control mode for the approach, in force constraint position control for contacting the object and in force control for holding the object. Slip is detected by observing the change in the center of pressure at the contact point between hand and object. The normal force target for the controller is increased as slip is detected and decreased as long as slip is absent. A similar system is described in (Al-Mohammed et al., 2018) that increases the applied force at the contact points once slip is detected. In addition, the grasping motion of the robot is stopped until the grasping force is adapted.

A human-inspired grasp stabilization controller based on tactile feedback is presented in (Veiga et al., 2020), where each finger is independently controlled based on slip prediction and a leaky integrator-based velocity controller. The leaky integrator for the velocity command is implemented a weighted sum with weights smaller one, of the last velocity command and a value that is positive if slip is predicted and zero otherwise. The independent control of individual fingers has been shown to ensure stability of a grasp in complex in-hand-manipulation tasks while avoiding complex coordination between fingers. (Nakagawa-Silva et al., 2019) develop a biology-inspired neuromorphic controller where slip events are encoded by spikes and used as input for a monotonic PI position controller. For slip detection the current sensor signal is compared to the last signal and if a threshold is exceeded, a spike is generated. The number of spikes is then used as the input of a PI controller for controlling the position. The controller is monotonic, meaning that the fingers can only close, not open.

Object Stiffness Estimation

A third class of approaches estimates the stiffness of the grasped object to guess the amount of applied normal force. (Romano et al., 2011) estimate the stiffness based on the distance change between the gripper yaws during initial contact. A similar approach is used in (Deng et al., 2017) and (Ji et al., 2019) where it is combined with slip detection to adjust the normal force during grasping. (Deng et al., 2020) utilize an online method for simultaneous detection of contact events and object material based on tactile data.

2.3.2. Controllers for the Complete Grasping Process

Few works approach the problem of developing grasping controllers that adapt grasping forces during all different phases of a grasp and manipulation task, beginning with closing the fingers around an object, lifting, manipulating, placing and releasing the object.

(Yamaguchi and Atkeson, 2017) implement four different behaviors for gentle closing, holding, handover and in-hand manipulation. The authors utilize feedback from a vision-based tactile sensor measuring normal and shear forces, and detecting slip. The behaviors are evaluated individually, chaining of the behaviors into a complete grasping and manipulation task is not evaluated. Based on the neuroscientific findings on the human grasping strategy in (Johansson and Flanagan, 2009a), the authors implement a grasp strategy divided into individual controllers for the phases *close, load, lift and hold, replace, unload* and *open*. The events are derived from pressure sensor arrays attached to the fingertips of a two finger gripper and a hand-mounted accelerometer. The grasp strategy was evaluated against the baseline approach of always closing the gripper with full force. While the baseline destroyed or damaged 30 objects used in the evaluation, the proposed grasp strategy only crushed one object while not significantly increasing the amount of dropped objects. The work demonstrates how tactile feedback can be used to control complete grasping and manipulation tasks on a robot autonomously.

Together with a prosthetic hand with embedded shear force sensors, (Zhang and Jiang, 2018; Zhang et al., 2018) propose a human-inspired grasp phases control scheme for the phases *load, hold* and *unload*. The prosthesis user first selects individual fingers of the hand and brings them into contact with the object using EMG signals from six electrodes. The fingers then apply force to the object based on friction coefficient estimation and slip detection. The unload phase is triggered by a decrease in the ratio between shear and normal forces, while opening of the hand is triggered manually by the user using EMG signals. The mathematical formulation and implementation of the controllers is not disclosed. The control scheme is demonstrated in trials with five able-bodied subjects and an amputee grasping four different objects, showing an average increase of grasp success.

2.3.3. Discussion

Most related work in sensor-based grasping primarily focuses on stable lifting and holding unknown objects. Through the research in theses works three main strategies for force control have been established and strengths and limitations of the respective approaches are evident. These are discussed in the first part of this section. The second part discusses limitations in works considered with providing controllers for most or all phases observed in human grasping.

Force Control for the Phases Load, Lift and Hold

Control of grasping force to stabilize a grasped object is well-researched. These controllers operate in the phases the phases *load*, *lift* and *hold* . For the force control necessary in these phases, three main strategies are considered.

Methods based on *Object Stiffness Estimation* estimate the required grasping force based on the stiffness of the grasped object. This method is simple, as only the length of travel of the fingers or gripper yaws between the moment of contact to reaching a set force threshold needs to be considered. Hence only normal force sensors are required, simplifying the required sensor setup. Yet, the estimate of required normal force based on object stiffness is just a heuristic, failing especially for stiff yet fragile objects like raw eggs.

Slip Detection based methods try to detect vibration events at the interface between the hand or gripper and the object. If such an event is detected usually a simple reflex is triggered to tighten the grasp. Detection of slip requires either dedicated sensors like floating accelerometers at the contacting surfaces or analysis of the high frequency components of other tactile sensor modalities like normal force. Often the sensor signals are subjected to a Fourier or wavelet transform to isolate signal patterns characteristic for slip events, increasing the computational complexity. While individual works consider the problem of slip prediction, the majority of slip-based grasp controllers act reactively, slip is not prevented. If multiple slip events occur, the object can slip far enough inside the grasp to change its pose or completely fall out of the hand.

Friction Coefficient Estimation based methods estimate the friction acting between the gripper or hand by monitoring the ratio between normal and shear forces measured at the points of contact. If the friction is low, the normal force can be increased or safely decreased if the friction is very high. This has the advantage that the estimate for the required normal force is independent of object stiffness and the estimate can be dynamically adapted. For this method to work reliably,

the contact surfaces must be equipped with shear force sensors, increasing the complexity of required sensorization. Since the friction is different for each object, either a static friction value can be used as reference that is considered to be safe or the friction is estimated during initial contact and lifting of the object. Friction coefficient estimation tends to fail for objects that are crumbly like bread or dusty. The minimum required friction can for example be estimated using Slip Detection.

Due to the various advantages of force control based on *friction coefficient estimation* regarding stability, the controller for the phases load, lift hold and replace in the thesis utilizes a friction coefficient based controller with a fixed value for the minimal desirable friction.

Limitations in Kinematics, Sensorization and Control of Holistic Approaches

Works presenting a more holistic approach to grasping and manipulation akin to human grasping, i. e. including closing of the fingers, replacing objects and opening the fingers, are rare. These works, namely (Romano et al., 2011; Yamaguchi and Atkeson, 2017; Zhang and Jiang, 2018), show great success in handling arbitrary objects in a reliable manner, showing the potential of a more human-like approach. Yet, several limitations can be identified that are addressed in the thesis.

All works that consider the *Complete Grasping Process* make use of either a parallel gripper (Romano et al., 2011; Yamaguchi et al., 2018) or manually pre-determine the fingers that are involed in the grasp (Zhang and Jiang, 2018). The automatic selection and coordination of all fingers is not considered in (Zhang and Jiang, 2018) and not applicable in case of parallel grippers. In the case of (Zhang and Jiang, 2018) this means that the prosthesis user has to manually bring the selected fingers into contact with the object before autonomous force control is started.

The yaws of parallel grippers are relatively easy to sensorize with a flat sensor matrix, so that objects only contact the gripper at sensorized surfaces. A humanoid hand exhibits a far more complex geometry. The object might contact surfaces on the fingers and the hand that are not equipped with sensors, increasing the uncertainty of the available sensor data. Individual fingers might contact the object at an angle, right at a sharp feature or might miss the object entirely. Almost all works restrict contact points between object and hand or

gripper to surfaces that are sensorized, like (Wettels et al., 2009; De Maria et al., 2015; Su et al., 2015; Kaboli et al., 2016; Ajoudani et al., 2016; Takahashi et al., 2008; Al-Mohammed et al., 2018; Veiga et al., 2020; Nakagawa-Silva et al., 2019; Romano et al., 2011; Yamaguchi and Atkeson, 2017). The authors in (Zhang and Jiang, 2018) also concentrate on pinch and tripod grasps that contact the object only on the sensorized fingertips.

Grasping starts with bringing the hand into close proximity of the object and then closing the fingers to make initial contact. (Yamaguchi and Atkeson, 2017) describe an controller for gentle closing of the hand, stopping the gripper yaws as soon as fixed threshold of normal force is reached. The same strategy is employed in (Romano et al., 2011) and in (Zhang and Jiang, 2018). The use of proximity sensors for controlling the finger speed during closing to not impact the object with high velocity is not considered.

In contrast to related wroks, the grasp-phases controller developed in the thesis implements all phases observed in human grasping in a fully autonomous manner. All fingers attempt to grasp and are automatically disabled if they miss the object and opening the fingers is automatically coordinated. The approach of the fingers is monitored using proximity sensing to enable fast closing of the fingers and slowing them down as they approach the object. Grasping in this thesis is not restricted to contacting the object with sensorized parts of the hand. To deal with the uncertainty, the controller in this thesis makes use of multimodal sensor data to verify individual measurements with measurements from a different modality.

3. Anthropomorphic Hands with a Multimodal Sensor System

Perception of a hand's close environment as well as interactions with the environment are crucial to dexterous grasping and manipulation. The human hand employs a multimodal sensing system with hundreds of sensors per square centimeter for tactile sensing alone, in addition to proprioception and visual cues. To apply human-inspired grasping strategies, a technical realization of these sensor modalities must be integrated into the mechanical structure of an anthropomorphic hand.

This chapter hence details the efforts made in this thesis to integrate a multimodal sensor system into anthropomorphic hands and especially fingers, as these are the main tool to interact with objects. Three different contributions are made. First, the development of a male and female hand prosthesis that embeds a sensor system and an embedded system directly in the palm (Section 3.1). As the integration of sensors into the fingers while enabling free scalability of these fingers is especially challenging, these developments are presented in detail in Section 3.2. Section 3.3 then introduces a soft finger variant of the rigid fingers described in the sections above. Lastly, the design of two embedded system variants for sensor readout and on-board control is presented in Section 3.4.

3.1. The KIT Prosthetic Hands

The following section has been published in (Weiner, Starke, Rader et al., 2022) and is inclueded here with changes (CC BY 4.0). The contribution of the theses is the sensorization of the palm, the implementation of the embedded system and a novel design for the underactuated mechanism. Hand prostheses allow amputees to regain autonomy and abilities in their daily life. Recent advances in prosthetic hand development have led to sophisticated multiarticulate devices. However, the rejection rate of myoelectric prostheses is very high with 44 %

(Salminger et al., 2020). One reason for this problem arises from limitations in terms of intuitiveness-of-use and a high level of user control effort needed to execute grasping tasks. These limitations can be relaxed by the integration of intelligent hardware and software. In terms of hardware, underactuated mechanisms have proven to be a very promising way to design robot hands with a small number of active Degree of Freedoms (DoFs) as shown for example by Fukaya et al. (2000), Belter and Dollar (2013) and Catalano et al. (2014) among others. Such hands are able to adapt to the shape of objects to reliably execute grasps while exploiting the physical interaction with the object. In addition, intelligent control strategies significantly reduce the cognitive burden on the user by taking information about the environment and user intention into account to autonomously select suitable grasps while keeping the user in the loop. The advantages of such approach has been demonstrated by several recent developments e. g. by Došen et al. (2010), Markovic et al. (2015) and Ghazaei et al. (2017) among others. However, semi-autonomous control requires profound knowledge about the environmental situation and the user intention, which must be acquired by an appropriate sensor system and sufficient computing resources to extract such knowledge from sensor data.

The remainder of this section presents recent work on the development of highly integrated prosthetic hands that are equipped with on-board sensors and computing power to support the realization of semi-autonomous grasping. Contributions to the prosthetic hands made in this thesis are the design of a novel adaptive underactuated mechanism based on the TUAT/Karlsruhe mechanism (Fukaya et al., 2000) for the female hand, the integration of sensors into the palm and design of the embedded system. Furthermore, this thesis contributed to the mechanical design, especially to the arrangement of the individual components. Although this thesis also contributed to the older male version of the hand (Weiner et al., 2018b), the focus in this section lies on the newer female hand, which will be compared to the older male hand in relevant aspects. The hands, as depicted in Figure 3.1, are driven by two DC motors, one motor for the thumb and one for the fingers, with a total of 10 DoF. Specifically, the most recent version of the prosthetic hand, the female version is presented and compared to the previous male version. The female hand which is based on the male hand regarding the design of prosthetic hands by Weiner et al. (2018b) and in-hand visual data processing for object detection by Hundhausen et al. (2019). The female prosthesis extends previous work on the male hand in terms of sensing and visual perception capabilities, underactuated mechanism and shows the scalability of the design to different hand sizes.

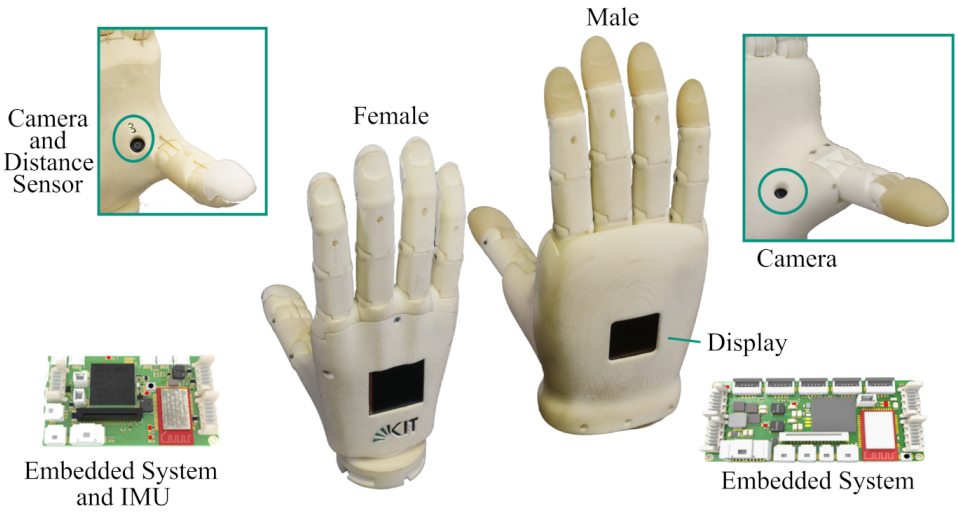

Figure 3.1.: The KIT Prosthetic Hands; female (left) and male (right) intelligent hand prostheses designed for semi-autonomous grasp control. Each hand has two Direct Current (DC) motors actuating 10 DoF via an underactuated mechanism. Each hand is equipped with a camera in the palm, Inertial Measurement Unit (IMU) and a distance sensors (female version) as well as an integrated embedded system for in-hand sensor data processing and control. Reprinted from (Weiner, Starke, Rader et al., 2022) with changes (CC BY 4.0).

The section is organized as follows: In Subsection 3.1.1 the key requirements governing the development of our hand prostheses are explained. The mechanical design as well as the sensors and embedded system are detailed in Subsection 3.1.2. Subsection 3.1.3 describes experimental results regarding main characteristics and real-world grasping studies. The section concludes with a summary and discussion of the presented hand (Subsection 3.1.4).

3.1.1. Key Requirements

To provide support for the user performing diverse Activity of Daily Livings (ADLs), as for example food preparation, housekeeping or tool use among others, a prosthesis has to be reliable and versatile in terms of its grasping capabilities, i. e. it should be able to successfully perform a wide variety of ADLs (Matheus and Dollar, 2010). The user expects their prosthesis to be effortless and intuitive despite the inherent complexity of the mechatronics and control (Cordella et al., 2016). The pivotal point of our hand development is therefore to endow prosthetic hands with intelligent grasping capabilities to support

intuitiveness-of-use and to reduce the cognitive burden of the user. In this work, we strive for intelligent hand mechatronics, that provide the sensor information and capabilities to render intuitive, partially autonomous grasp control possible. In the following, we discuss the key requirements that should be taken into account in the context of the development of such prosthetic hands. These concern the simplicity of mechanical design, the ability to perceive and interpret the current scene, the computing system needed for sensor data processing and control as well as requirements regarding size, weight and appearance of the hand. Underactuated mechanical designs have shown how grasping behavior can be achieved by intelligent hand and finger mechanisms that are able to autonomously self-adapt the hand morphology to the object shape, see (Pfeifer and Gómez, 2009) and (Carrozza et al., 2006). This allows the realization of basic grasping by exploiting the interaction of the hand with the object while using simple and often none precise control.

While such self-adaption of the hand reduces the control complexity for closing the hand, it does not simplify other parts of a grasping action for the user. This includes the selection of a grasp type, hand preshape and hand orientation, which depend on the object to be grasped and on task-specific constraints. Thus, an intuitive-to-use prosthetic hand should be able to autonomously determine suitable grasps, hand preshapes and orientations based on the available object information and the user intention. To keep the human in the loop, the execution of the different parts of a grasping action should always be supervised by the user leading to semi-autonomous grasping behavior. Different semi-autonomous control schemes have been proposed in literature and have proven to reduce the cognitive burden for the user (Došen et al., 2010; Markovic et al., 2015; Ghazaei et al., 2017).

To achieve such semi-autonomous grasping behavior, a multi-modal sensor system is needed to perceive the scene, extract important object information as well as to capture user's state and intention. Visual perception plays a key role for scene understanding, in particular for object detection that is needed to generate suitable grasps. Thus, vision systems have been a central part of semi-autonomous grasping setups, with cameras attached to the human body or the environment to provide the necessary information. In our work, we integrate a camera, an IMU and a distance sensor in the prosthesis to provide a fully integrated system enabling semi-autonomous grasping. In addition, according to Cordella et al. (2016), providing feedback to the user about the state of their prosthetic hand is important and should be considered. For processing and interpretation of multi-modal sensory data, appropriate computing resources

are needed that should be integrated in the hand while taking into account space limitations and energy consumption. In addition, resource-aware image processing and machine learning methods are needed.

Finally, the hand needs to comply with the general design requirements for prosthetic hands in terms of size, weight, grasp force, speed and appearance (Cordella et al., 2016; Pylatiuk et al., 2007; Wijk and Carlsson, 2015; Schweitzer et al., 2018). Thus, the design of the prosthetic hand should take into account the scalability in size to fit a large portion of the population. To show the feasibility of integrating the functions described above within the severe space limitations of prostheses, we design a hand with the size of a 50^{th} percentile female hand according to the German standard specification (DIN 33402-2). According to the literature, the weight of the prosthetic hand should not exceed 400 g to match the weight of a human hand (Kaye and Konz, 1986). Further, the grasping force and closing speed of the hand should be comparable to commercial hands, as reported in (Belter and Dollar, 2013).

3.1.2. Design and Mechatronics

The female KIT Prosthetic Hand is an underactuated myoelectric prosthetic hand driven by two DC motors and controlled via muscle signals extracted by two Electromyography (EMG) electrodes. In this subsection, we present the mechanical and electrical design of the female prosthesis offering mechanical grasp support via underactuation and providing a platform for intelligent and context-aware control algorithms. The advances in design are shown in comparison to the male prosthesis described in (Weiner et al., 2018b).

Actuation and Adaptive Mechanism

The design of the prosthesis incorporates two DC motors (2224U012SR, Faulhaber) that are equipped with relative encoders (IEH2-512, Faulhaber) and a planetary gear (Series 20/1R, Faulhaber) with 23:1 transmission. The first motor drives the thumb flexion. All four fingers are actuated together by the second motor via an underactuated mechanism. Both versions of the mechanism in the male and female hand are depicted in Figure 3.2.

For the male hand, we presented the mechanism in Figure 3.2 consisting of a rocker that is centrally pulled by a tendon on pulley ③ connected to the motor at ④. The tendons ⑥ and ⑦ connecting two fingers each are fixed on either

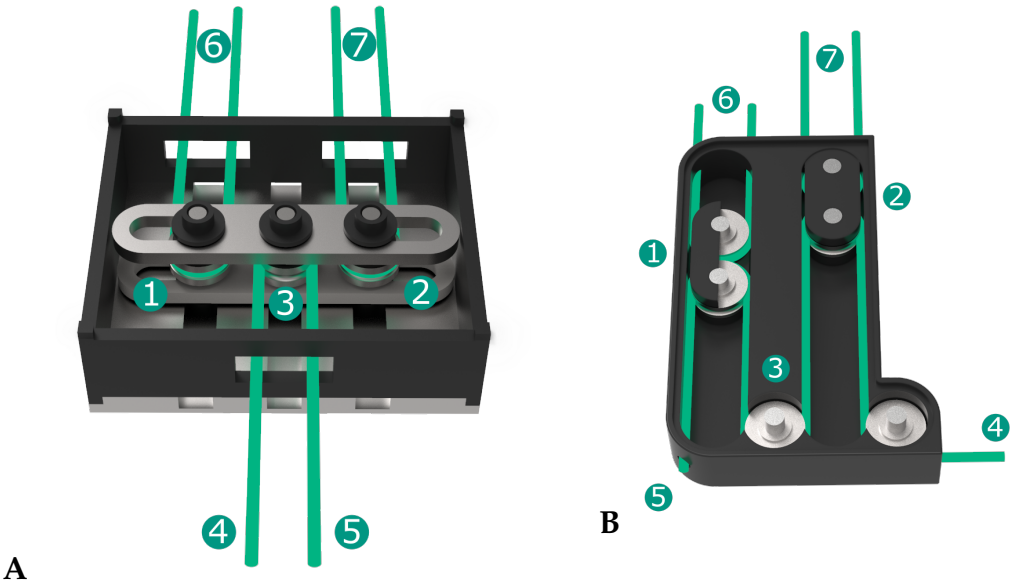

Figure 3.2.: Underactuated force distributing mechanism for the fingers; the mechanism in the male hand connects two fingers by a single tendon and the pairs of fingers by a lever (A); the mechanism in the female hand actuates pairs of fingers by free floating sliders interconnected by the motor tendon B). Reprinted from (Weiner, Starke, Rader et al., 2022) without changes (CC BY 4.0).

side of the lever bar and rotate around the floating pulleys ① and ②. As long as all of the fingers can close freely, all finger tendons are pulled equally causing finger flexion. If one finger is blocked by an object, the tendon turns around its pulley, thereby further closing the second finger connected to the same tendon. If both fingers connected to a tendon cannot close any further, the lever of the mechanism rotates and allows the other two fingers to continue closing. This mechanism design provides the prosthesis with the ability to wrap around arbitrarily shaped objects without the need of complex control input.

In the female hand, the mechanism is further improved regarding the required input force, sizing and friction. The lever is replaced by two separate sliders ① and ② consisting of two connected pulleys. The sliders are free floating and move along their individual guides. The tendon coming from the motor at ④ is led around one pulley of slider ②, a fixed guiding pulley ③ and to slider ①, before it is fixed at the housing at ⑤. The tendons ⑥ and ⑦ connecting two fingers each are led around the second pulley of one slider each. By pulling the motor tendon, the force is still equally distributed to all four fingers by similarly actuating both sliders. The distribution between two fingers remains

the same as in the first hand version while the lever is replaced by the two sliders distributing force between the individual pairs of fingers.

Apart from the reduced dimensions of the mechanism, the additional redirection of the tendon between both sliders results in a force transmission ratio of 2:1, thereby doubling the finger force compared to the tendon force on the motor pulley. Together with a decrease of the diameter of the motor pulley from 16 mm to 8 mm, which corresponds to an additional transmission ratio of 2:1, this allows the reduction of the transmission gear of the motor by factor four from 86:1 in the male hand to 23:1 in the female hand. Therefore, the gear needs one reduction stage less, hence making the gear shorter and lighter while also increasing transmission efficiency.

As the sliders are held in constant tension between motor and finger tendon, they are free-floating and thereby cause no friction against the mechanism walls. All pulleys are supported by ball bearings. This further reduces the friction within the mechanism, thereby increasing the resulting finger force. The design with individual sliders makes the mechanism suitable to be used with other finger designs. This has been shown in the development of the KIT Finger-Vision Soft Hand described by Hundhausen et al. (2020), in which three fingers are driven with an adapted version of this mechanism.

Mechanical Design

The mechanism and motors are placed within the palm of the hand together with the sensors and the embedded system, as shown in Figure 3.3. The male and female prostheses have the size of a 50$^{\text{th}}$ percentile male and female hand, respectively, according to the German standard specification (DIN 33402-2). Individual finger segment lengths are based on the human hand length study by Vergara et al. (2016). The dimensions of both prosthetic hands are listed in Table 3.1.

Despite a reduction of the integration space by 30.9 % compared to the male hand, all hardware components including the two motors, the underactuated mechanism, sensors and the embedded system are integrated into the palm of the female prosthesis. The fingers are designed based on a Computer Aided Design (CAD) model, which allows scaling of the hand according to the size of the user's able hand. To support a lightweight design, the housing, finger phalanges and mechanism sliders are 3D-printed using selective laser sintering from polyamide, a robust, yet flexible plastic.

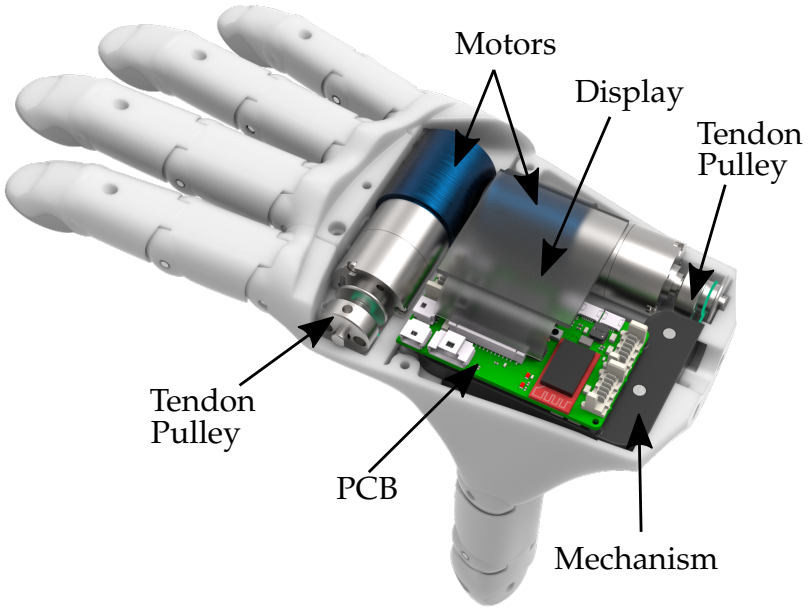

Figure 3.3.: The female prosthesis with motors, mechanism and Printed Circuit Board (PCB) integrated into the palm. Camera and distance sensor are mounted below the mechanism. The mechanism in black is mounted below the PCB. The display is fixed on top of the PCB in the dorsal housing. The display is rendered semi-transparent to make the components underneath visible. Reprinted from (Weiner, Starke, Rader et al., 2022) without changes (CC BY 4.0).

The fingers are actuated by 0.4 mm Dyneema tendons. Each finger comprises actuated flexion in the metacarpophalangeal (MCP) joint and the Proximal Interphalangeal (PIP) joint. The PIP joint is fixed at an angle of 20°. The resulting 10 joints are equipped with ball bearings and the tendon is routed through Teflon tubes (PTFE) to minimize friction. Torsion springs are included in the finger joints and support the passive extension of the fingers. A higher pretension of the springs in the PIP joints leads to a higher closing speed of the MCP joints compared to the PIP joints. This results in a human-like spiral fingertip closing trajectory, as shown by Kamper et al. (2003). The fingers are attached to the hand by a mechanical interface, allowing the fingers to be exchanged for different versions.

The fingertips are equipped with high friction finger pads to enhance the friction with the grasped object and thereby lower the required force to perform a stable grasp. The pads cover the palmar side of the medial and distal phalanges and envelop the tip as well as radial and ulnar side of the distal phalanx. They are cast from silicone and glued to the fingertip housing structure.

Table 3.1.: Dimensions of the KIT prosthetic hands. Reprinted from (Weiner, Starke, Rader et al., 2022) without changes (CC BY 4.0).

Hand Part		Male (mm)	Female (mm)
Palm	Length	111	100
	Width	87	77
	Depth	30	26
Thumb	Proximal Phalanx	37.0	32.7
	Distal Phalanx	37.7	33.2
Index Finger	Proximal Phalanx	29.9	27.0
	Intermediate Phalanx	28.0	26.4
	Distal Phalanx	27.1	25.5
Middle Finger	Proximal Phalanx	33.6	30.3
	Intermediate Phalanx	32.3	30.4
	Distal Phalanx	28	26.3
Ring Finger	Proximal Phalanx	30.1	26.9
	Intermediate Phalanx	31.3	29.3
	Distal Phalanx	28.6	26.8
Little Finger	Proximal Phalanx	22.8	20.5
	Intermediate Phalanx	23.9	22.6
	Distal Phalanx	27.3	25.7

Embedded Sensor System and Electronics

Both male and female prosthetic hands contain a multi-modal sensor system, a display and an embedded system to support intelligent sensor data processing and control without the need for external devices such as smartphones. To gain information about the proximate surroundings of the hand, the prostheses embed a camera (OV2640, OmniVision) at the base of the thumb. The camera module has a size of 8 mm×8 mm×6.3 mm and is connected to the processor's digital camera interface (DCMI) by a 24 pin flat-flex cable. The camera is configured to provide a 176 × 144 pixel RGB image at 10 frames per second. In the female prosthesis, a Time of Flight (ToF) distance sensor (VL53L1X, STMicroelectronics) placed close to the camera is used to measure the distance of a target object to the hand. Relative motor encoders and, in the female version, an IMU (BNO055, Bosch Sensortec) located on the embedded system's PCB provide proprioceptive information. In addition, the state of the users forearm can be estimated using the IMU.

An OLED display in the back of the hand provides feedback to the user about the current status of the hand. This can be utilized in semi-autonomous control schemes to show the proposed grasp type and the orientation for a recognized object. All sensors, motors and the display are connected to an embedded system in the palm of the hands. A detailed overview of the embedded system inside of the female hand is given in subsection 3.4.1.

3.1.3. Evaluation

The female prosthetic hand is evaluated and compared to the male prosthetic hand to assess the improvement of the design. The evaluation includes the hand characteristics in terms of grasping force, closing speed and hand weight. In addition, an assessment of grasping functionality using an adapted version of the YCB Assessment Protocol Calli et al. (2015) is performed and a task-oriented evaluation of object grasping and manipulation is conducted. The context information provided by the multi-modal sensor system is evaluated in a sensor-based grasping experiment.

Prosthesis Characteristics

Grasping Force: The grasp force of the prosthesis in case of a cylindrical power grasp is assessed using a sensorized wooden cylinder of 49 mm diameter that integrates a 6D force/torque sensor (Mini 40, ATI Industrial Automation) as shown in Figure 3.4a. The cylinder is grasped by the prosthesis with the thumb and the fingers touching on opposite sides of the sensor and held vertically. The individual finger forces are measured by positioning the flat hand directly over the force/torque sensor. By closing the hand, one finger is pressed onto the sensor while the others close freely. This procedure is performed for every finger. Both measurements are repeated 15 times each.

The cylindrical power grasp force amounts to a mean of 24.2 N with a standard deviation of $\pm$1.9 N for the male prosthesis and 40.5 N$\pm$8.1 N for the female hand. The mean finger forces range between 6.2 N to 8.2 N and 9.0 N to 12.3 N for the male and female hands respectively. The individual forces of the different fingers are shown in Figure 3.4b. The thumb grasp force in an extended configuration amounts to 53.1 N$\pm$1.4 N.

Speed The hand closing time is measured in an experimental setup, in which we track the fingertip positions of index and thumb in image sequences. To

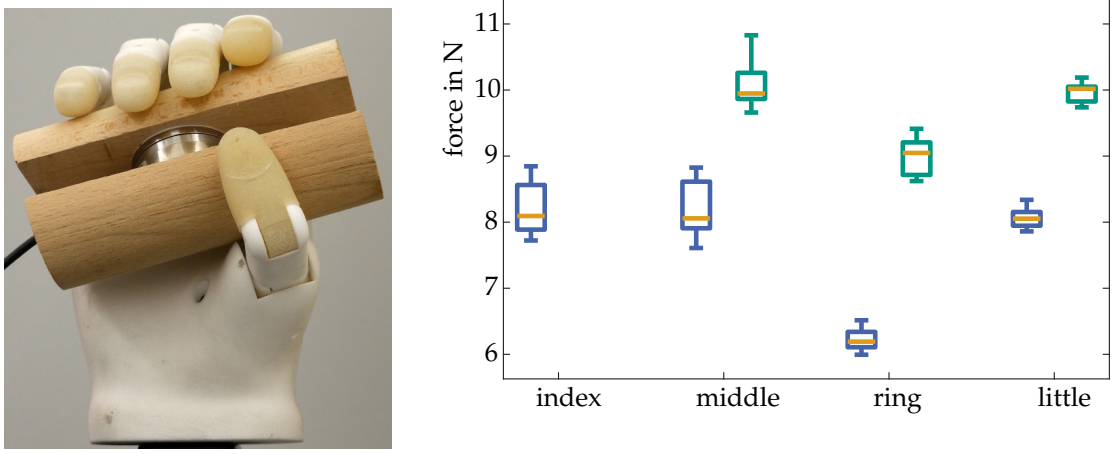

(a) (b)

Figure 3.5.: (a) Measurement setup for the measurement of cylindrical grasping forces. (Weiner et al., 2018b) (b) Fingertip forces of the male and female prosthesis. The orange line marks the median force, the box boundaries denote the first and third quartile and the outer lines depict the extrema of the respective fingertip force. Reprinted from (Weiner, Starke, Rader et al., 2022) without changes (CC BY 4.0).

determine the time, we repeated the experiments five times. The hand was placed in front of the camera lying on the back of the hand on a flat surface, exposing thumb and index finger to the camera.This orientation of the hand represents the worst case for fast closing, as gravity in this orientation extends the fingers and is hindering fast acceleration of the fingers, whereas rotation of the hand by 180° would result in gravity-assisted finger closing. The finger tips were marked using red tape for color-based tracking. The tracking of one corner of the red tape was performed using the video tracking software *kinovea*[1].While the male hand closes in 1.32 s±0.04 s, the female hand exhibits a closing speed of 0.73 s±0.02 s. The nominal maximum motor speed is kept constant for both versions.

Weight and Cost The female prosthesis weighs 377 g and requires material costs of 896 €, as shown in Figure 3.6. The male hand has a weight of 670 g and material costs of 1008 €. The weight reduction is achieved in large parts

[1]https://www.kinovea.org/

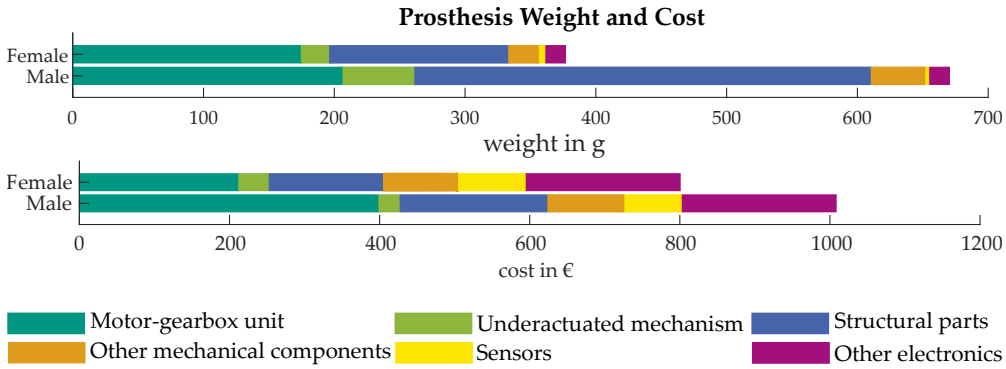

Figure 3.6.: Distribution of weight and cost among the components of the male and female KIT Prosthetic Hand. Reprinted from (Weiner, Starke, Rader et al., 2022) without changes (CC BY 4.0).

by optimizing the structural 3D-printed parts for the palm. In contrast to the mechanism in the male version, which was milled from aluminum, the mechanism in the female hand is also 3D-printed, reducing the weight by 60 %. Due to the additional transmission ratio of 2:1 in the mechanism and reduction of the diameter of the motor tendon pulley, weight is saved as the motor requires one reduction gear stage less.

Grasping Ability

We evaluated the grasping and manipulation abilities of the hands using 1) the *YCB Gripper Assessment Protocol* as proposed by Calli et al. (2015) to assess grasping abilities and 2) a second *task-oriented protocol* for assessing the hand performance in activities of daily living (ADL).

Gripper Assasment Protocol The general grasping ability is assessed based on the YCB Gripper Assessment Protocol. The procedure consists of grasping each object from a table, holding it for 3 s and rotating it by 90°. In contrast to the original protocol, we include all object categories from the *YCB Object Set* except for the task items category. This category, containing e. g. a peg-in-hole board or the assembly of an airplane toy, is excluded from the evaluation as we focus on the assessment of the hand grasping abilities. Altogether, 60 objects were tested. No position offsets are applied to the objects as these are compensated by the user.

The procedure was applied to both the male and female prosthetic hand while being manually controlled by a human operator. One point is scored if the

object is successfully lifted and held. A second point is scored if the object does not move or slide inside the hand, a third point is scored if the object remains grasped after the rotation and the fourth point is scored if the object does not move inside the hand after rotation. The maximum score that can be achieved for each object is four. For articulated objects (table cloth, chain, rope, t-shirt), the object is grasped and lifted three times and half a point is granted for each successful attempt.

The scores were 193 and 203.5 of the possible 230 points for the male and female hand respectively. In total 85.2 % of all objects could be grasped with the male hand and 91.8 % with the female hand. Both hands encounter difficulties in grasping thin and small objects like credit cards, nails and washers. Despite the smaller size of the female hand, there are no notable shortcomings in grasping large objects, like the wood block or the mini soccer ball from the YCB Object Set. Both hands are able to lift all heavy objects from the YCB object with a full score, for example the power drill, the table cloth and the wood block. The skillet could be lifted at the handle, but moved inside the hand during hand rotation due to the high torque on the handle.

Task-Oriented Protocol The female hand is additionally evaluated with a task oriented protocol of common daily life activities. To this end, the prosthesis was mounted on a shaft, which can be worn below the forearm of the able hand and several activities of daily living were performed using the prosthesis. The tasks are selected based on the objects and activities proposed by Matheus and Dollar (2010). The list of the tasks is shown in Figure 3.7.

The execution of every task is repeated five times. The task execution quality is assessed with a score between 0 and 3 points. The used scoring system is designed as follows: one point is granted for achieving a stable grasp, a second point is granted for successful accomplishment of the task goal and the third point is granted when the task execution is done in a natural and comfortable manner compared to its execution with two able human hands. As an example, for the writing task, the first point is scored if the pen is stably held in the hand, the second point for writing the requested sentence on a piece of paper in a readable manner and the third point is granted only if the handwriting looks natural, the task is executed in a comfortable manner and the writing time is not disproportionally long. As defined in the Southampton Hand Assessment Procedure (SHAP) proposed in Light et al. (2002), each task needs to be solved within eight times the time needed by an able-bodied person to be not considered

disproportionally long. If the task execution requires more time, it can only be rated with two points at maximum.

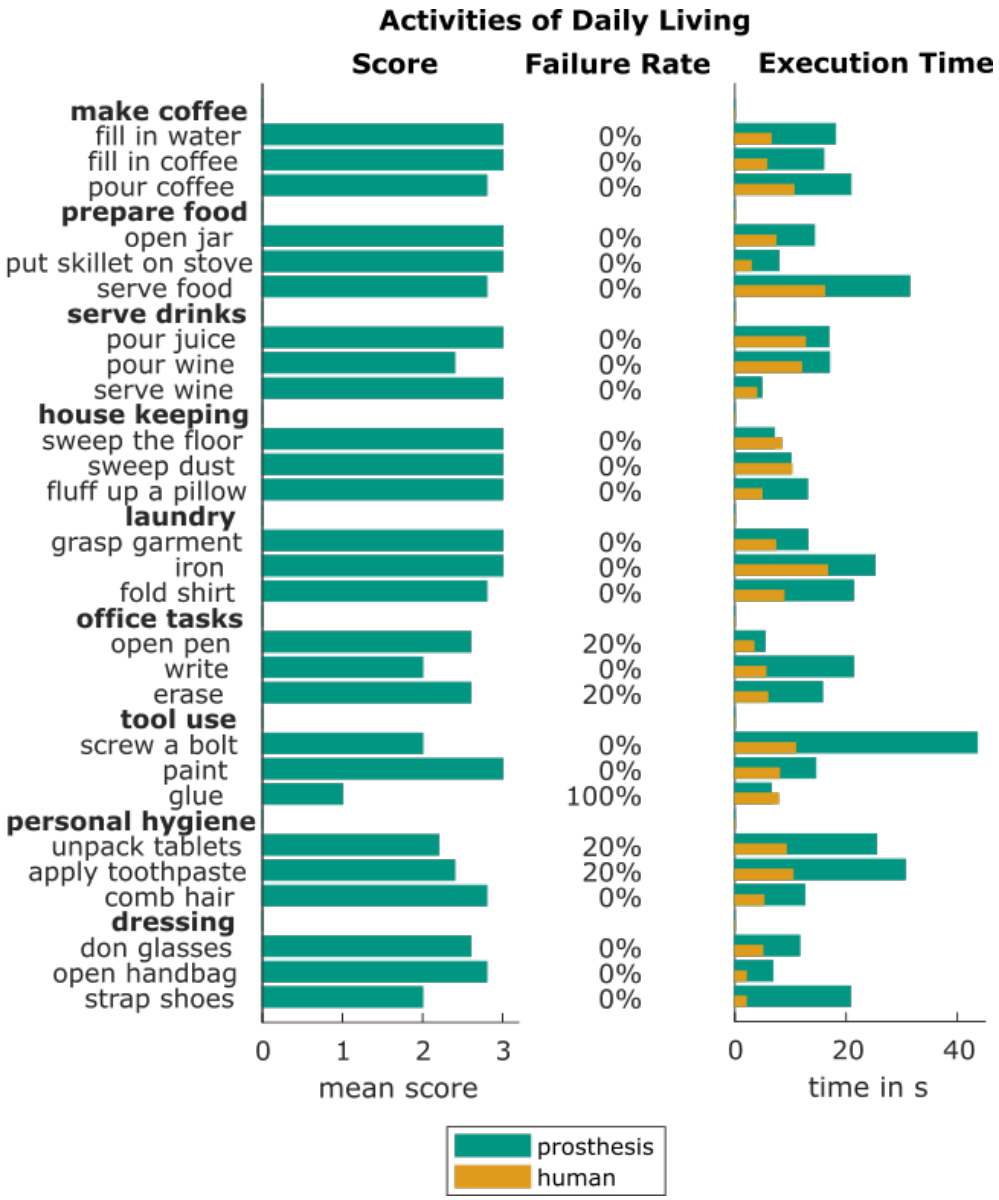

Figure 3.7.: Tasks performed in the task-oriented protocol with the mean prosthesis scores, ranging between 0 for the hand being unable to grasp the object to 3 for a comfortable task execution, the rate of failed task executions over five trials and the mean execution times with the prosthetic hand and an able human hand. Reprinted from (Weiner, Starke, Rader et al., 2022) without changes (CC BY 4.0).

The scores and execution times achieved with the female prosthesis are shown in Figure 3.7. In addition, the task failure rate over all five executions of each task is given. Over all activities, the task was not fulfilled successfully in 6.7 %

of all executions. The overall score of 88.6 % of achievable points indicates a satisfying functionality of the hand in performing activities of daily life.

The prosthesis was especially successful in executing everyday household activities like food preparation, house keeping and laundry. Lower task evaluation scores are mainly seen in office tasks as well as medicating and bathing tasks. This is due to the fact, that these tasks require more complex grasping and prehensile in-hand object manipulation. The only task that could not be accomplished by the prosthesis was gluing with a hot glue gun. While the gun could be grasped, the trigger could not be pressed by the index finger. The task of screwing a bolt into a nut was especially challenging, since the hand is not able to turn the screw driver within the hand, but instead the full hand needs to be rotated with the screwdriver. This results in unnatural and uncomfortable whole-body compensatory movements. No task took more than eight times the time of an execution with two able human hands. Strapping a shoe was the only task that exceeded the defined time constraint because the task took 10.4 times the time needed by a human with two able hands.

Sensor-Based Grasping

The merit of the multi-modal sensor system for grasp control is evaluated in the context of sensor-based grasping (see Figure 3.8). All sensor readings are recorded and evaluated during a grasping sequence of daily living activity. In the sequence, a bottle of coke is grasped with the prosthesis, opened and the coke is poured into a glass. After the bottle is placed back on the table, a lemon is grasped and held firmly. A slice is cut off with a knife in the second hand and the lemon is placed on the table. The lemon slice is inserted into the glass of coke with the able hand. Before grasping, an image of the object is captured by the hand's integrated camera and the object recognition is run on the in-hand integrated embedded system. Figure 3.8 shows the experimental procedure, the sensor readings and results of the object recognition. The camera image for object recognition is shown together with the recognition probabilities for all 13 trained objects in the bottom row. The correct object, being coke and lemon respectively, is marked in orange in the bar chart diagrams. In both cases, the object recognition returns the highest probability for the correct object, allowing for object-specific grasp control.

The sensor readings for five executions of the task are shown in the middle of Figure 3.8. The associated sensor readings are plotted in solid lines for an exemplary execution and in transparent lines for the remaining four executions.

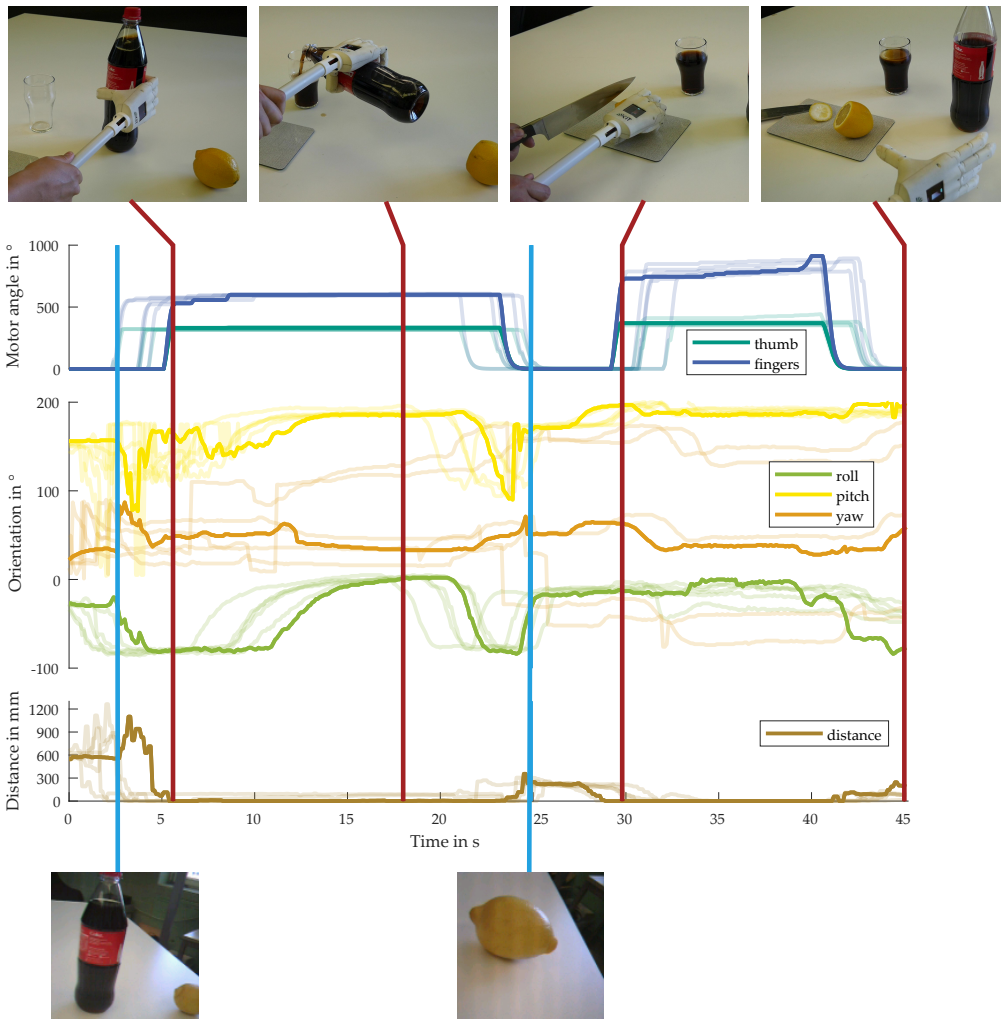

Figure 3.8.: Sensor readings while pouring coke into a glass and adding a slice cut off from a lemon. Graphs show an exemplary measurement of the motor positions, hand orientation from the IMU and object distance. Four additional experiments printed in the background underline the reliability of the sensor data. Important events of the grasping process are marked by dashed lines and corresponding images of the scene are shown above the graphs. The triggering of the object recognition is marked by dotted lines and an images captured by the hand camera together with the object recognition probabilities are shown below the graphs. The recognition probability of the coke bottle and lemon respectively are marked in orange in the bar chart, indicating the object was recognized correctly based on visual information. Reprinted from (Weiner, Starke, Rader et al., 2022) without changes (CC BY 4.0).

All sensor readings have been normalized over the execution time, to show the similarity of the acquired sensor data throughout several executions. Grasping the bottle is finished after 5.2 s, which is clearly visible in the motor position data. Similarly the bottle is placed on the table after 23.3 s, coincident with the motor position moving back to the initial state. Grasping and releasing the lemon occur at 29.9 s and 40.6 s respectively.

Approaching the object can also be inferred from the distance sensor in the palm, which shows a decrease of the object distance from 379 mm to 15 mm between 3.6 s and 5.1 s. The grasping action can therefore be controlled based on the distance to the object provided by the distance sensor. As the ball of the thumb does not touch the bottle, the distance sensor does not decrease to zero throughout the grasp. The release of the object, which is also visible in the finger motor positions, is consequently followed by an increase of the object distance starting after 24.6 s.

The orientation data from the IMU provides additional information about the grasp. Figure 3.8 shows the hand orientation in the hand coordinate system. Several rotations of the prosthesis throughout the manipulation action can be recognized. The recording starts with the hand in a horizontal position and the palm facing towards the table. After 11.1 s, when the bottle is grasped and opened, the prosthesis starts rotating with the bottle to pour coke into the glass. This is visible in the roll angle of the IMU. Once the pouring action is finished and the hand is rotated back, the placement of the bottle can be recognized based on the distance sensor data. The disturbance induced by opening the bottle and placing it back on the table can be seen in the hand's pitch angle. To grasp the lemon, the hand is again horizontally orientated, as visible in the roll angle of the IMU.

The experiment exemplifies that information about the current phase of an object grasping and manipulation task can be inferred from sensor data and can be used for semi-autonomous grasp control.

3.1.4. Discussion

We present the KIT Prosthetic Hands as an example for intelligent prostheses equipped with abilities needed for the realization of semi-autonomous grasping. The hands are designed to support users in grasping objects to master daily life activities. The intelligence of the hands is achieved by combining adaptive underactuated mechanisms with a multi-modal sensor system and an embedded

Table 3.2.: Key characteristics of the male and female KIT prosthetic hands. Reprinted from (Weiner, Starke, Rader et al., 2022) without changes (CC BY 4.0).

Prosthesis	Percentile	Weight	Material Cost	Embedded Sensors	Grasping Force	Closing Speed	YCB GAP Score
Male	50th male	768g	1008€	Camera	24.2±1.9 N	1.32±0.04 s	193
Female	50th female	377g	896€	Distance, IMU, Camera	40.5±8.1 N	0.73±0.02 s	203.5

system for onboard processing of sensory information and control. Thanks to the underactuated mechanism, high grasp forces can be achieved. The on-board processing of multimodal sensor information relevant to the current task allows the implementation of semi-autonomous grasping behaviors.

The hand's size and weight comply to the requirements for a hand prosthesis. With its total weight of 377 g, the hand is lighter than any commercial myoelectric prosthetic hand as presented in Table 2.1, and is comparable to the human hand with approximately 400 g (Kaye and Konz, 1986). Compared to the male hand, the female hand shows a reduction of 44 % in weight and 30 % in cost. As shown in Figure 3.6, this is achieved by a significant improvement in lightweight design of mechanism and structural hand parts as well as the 3D-printed design of the mechanism without custom metal parts. Compared to the male hand, the closing time of the female prosthesis is decreased by 0.59 s to an absolute closing time of 0.73 s. This increase in speed is achieved by the improved mechanism design and the shorter finger dimensions requiring a smaller tendon deflection. The hand provides a cylindrical grasp force of 40.5 N and a mean fingertip force of 10.3 N within the four fingers. Compared to the male hand, the increase of the finger forces amounts on average to 35.2 %. This is within the range of commercial and research prosthetic hands as e. g. the iLimb Pulse (Belter and Dollar, 2013) or the SSSA-MyHand in (Controzzi et al., 2017). With 53.4 N, the thumb is capable of providing a significantly higher force to counteract the four fingers.

The evaluation of the prosthesis based on the YCB Gripper Assessment Protocol shows a grasp functionality of 91.8 % in grasping everyday objects and the prosthesis achieves a score of 88.6 % in the execution of daily activity manipulation tasks. This shows the potential of the hand to support users throughout their daily life spanning food preparation, household and hygiene tasks, but also

Figure 3.9.: The KIT Sensorized Soft Hand (left) and KIT Finger-Vision Soft Hand (right) inspired by the prosthetic hand development. Reprinted from (Weiner, Starke, Rader et al., 2022) without changes (CC BY 4.0).

including their professional life, exemplary shown in office and workshop activities. The improvements of the female prosthetic hand over the male version are summarized in Table 3.2.

With these achievements, we provide important prerequisites for novel generation of prosthetic hands that integrate multi-modal sensing and computing for the realization of semi-autonomous grasping and improving the way how users can interact with their prosthetic hands in an easy and intuitive way. We believe that the hardware design of the KIT Prosthetic Hand as an intelligent and functional hand prosthesis provides a powerful platform for the development of intelligent, semi-autonomous control algorithms.

Important to mention is also the fact that the underactuated mechanisms used in the KIT prosthetic hands served as the basis for the development of the hands of the humanoid robot ARMAR-6 by Asfour et al. (2019). In addition, the new version of prosthetic hand, the female version, served as a basis for the development of several new soft humanoid robotic hands, the KIT Finger-Vision Soft Hand, see Hundhausen et al. (2020), and the KIT Sensorized Soft Hand with tactile sensing of the fingers, see section 3.3 and (Weiner et al., 2021). Both hands are shown in Figure 3.9. The hands allow an individual actuation of the thumb and the index finger. Both are driven by three motors and include an adapted version of the underactuated mechanism described in subsection 3.1.2, that is designed to drive only three fingers with the same motor.

3.2. Scalable Sensorized Rigid Fingers

The development of fingers for anthropomorphic hands is driven by two main requirements. First, the fingers should include a multimodal haptic sensor system that is able to sense normal and shear forces, joint angles as well as proximity. Second, the fingers should be freely scalable according to human hand dimensions. This allows to manufacture fingers that reflect the different sizing of index, middle, ring and little finger for a given hand size and allow to build hands with different sizes, all from a single finger model. Scalability is hence a key feature, which is addressed in the thesis. Not only the mechanical model has to scale, the sensor system has to adapt to the different sized fingers as well.

The mechanical model of the finger described in the following is designed such that changing of a few high-level parameters adapts all dimensions of the model automatically. The sensor system is divided into modules that can be freely combined to cover the maximum space available for the scaled finger. These fingers could be scaled to match both prosthetic as well as humanoid robotic hands, as shown in Figure 3.10b. Individual sensor modalities are exchanged to allow for higher sample rates of the system and additional sensor modalities like an accelerometer and a distance sensor are added to the system. An overview of the sensor system and cabling in the fingers is given in Figure 3.10a.

Due to the complexity of the problem, development of the finger model has been conducted iteratively. For the first version of the fingers, described in (Weiner et al., 2018a), a model was derived that included a multimodal sensor system mounted on flexible Printed Circuit Boards (PCBs), but was not easily scalable. The second version of the fingers, published in (Weiner et al., 2019), improves upon the first version by introducing both a scalable mechanical model as well as a strategy to scale the sensor system. Another aspect improved in this version is assembly and availability of parts, since the flexible, non-scalable PCB in the first prototype is replaced by standard rigid PCB and Flat Flex Cables (FFCs). The use of small modules of standard PCBs to form a variable-sized and scalable system as well as the use of readily available digital sensors has been inspired by the robot skin presented in (Cheng et al., 2019).

The following sections up to the conclusion are reprinted from (Weiner et al., 2019) with changes (CC BY 4.0).

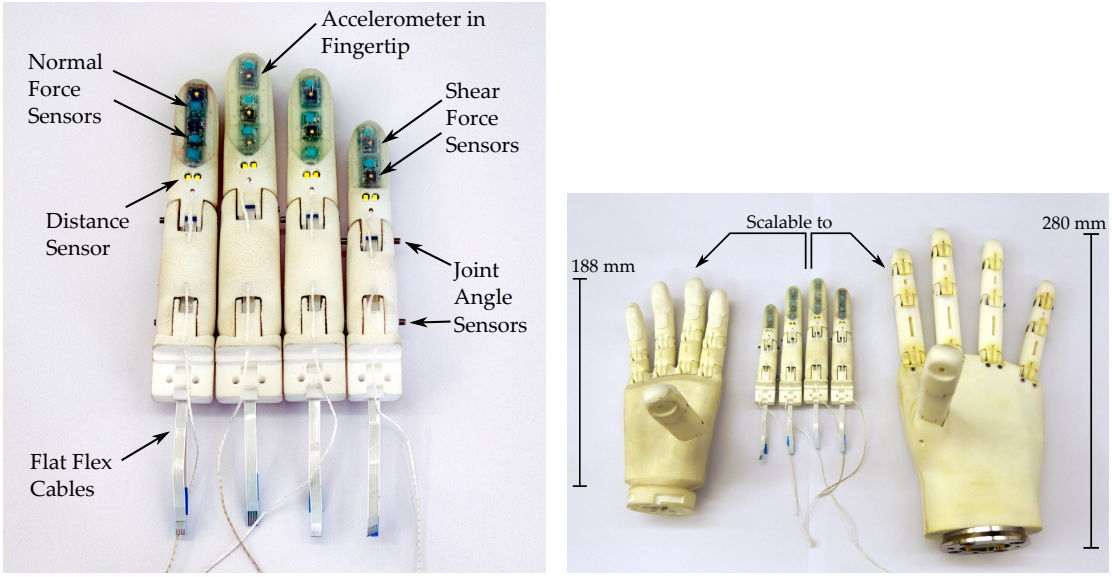

(a) (b)

Figure 3.10.: (**a**) The four manufactured demonstrators derived from the scalable model. (**b**) A comparison of the physical demonstrators with male KIT Prosthetic Hand (left) and the robotic KIT ARMAR-6 Hand (right). Reprinted from (Weiner et al., 2019) without changes (CC BY 4.0).

3.2.1. Design of Scalable Anthropomorphic Fingers

Our approach to implementing a multi-modal sensor system into an anthropomorphic finger combines a completely parametrized Computer Aided Design (CAD)-model with a modular electronic system consisting of commercially available sensors and standard PCBs. For force sensing we combine and extend methods described in (Tenzer et al., 2014) and (Tomo et al., 2016b). Additionally, we incorporate distance, vibration and joint angle sensing into the system. Mechanical parts are realized using 3D-printing. In this section, we describe the interplay of mechanical scalability and electrical modularity and how these two central concepts are implemented in detail.

Scalable Model

For the mechanical structure of the fingers we created a single scalable CAD-model of the finger. It is based on a skeleton that contains all important features of the finger, as can be seen in Figure 3.11. Based on this skeleton, the three individual parts for knuckle, proximal and distal phalanx are derived by referencing the sketches in the skeleton model. The skeleton can be parametrized using

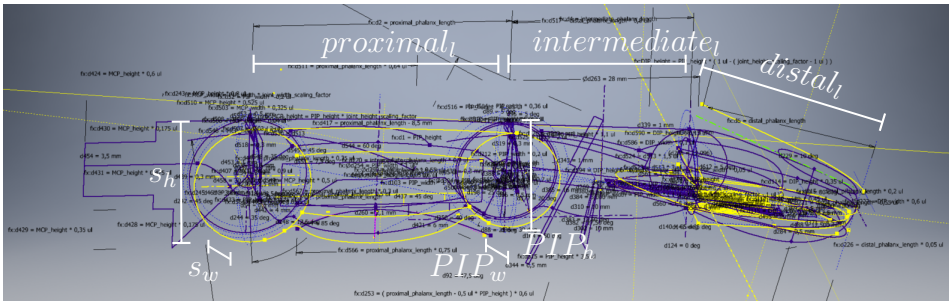

Figure 3.11.: Skeleton sketches used for the individual phalanges. The seven high-level parameters are used in these sketches to derive all dependent dimensions of the finger. Reprinted from (Weiner et al., 2019) without changes (CC BY 4.0).

seven high-level parameters that can be set independently of each other. These parameters define the width and height of the Proximal Interphalangeal (PIP) joint (PIP_w and PIP_h) as well as the lengths of the proximal, intermediate and distal phalanx ($proximal_l$, $intermediate_l$ and $distal_l$). Two additional parameters s_w and s_h represent scaling factors that are used to determine the width and height of the Distal Interphalangeal (DIP) and metacarpophalangeal (MCP) joints as follows:

$$\begin{aligned} MCP_w &= PIP_w \cdot s_w & \qquad DIP_w &= PIP_w \cdot (1 - (s_w - 1)) \\ MCP_h &= PIP_h \cdot s_h & \qquad DIP_h &= PIP_h \cdot (1 - (s_h - 1)) \end{aligned}$$

The scaling factors s_w and s_h are calculated as the average ratios of joint height divided by joint width as measured in (Vergara et al., 2018). If desired, the height/width of all joints can also be changed individually and independently by replacing the above calculations for MCP and DIP in the root sketch with independent scalar values.

The seven high-level parameters (PIP_w, PIP_h, $proximal_l$, $intermediate_l$, $distal_l$, s_w, s_h) define lengths and radii in a root sketch, together with basic definitions of useful axes and planes. This root sketch is referenced by further sketches in the model that define further features like loft guides or faces needed for extrusions. The model makes use of splines, which allow for round and smooth shapes. To keep the number of spline parameters small, we define the whole shape of the finger with as few splines as possible and use a small number of control points for each spline. Once the whole skeleton is defined as a set of sketches, the three individual parts of the fingers are designed by deriving relevant sketches from the skeleton and building the geometry based on these sketches. In addition to the seven high-level parameters, the model contains 257 other parameters,

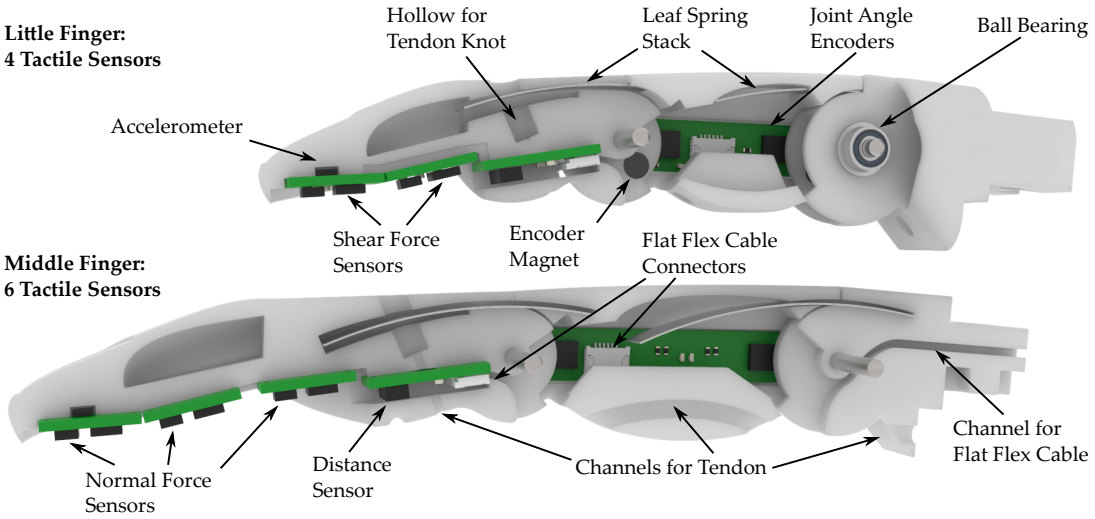

Figure 3.12.: Section view of the little and middle finger with the model scaled to the 50th percentile female dimensions. The section view of the little finger shows the joints of the finger while the deeper cut into the middle finger shows the paths for both the FFCs and the tendon. Reprinted from (Weiner et al., 2019) without changes (CC BY 4.0).

which are either derived from the high-level parameters or are constant like fittings, so that a change in high-level parameter values results in a change of the dimensions of the entire finger.

The parameters can, for example, be set to match the measured dimensions of the able hand of an amputee. We successfully tested the model using the 5th percentile female hand dimensions as well as the 95th percentile male hand dimensions. Figure 3.12 shows two specimens of the developed CAD-model scaled to the dimensions of the little and middle finger sized according to a median female hand.

In addition to human sizing, special attention was given to the anthropomorphic shape of the fingers, which is an important factor especially for the acceptance in prosthetic applications (Cordella et al., 2016). In Figure 3.13, the profile of a physical demonstrator is shown.

We consciously made the decision to fuse the distal and intermediate phalanx into one part. Each finger hence has two joints, the MCP joint and the PIP joint. Omitting the DIP joint reduces the complexity of the assembly and allows for sufficient space in the distal part to house the sensor system. This is a common design choice for both commercially available prostheses (Belter and Dollar, 2013) as well research prostheses and humanoid robotic hands (Piazza et al., 2019).

Figure 3.13.: Profile of the ring finger showing a curved design for the individual phalanges. Reprinted from (Weiner et al., 2019) without changes (CC BY 4.0).

The individual components for the fingers are 3D-printed from Nylon (PA 2200) using Selective Laser Sintering (SLS) to enable individualized sizing as needed.

Joint Structure and Actuation

Each finger consists of three individual parts, the distal/intermediate phalanx, the proximal phalanx and the knuckle, as well as two joints, the MCP joint and the PIP joint, that connect the phalanges. Each joint is supported by two miniature metal ball bearings to reduce friction to a minimum. The joints are actuated in flexion direction by a tendon that is located on the palmar side of the fingers. Actuation via tendons was chosen as it does not require levers inside of the finger, hence leaving necessary space for the electronics and cables.

Each joint is extended by a stack of leaf springs, as opposed to the torsion springs, that are used in the previous version of the KIT male prosthetic hand (Weiner et al., 2018b), in order to free up space in the joints for sensors and their cables. The leaf springs are installed completely inside each finger and are not visible from the outside. The pockets for holding the leaf springs are slightly curved to minimize friction and simultaneously create pretension in the springs. One end of the leaf springs is glued into the phalanx, the other slides in and out of the pocket. In order to decrease the friction between the finger material and leaf springs, we created a hollow space inside the finger. Both the distal/intermediate as well as the proximal phalanx are hollow for the most part to allow the springs to extend without friction and in order to save weight. We used spring steel with 0.1 mm thickness as the leaf spring material. Each joint is equipped with a stack of three leaf springs to reach a sufficiently high torque.

Embedded Sensor System Overview

As shown in Figure 3.10a and Figure 3.12, a customizable number of sensors can be integrated into a finger, depending on the finger pad area available for the integration of tactile sensors. The middle, and thus largest, finger used in this work, shown in the bottom of Figure 3.12, contains a total number of ten sensors, which include two joint angle encoders, a distance sensor, three normal force sensors, three shear force sensors and one accelerometer. The sensor PCBs are connected to the controller using FFCs via connectors on the joint angle encoder and distance sensor PCBs (see Figure 3.12), while the tactile sensor PCBs are connected through magnet wires (see Figure 3.15).

Sensor Placement Experiments

In order to find the optimal configuration and placement positions of the tactile sensors in each finger, we conducted tests to determine which surfaces of each finger are in contact when grasping different objects. These experiments were carried out prior to the definition of the tactile sensor layout and their results were used to define the area on the finger that should be covered with tactile sensors. We used the KIT female prosthetic hand (see section 3.1), as well as five objects (banana, baseball, bowl, drill, spam) from the YCB object set (Calli et al., 2015) and two objects (cola, green cup) from the KIT object set (Kasper et al., 2012), in order to have a variation of shapes and sizes. The outside surface of each object was painted green, after which the object was immediately grasped using either a top or a side grasp (approaching the object from the top or the side, respectively). From the experiments it is evident that the finger area that is in contact with most objects is the finger pad, especially that of the index finger. Examples of the experiment results can be seen in Figure 3.14. Thus, contact forces and slip can be measured most accurately by placing sensors in these areas.

Sensor System Configuration

We use a combination of three types of sensors to acquire a wide range of tactile information in the available finger pad area, shown in Figure 3.15. The normal force sensors (NPA201, NovaSensor) are based on ideas presented in (Tenzer et al., 2014). In contrast to the design by Tenzer et al. used, they are constructed by leaving a small pressure chamber in the silicone above the barometric pressure sensor by casting small pressure chambers out of silicone, which

(a) cup side (b) spam top (c) bowl top (d) bottle side (e) drill side

Figure 3.14.: Finger contact surface experiment examples for different grasps. Reprinted from (Weiner et al., 2019) without changes (CC BY 4.0).

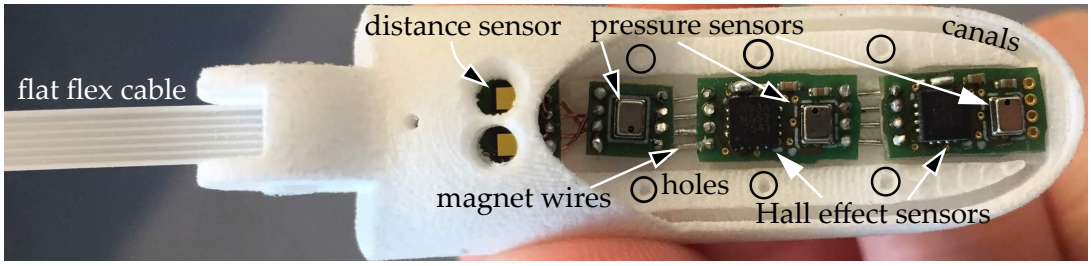

Figure 3.15.: The individual tactile sensor PCBs, containing normal and shear force sensors and an accelerometer, as well as the distance sensor and design details are shown. Reprinted from (Weiner et al., 2019) without changes (CC BY 4.0).

are placed on the sensor after curing.When a force is exerted on the silicone in vicinity to the sensor, this force compresses the pressure chamber which in turn is measured as an increase in pressure by the sensor. These sensors will be called barometer-based sensors in the rest of this section. While estimating forces only in one direction, they are very sensitive and offer a high resolution. The shear force sensors (MLX90393, Melexis) are based on work presented in (Tomo et al., 2016a) and (Tomo et al., 2016b). They can be used to estimate both normal and shear forces and offer a larger measurement range than the normal force sensors at the cost of reduced resolution and non-linearity. These sensors will be called Hall effect-based sensors in the rest of this section. The normal force estimation is hence performed using different measurement principles for each sensor, enabling a more accurate overall measurement through sensor fusion.

An accelerometer (BMA456, Bosch Sensortec) with a sample rate of 1.6 kHz is mounted at the back of the most distal sensor PCB. It can be used to detect slip of grasped objects as it is, unlike the normal and shear force sensors, able to achieve the necessary sampling rates for this task.

To gain additional information even before contact is made with an object, we added a distance sensor into the finger, shown in Figure 3.15. The sensor is a Time of Flight (ToF) device that is able to measure the distance of objects independent of their reflectance (VL53L1X, STMicroelectronics). The distance information acquired with this sensor can for example be used to control the hand to automatically close the hand as soon as it is close enough to an object to grasp.

All sensors are commercially available sensors that integrate all signal conditioning and digitalization circuits. All sensors also include a temperature sensing element that can be sampled together with the main sensor signal. This way no additional electronics are needed for signal processing. All sensors communicate using the two-wire Inter-Integrated Circuit (I^2C) communication bus. Together with the supply voltage lines, only four wires are needed to operate and read out all sensors. As there are no commercially available FFCs and connectors with four terminals, the smallest available configuration with six terminals is chosen to connect the sensor system to a central processor, typically inside of the palm of the robotic hand.

Manufacturing Process

Assembly of the fingers starts by connecting the PCBs with the sensors with short wires and gluing them into the mechanical parts. The mechanical structure of the fingers contains special grooves where the cables are situated, protecting them from any mechanical stess.

We then use the methodology described in our previous work (Weiner et al., 2018a) to cast the normal and shear force sensors in silicone rubber, using the shear force and placeholder magnets shown in Figure 3.16a. For the Hall effect-based sensors a thin pad of silicone with Shore A (ShA) hardness 13 is glued to the top of the sensor using silicone glue. A magnet is placed on the center above the sensor and a drop of silicone is used to fix the magnet to the silicone pad.

For the barometer-based sensors a small mold is placed around the sensor. A small magnet is placed directly above the opening in the casing of the barometric pressure sensor and the mold is filled to the top of the magnet with silicone

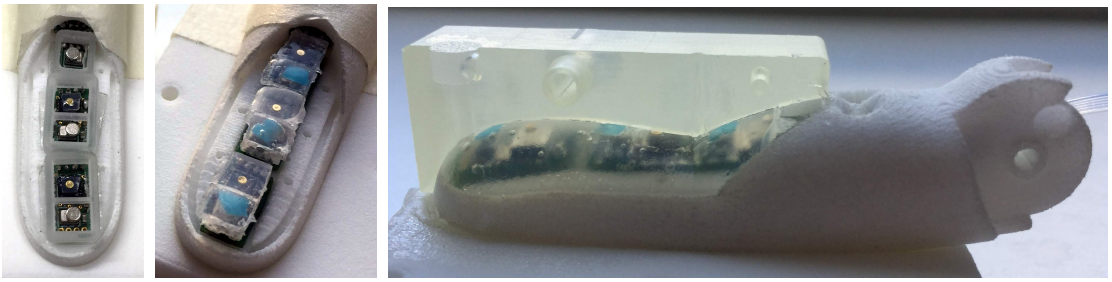

(a) (b) (c)

Figure 3.16.: (**a**) The molds for the silicone rubber casting process are placed directly into the finger. (**b**) The individual sensors have been cast in rubber. The next step is to cast the remaining finger pad area in rubber. (**c**) The result of the casting process of the finger tip and one half of the used mold is shown. A silicone canal is used to inject silicone rubber into the molds. Reprinted from (Weiner et al., 2019) without changes (CC BY 4.0).

(PCB 45). Since the housing of the pressure sensor is magnetic, the magnet is tightly held in place. As soon as the silicone is hardened, the magnet is removed. The resulting hole forms the walls of the pressure chamber above the sensor. The hole is then covered with a thin sheet of silicone (ShA 22) and fixated by a drop of silicone. Both molds for Hall effect-based and barometer-based sensors and placeholder magnets are shown in Figure 3.16a. The 3D printed molds, depicted in Figure 3.16b, can be placed directly onto the PCBs glued into the finger. The individual sensors are cast in rubber as shown in Figure 3.16a, the result of which can be seen in Figure 3.16b.

The entire area of the finger pad is then cast in an additional layer of silicone rubber (ShA 13), shown in Figure 3.16c. In order to ensure sufficient stability of the silicone layer, holes and canals with undercuts, as shown in Figure 3.15, are integrated into the finger tip. This design allows for increased adhesion of the silicone to the 3D printed material. Compared to the previous work, a larger part of the fingertip is cast in silicone rubber to enable a configuration with a larger number of sensors. This also contributes to an improved grasping behavior as the silicone rubber is more elastic and has a higher friction coefficient compared to the 3D printed material (Or et al., 2016).

Joint Angle Measurement

Additionally required for the forming of pre-grasps are joint angle encoders that determine the rotation angle of each joint and can be used to control and adjust the finger flexion. One possibility to measure joint rotation angles is to place a

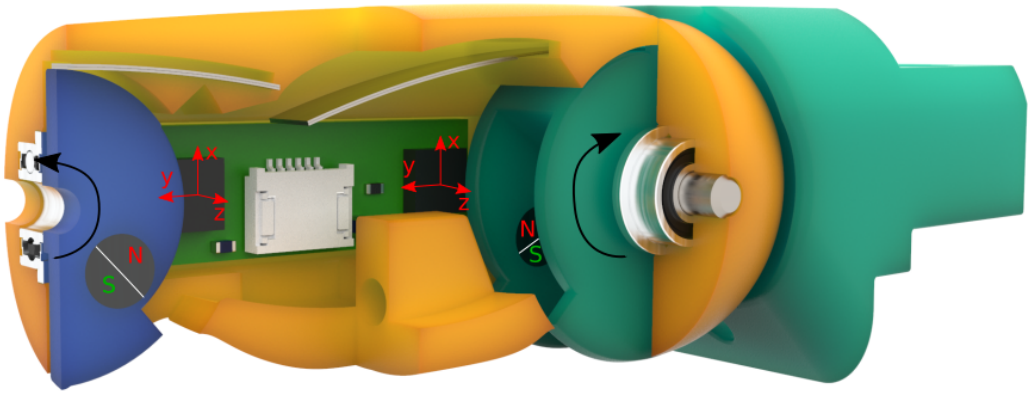

Figure 3.17.: Section view of the little finger, with the distal/intermediate phalanx in blue, the proximal phalanx in orange and the knuckle in green, showing the joint angle encoders and magnets used to determine the joint rotational angles. Reprinted from (Weiner et al., 2019) without changes (CC BY 4.0).

diametrically polarized magnet directly on the joint axis that rotates with the joint. A Hall effect sensor that is placed directly above the magnet is then able to measure the change in magnetic field strength induced by the rotation of the magnet. As the Hall effect sensor outputs the magnetic field strength in x, y and z direction, these values can be used to derive the rotation angle of each joint.

To calculate the rotation angle α_z around the z axis, the following equation is used, where x_{Mag} and y_{Mag} are the magnetic field strengths in x and y direction, respectively:

$$\alpha_z = \arctan 2(y_{Mag}, x_{Mag}) * \frac{180°}{\pi} \tag{3.1}$$

In this work, however, we perform this measurement off-axis both for the magnet and the sensor (MLX90393, Melexis), due to space constraints in the joints, which is shown in Figure 3.17. The magnets are glued into the distal/intermediate phalanx (blue) and the knuckle (green), and rotate around their respective joints when these are rotated. At 45 degrees rotation the magnets are positioned directly above the sensors, so that they have the same distance between each other at 0 and 90 degrees, which corresponds to the minimum and maximum angle, respectively, of all joints. The above stated Equation 3.1 can nevertheless be used to provide an approximation of the joint rotation angle using this off-axis measurement. However, when the placement of the magnet above the sensor changes in x or y direction, the magnetic field strength and therefore sensor output of the Hall effect sensor changes. Therefore, an experiment is necessary to determine the correlation between the sensor output and the actual rotation angle, which is described in subsection 3.2.2.

	Index	Middle	Ring	Little
Finger Length	80.64	90.02	83.98	66.17
Proximal Phalanx Length	34.15	38.15	34.45	27.05
Distal Phalanx Length	46.49	51.87	49.53	39.12
Proximal Phalanx Height	17.28	17.28	17.28	17.28
Distal Phalanx Height	14.4	14.4	14.4	14.4
Proximal Phalanx Width	18.7	20.13	18.81	16.5
Distal Phalanx Width	17	18.3	17.1	15

Table 3.3.: Dimensions in [mm] of the finger demonstrators. Reprinted from (Weiner et al., 2019) without changes (CC BY 4.0).

As the PCB for the joint angle encoders contains just two sensors and a connector, it is fairly easy to adjust the distance between the two sensors for different finger sizes directly in the PCB layout. We hence produced PCBs in three different sizes for the little finger, the middle finger, and the other two fingers which can accommodate the same PCB size due to their similar dimension.

Physical Demonstrators

The physical demonstrators developed in this work were sized according to the 50^{th} percentile female dimensions as described by the German standard specification (DIN 33402-2) in finger length and additional dimensions as identified in (Vergara et al., 2018). The dimensions for all fingers and segments are shown in Table 3.3. As the range for prosthetic and humanoid robotic hand sizes varies greatly, we have chosen dimensions at the smaller end of the range to ensure that the model and electronics can be used in even small hands and can consequently also be easily modified and extended for larger hands.

Through the use of additive manufacturing for mechanical parts, commercially available sensors and standard manufacturing techniques for the PCBs the price for an individual finger can be kept below 70€.

3.2.2. Experimental Characterization

A series of characterizations were conducted on the physical demonstrators to assess the performance of the sensors individually and as a whole system. For the experiments regarding normal and shear forces, as well as an experiment determining the spatial resolution of the sensor setup, a two-axis linear table is used, shown in Figure 3.18. Each axis is a precision linear stage (PT4808, MM

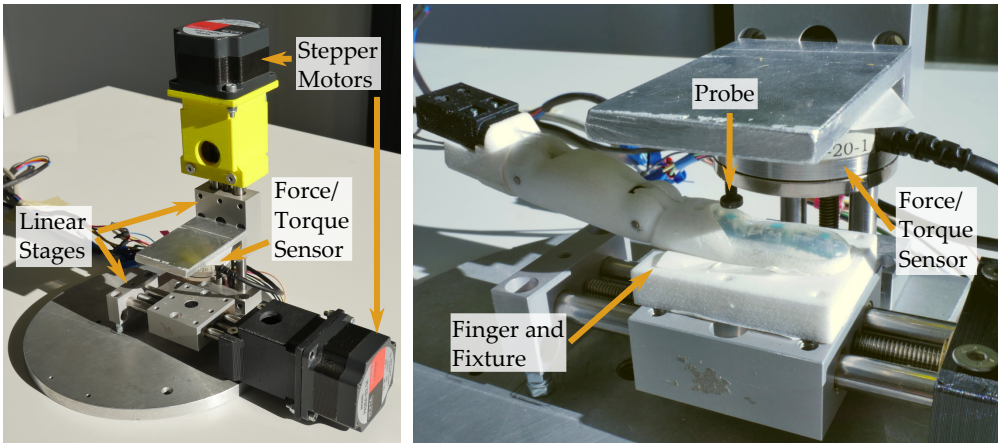

Figure 3.18.: Linear table for normal force, shear force characterization and spatial mapping experiments. Reprinted from (Weiner et al., 2019) without changes (CC BY 4.0).

Engineering GmbH) with 0.5 mm displacement per turn attached to a stepper motor with 200 steps per turn. A force/torque sensor (Mini 40, ATI Industrial Automation) is mounted on one axis and equipped with a cylindrical probe with a diameter of 5.3 mm, which is small enough to allow applying loads to individual sensors. A sensorized finger can be attached to the other axis, enabling the probe to apply normal forces to different parts of the finger along one axis, as well as shear forces when the finger is moved while normal forces are applied.

The communication with the sensors during the experiments was implemented on the embedded system also used in male the KIT prosthetic hand as described in subsection 3.4.1.

In general, we incorporated sensors from different fingers into the experiments to examine if they exhibited similar characteristics. The following experiments for the tactile sensors were intended to determine that the methods described in (Tomo et al., 2016a,b; Tenzer et al., 2014) and (Weiner et al., 2018a) could be successfully adapted despite differences in design like smaller magnets and the curved shape of the finger. A thorough characterization of the tactile sensor technologies used in this work is conducted in the works above. The experiments primarily give an overview of the quality, correlation and coherence of the signals generated by the different sensor modalities.

To be able to identify the individual tactile sensors for the experiments we adopted the following naming scheme: the sensor names started with the beginning letter of the finger they were included in: I for index finger, M for middle finger, R for ring finger, and L for little finger. The second letter denoted

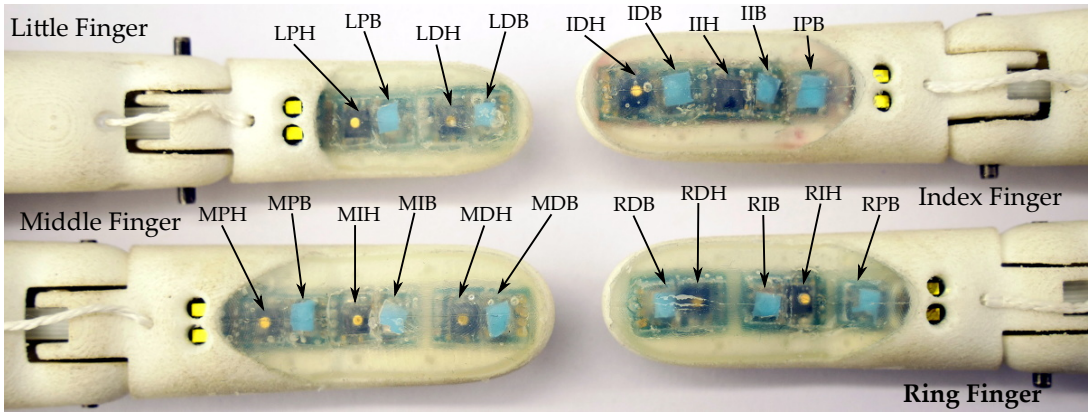

Figure 3.19.: Identifiers for all sensors on all physical demonstrators. The identifiers are named after the first letter of the finger name, their position inside the finger and the sensor type. Reprinted from (Weiner et al., 2019) without changes (CC BY 4.0).

the position inside the finger: D for distal, I for intermediate and P for proximal. Note that the little finger did not have intermediate sensors. The third letter distinguishes the type of sensor—H for Hall effect-based sensors and B for barometer-based sensors. The Hall effect-based sensor at the tip of the index finger would hence be IDH. An overview over the positions of all tactile sensors and their corresponding designators in all physical demonstrators can be seen in Figure 3.19.

Normal Force Sensor Characterization

Two types of normal force sensors are integrated into the fingers. The barometer-based normal force sensors are able to resolve small forces but also saturate at comparatively low forces. The Hall effect-based sensors do not offer the same level of resolution but are able to measure magnitudes higher forces before saturation sets in. For the normal force characterization, we used the aforementioned linear table (see Figure 3.18) to allow applying and measuring well-defined forces. In Figure 3.20 two measurements for Hall effect-based sensors ((a) and (b)) and two measurements for barometer-based sensors ((c) and (g)) are presented in green. The ground truth measurement of the force/torque sensor is plotted in orange (labelled F_n). These two measurements together are combined in the hysteresis plots ((d)–(f) and (h)) corresponding to the four sensor measurements (a)–(c) and (g).

To show the difference in resolution, we carried out an additional experiment, where a small metal plate was placed on the adjacent sensors RIB and RIH on

the ring finger. The plate distributes the load of any weight placed in its center evenly on the two sensors. For the experiment, consecutive weights with an increasing mass of 0.4 g, 0.85 g, 1.1 g, 2.2 g, 4.65 g and 10.75 g were placed on the plate. The resulting sensor readings can be seen in Figure 3.20 (i).

Both types of sensors are able to track the applied normal forces. Differences are visible in the hysteresis behavior as the barometer-based normal force sensors RDB and RPB show a more linear correspondence between their signals and the normal forces measured by the force/torque sensor. Furthermore, the hysteresis was directed in different directions for both sensor types while unloading the sensor. While the Hall effect-based sensors LDH and MIH show a notable lag when returning to the unloaded state compared to the ground truth, the barometer-based sensors overshot the unloaded state.

In terms of sensitivity, the barometer-based sensors have a clear advantage over the Hall effect-based sensor as can be seen in Figure 3.20 (i). The barometer-based sensor RIB show a discernible response even to the smallest weight of 0.4 g, whereas the noise in the signal of the Hall effect-based sensor RIH only allows the detection of the fourth 2.2 g weight with sufficient confidence. The barometer-based sensors saturate by design at 2.6 MPa which is only slightly above the maximum sensor readings observed during the above characterization at 2 N. The Hall effect-based sensors on the other hand show a clear signal at forces up to 5 N.

Overall the barometer-based sensors offer a good performance for low forces coupled with a comparatively low hysteresis. The Hall effect-based sensors offer a far wider sensing range at the expense of a more nonlinear behavior and a stronger hysteresis effect, which could arguably also be caused by the applied forces being higher.

Shear Force Sensor Characterization

To reliably allow applying shear forces, the force sensor without a probe was used to first apply a normal force of 5 N to the fingertip. The larger sensor surface compared to the probe then allowed to evenly shear the soft silicone material whereas a small probe would only cause a local and undefined distortion. As soon as the normal force threshold was reached, an increasing shear force was applied by the second axis of the linear table up to a limit of 2 N. After the limit was reached the shear force was lowered again until it reached a value close to zero. The direction of the exerted shear forces was chosen to correspond to one

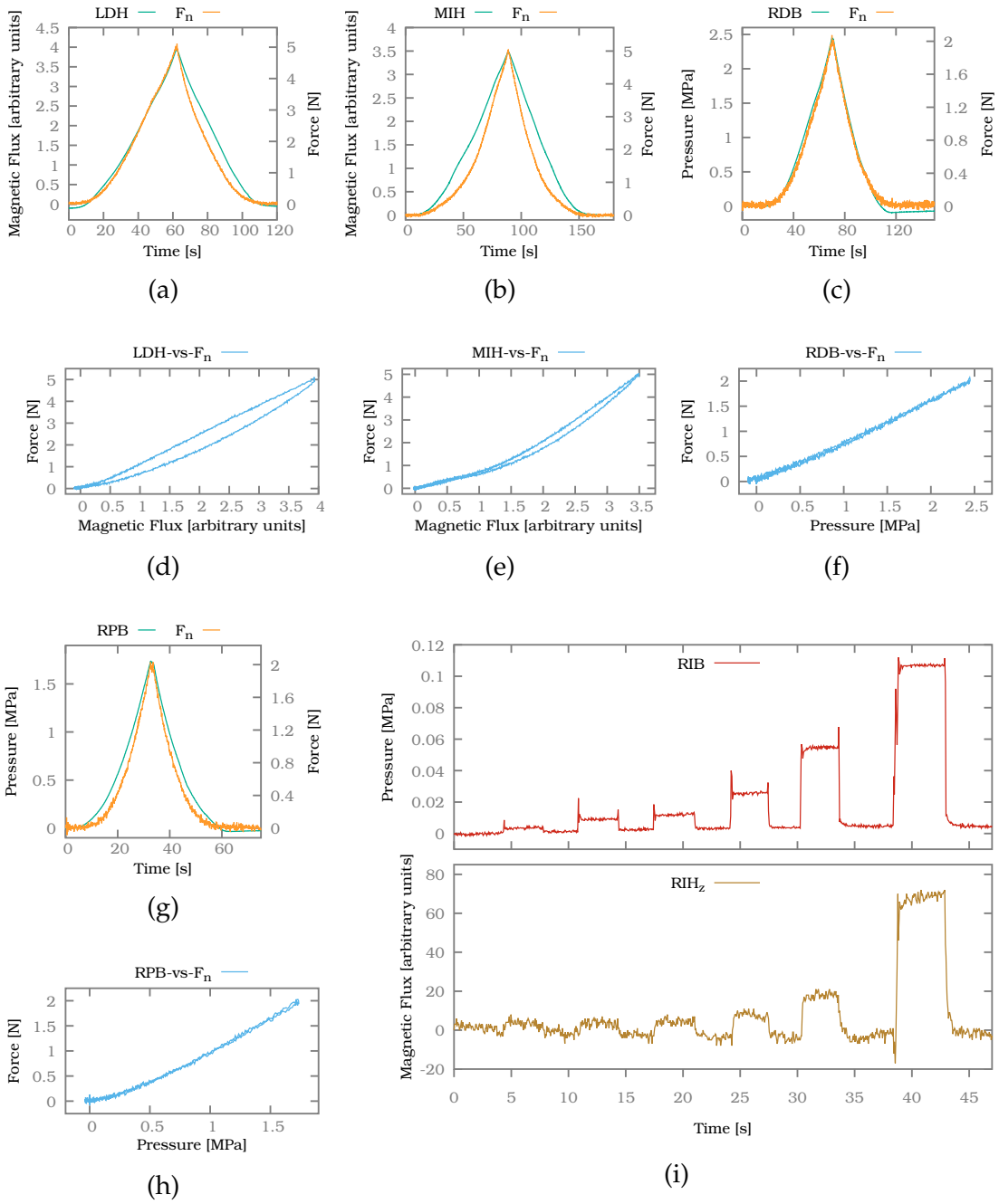

Figure 3.20.: (**a**) and (**b**) Normal force measurements for Hall effect-based sensors. (**d**) and (**e**) Corresponding hysteresis plots. (**c**) and (**g**) Normal force measurements for the barometer-based normal force sensors. (**f**) and (**h**) Corresponding hysteresis plots for the barometer-based sensors. (**i**) Weights distributed on a Hall effect- and barometer-based sensor. Reprinted from (Weiner et al., 2019) without changes (CC BY 4.0).

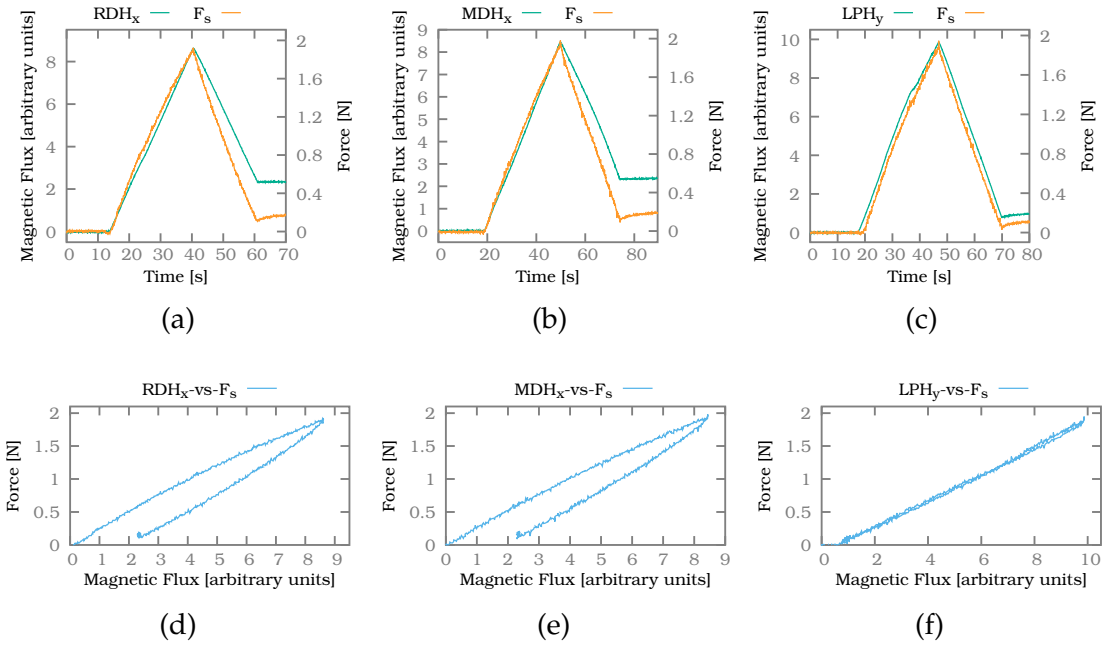

Figure 3.21.: Exemplary shear force measurements for sensor signals RDH_x **(a)**, MDH_x **(b)** and LPH_y **(c)** as well as the corresponding hysteresis plots **(d), (e), (f)**. Reprinted from (Weiner et al., 2019) without changes (CC BY 4.0).

of the two measurement axes of the shear force sensors in the fingers. For the characterization, shear force sensors in the ring finger (x-axis), middle finger (x-axis) and little finger (y-axis) were chosen. The resulting measurements can be seen in Figure 3.21. For each measurement, the shear force sensor signal as well as force/torque sensor values are plotted in diagrams (a)–(c) and corresponding hysteresis plots are provided in (d) and (e).

In general, the shear force sensors are able to correctly track the direction and rate of change of the applied shear forces. The amplitude of the signal is similar for all sensors, although not identical. Due to the anthropomorphic shape of the finger, the silicone is not evenly distributed onto the sensors but follows the curved shape of the human finger. Hence different sensors are covered by silicone of different heights as shown in Figure 3.13 and the amount of transduced pressure changes accordingly. In addition, the force/torque sensor is in almost all cases not perfectly aligned with the sensor plane since the PCBs for the sensors are mounted at a slight angle.

From the three hysteresis plots a significant hysteresis is noticeable for the sensors RDH_y and MDH_x. This is also evident at the end of the plots (a) and (b) as the signal of the shear force sensor remains notably higher than that of the force/torque sensor. For the shear force sensor LPH_y in the little finger, the

hysteresis is much less noticeable. As the little finger is the smallest, the silicone layer on top of the sensor, as well as the overall amount of silicone, is smaller than for the middle and ring finger. Hence the effect of hysteresis should also be reduced for this finger. During the characterization we found no sign of crosstalk between the sensors, meaning the magnet on one Hall-effect-based sensor did not affect the other Hall effect-based sensors. There was also no noticeable crosstalk between the Hall effect-based tactile sensors and the joint angle encoders.

It can be concluded from the above observations that the shear force sensor signals are able to track direction and dynamic of shear forces well. The sensors exhibit notable hysteresis for slow dynamic loads. The shape of the finger does not seem to influence the sensor performance too much.

Joint Angle Sensor Characterization

Due to space constraints the measurement of the joint rotation angles is performed off-axis (see subsection 3.2.1). Therefore, an experimental characterization, shown in Figure 3.22a for the MCP joint of the index finger, was necessary to determine the correlation between the calculated sensor output α_z (using Equation 3.1, based on the magnetic field strengths x_{Mag} and y_{Mag} in x and y direction) and the actual rotation angle of the joint. To determine this correlation, we moved each joint of each finger incrementally in steps of 5°, starting at 0° and ending at 90°, which corresponds to the minimum and maximum rotation angle of each joint, respectively. To ensure that only the correct joint was rotated, we fixed the other joint during the measurements. At each step the sensor output (α_z) and rotation angle were recorded, after which the joint was rotated five degrees further. The resulting correlation between rotation angle and sensor output was then used to obtain a 3rd order polynomial approximation for each joint, shown for the MCP joint of the index finger in Figure 3.22b. This approximation can be used for the real-time control of the finger to directly calculate the rotation angle of each joint during the data processing step.

As the rotational orientation of the diametrically polarized magnet can not be exactly controlled during assembly, this polynomial approximation needs to be experimentally determined for each joint individually if accurate joint angle measurements are needed. The position of the PCBs with the Hall effect-based sensors inside the proximal phalanx can also vary slightly. Alternatively, the curve can be linearly interpolated using the lowest and highest measured value for increased calibration speed at the cost of angular resolution.

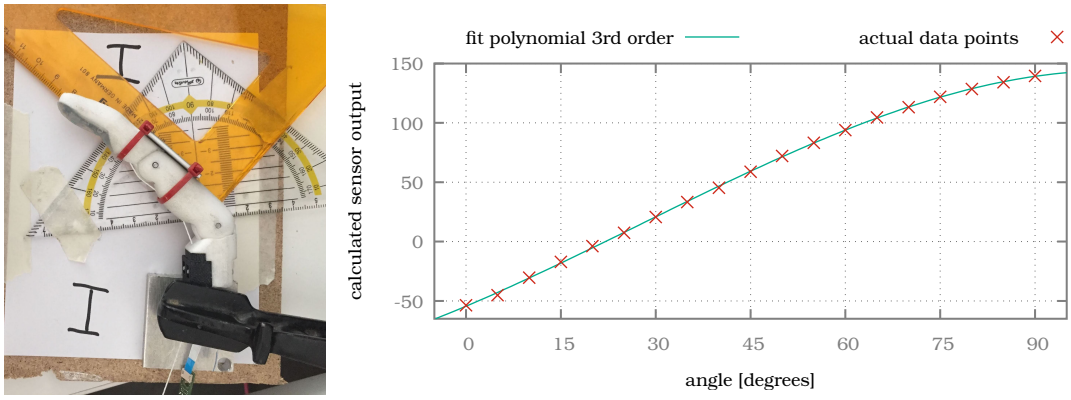

(a) (b)

Figure 3.22.: (**a**) The PIP joint is fixed and the MCP joint is incrementally rotated by 5° while the sensor output data are acquired, to determine the correlation between sensor output and actual rotation angle. (**b**) The resulting data points and 3rd order polynomial approximation. Reprinted from (Weiner et al., 2019) without changes (CC BY 4.0).

In addition to calibration, we investigated the influence of crosstalk between the magnet of one joint and the Hall effect-based sensor of the other joint. For this experiment, the distal joint was fixated and the proximal joint actuated across the full range while recording the values of the distal sensor. For the little finger, with a minimal distance of 16.7 mm between distal Hall sensor and proximal magnet, we measured a maximum of 1.1° of crosstalk. The other fingers do not show significant crosstalk as the distances between sensor and magnet are larger (23.3 mm for index/ring finger and 27.3 mm for the middle finger).

Object Grasping and Slip Detection

To evaluate the performance of the multimodal sensor system, we devised a grasping experiment where an object is grasped, held and released using two sensorized fingers. During the holding phase slip is induced. For this experiment the little and ring finger are fixed in direct opposition to each other, meaning both sensor surfaces are roughly facing each other. The tendon of the little finger can be actuated manually so that an object can be grasped in a pinch grasp configuration (see Figure 3.23, top).

Using this setup, a wooden block of 4 cm × 4 cm × 20 cm and a mass of 215 g is grasped firmly. The holding force is then lowered until slip occurs, after which the grasp is quickly fastened again twice. Afterwards, the grasp is released. All normal-force, shear-force, accelerometer and joint angle sensors for both fingers are recorded simultaneously. The bottom part of Figure 3.23 shows the signals

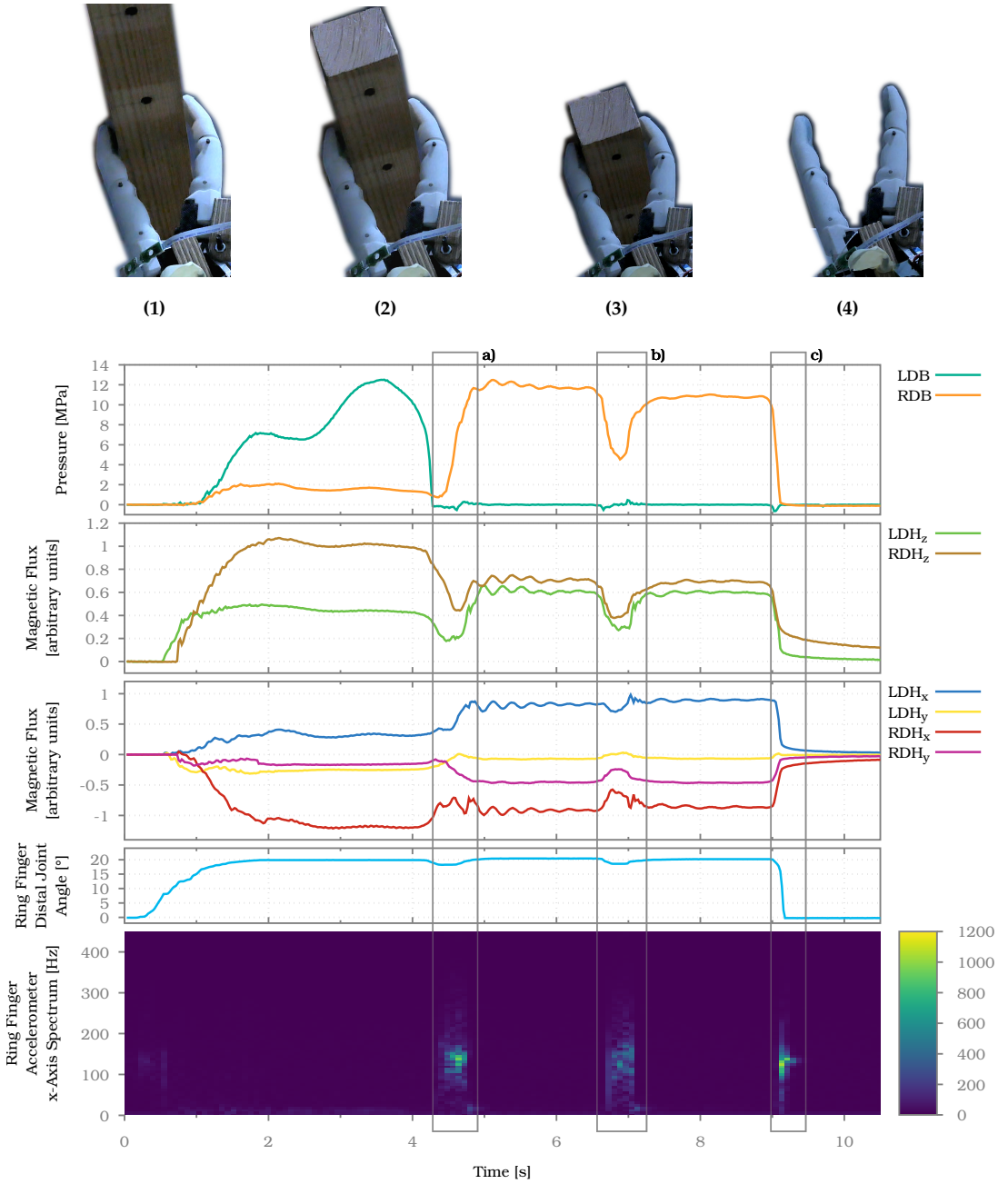

Figure 3.23.: Sensor signals recorded while grasping a block with two fingers in a pinch grasp configuration, letting the object slide twice and releasing the grasp. The top row images (1)–(4) show the static states between the slip events a)–c). Reprinted from (Weiner et al., 2019) without changes (CC BY 4.0).

of the different sensors throughout the experiment. For clarity only changing sensor values are plotted. To make the characteristic frequencies generated by incipient and gross slip visible, the accelerometer values are transformed using a Short-Time Fourier Transform (STFT).

At the beginning of the experiment the wooden block is grasped just above the centre of mass, as can be seen in Figure 3.23 (1). The distal barometer-based sensor of the little finger LDB and the distal Hall effect-based sensors LDH_z and RDH_z are loaded. This means that the point of contact on the little finger is located between the LDB and LDH sensors, whereas the contact point on the ring finger is close to the RDH sensor. Both shear force components LDH_x and RDH_x show a signal proportional to how near they are to the contact point, according to their normal force component. Since the shear force sensor in the ring finger is rotated by 180°, its values are negative, whereas the values of the shear force sensor in the little finger are positive.

After around 5 seconds the first slip event occurs, marked by box a) of Figure 3.23. Just prior to the event, grip strength is reduced as indicated by all sensors LDB, LDH_z and RDH_z. The reduction of grip strength also results in a slight reduction of the joint angle in the distal joint of the ring finger (fourth plot). The gross slip is detected by the accelerometer y-axis, as can be seen in the STFT of the signal at box a) (fifth plot). As soon as the slip occurs, the grip is manually tightened again. During the slip event, the contact point of the block on the fingers changes, as can be seen when comparing Figure 3.23 (1) and Figure 3.23 (2). On the ring finger the contact point moves between the sensors RDB and RDH, whereas on the little finger it moves away from LDB towards LDH. Hence the normal force sensor RDB gets loaded while RDH_z gets partly released. The opposite is true for the little finger. The slip event also induces a small pendulum motion on the wooden block around the two contact points which can be seen in the small waves in all loaded sensors after the first slip event.

The second slip event occurs at around seven seconds and is again induced by reducing the grip force, as can be seen in the signals of LDH_z, RDB and RDH_z. The joint angle also changes slightly as the grip is released. Again, the slip itself is clearly visible in the signal of the accelerometer in the ring finger. After the slip event the block is grasped near the top, as can be seen in Figure 3.23 (3). At around 10 seconds the grip is released, causing a very short but intensive slip event. The fingers are fully opened again, as can be seen in Figure 3.23 (4), and is also visible in the joint angle measurement. As can be seen in the last two seconds of the plot, the shear force sensors LDH and RDH exhibit hysteresis after unloading, whereas the normal force sensor RDB returns to zero immediately. The same holds true for the normal force sensor LDB at the time it is unloaded.

The experiment shows that distinct events during grasping, such as making or breaking contact, as well as gross slip, can be detected by not only one single

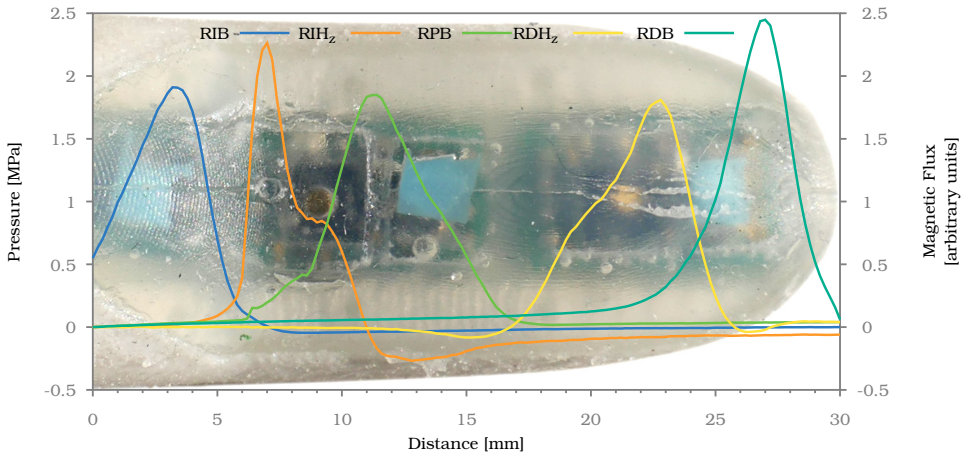

Figure 3.24.: Normal force signals for sensors of the ring finger while probed with 2 N of normal force along the axis from the proximal end of the fingertip to the distal end. The background image shows the approximate position of the probe on the finger at the time of each measurement. Reprinted from (Weiner et al., 2019) without changes (CC BY 4.0).

sensor modality but multiple different modalities. This allows for the fusion of sensor data from different modalities in order to gain more confidence for the detection of events during grasping.

Spatial Resolution and Sensitivity

The following experiment determines how the different sensors and sensor types in the fingertip, namely normal force and shear force sensors, respond to a fixed normal force applied at varying locations along the fingertip. The linear table, see Figure 3.18, is used to apply a normal force to the finger using the probe on the force/torque sensor. As soon as 2 N of normal force is reached, a measurement of the finger's sensors is taken. The probe is then lifted again and moved by 0.25 mm along the long axis of the fingertip. The probe is lowered again to apply force and read the resulting sensor outputs. This process is repeated incrementally, starting from the proximal end of the sensorized surface of the fingertip and ending at the distal end. Measurements were taken at an interval of 30 s to limit the influence of hysteresis on the experiment results. The result for the ring finger can be seen in Figure 3.24.

As can be seen, even a small probe of 5.3 mm could be detected almost everywhere along the fingertip. Only between 16 mm and 18 mm the probe remained hard to detect. Normally, the sensor response should be highest above the sensor

itself, so in the case of the barometer-based sensors at the position of the blue pad and in case of the Hall effect-based sensors around the golden magnet. As can be seen in the plot this was not the case. The spatial shift in sensor response can be explained by the uneven surface of the fingertip, which can be seen in Figure 3.13. Since the surface was not even, not all parts of the probe made contact with the finger at all positions. At the curved parts the contact area where smaller and more to the edge of the probe. This in turn shifted the positions of the signals perceived by the sensors.

Together with the observations from object grasping and slip detection experiment, it can be concluded that the spatial resolution of the finger is sufficient for use cases concerned with grasping and lifting objects of daily life, while for fine-grained manipulation tasks a higher sensor density is desirable.

3.2.3. Discussion

In this section we introduced the concept and implementation of completely scalable robotic fingers with a sophisticated multi-modal sensor system. The fingers are modelled using a skeleton-based parametric model that allows adaptation of all relevant finger dimensions. The embedded electronics is based on readily available sensors and rely on standard design and production techniques. Different sensor modalities have been included in the finger, namely normal and shear force sensors, a distance sensor, an accelerometer as well as joint angle encoders. In addition, each sensor chip includes a temperature sensing element. The sensor system is realized as a number of interchangeable modules that reflect the scalability of the mechanical model and allow easy adaptation of the sensor suit to different applications and finger sizes. All tactile sensors are encased in soft silicone while cables and other sensors are encapsulated in the finger itself to increase mechanical robustness. Conceptually, the sensor system is not limited to the presented sensors but can be completely exchanged with any sensor(s) that interface to an I^2C bus.

We characterized the tactile sensors, allowing for an informed comparison of two promising tactile sensing methods from literature and show how the detection of distinct events during grasping can benefit from a multi-modal sensor setup. The characterization regarding normal and shear force measurements (see subsection 3.2.2) for the tactile sensors have shown that these are susceptible to hysteresis induced by the silicone. Evaluation of multiple sensors in different fingers shows that this hysteresis, as well as the magnitude of response to forces,

is similar for all sensors of each type, indicating that the influence of different shapes of the fingers is minor. The large range of tested sensors also shows that the production process is reliable, as well as repeatable. The density of sensors in the finger is sufficient for the location of the point of contact with an object without larger blind spots (see Figure 3.24). Detection of distinct events during grasping and manipulation is not only dependent on tactile sensors but can be realized through sensor fusion of all available sensor data from distance sensors, accelerometers and joint angle encoders (see Figure 3.23). The accelerometers have also proven to be a valuable tool for gross slip detection despite being damped by soft material.

Integration of the fingers into an artificial hand will make it possible to evaluate different sensor fusion approaches to extract semantic information from the high dimensional sensor information of four fingers. The intention is to utilize the generated information in a similar way to the human, where individual events during grasping like making or breaking contact, lifting and slip seem to define sub-goals during the grasping process (Johansson and Flanagan, 2009a). Detection of such events allows breaking down and controlling the different phases of a grasp.

3.3. Soft Scalable Sensorized Fingers

While the rigid finger design presented in section 3.2 provides high robustness due to the strong plastic and rigid joints, only the distal phalanx is sensorized and covered in silicone. The proximal phalanx could only be sensorized in fingers with large dimensions, as the joints with their ball bearings take up most of the space inside the phalanx. The silicone is important, since it aids grasping since it conforms to the local geometry of the object and hence increases friction. Both these points are addressed with the development of soft sensorized fingers. Mechanically, these fingers are based on the design presented in (Hundhausen et al., 2020), where a leaf spring is combined with bone segments cast into silicone, to form a finger completely covered in soft material. Since the joints take up less space, it then becomes possible to cover the proximal phalanx with additional sensors. These fingers are used in chapter 5 for human-inspired autonomous grasp control. This section has been reprinted from (Weiner et al., 2021), "Detecting grasp phases and adaption of object-hand interaction forces of a soft humanoid hand based on tactile feedback", IROS 2021, ©2021 IEEE.

3.3.1. Mechanical Design

The mechanical design of the soft fingers is based on the soft fingers with integrated cameras from (Hundhausen et al., 2020). These fingers are comprised of 3D-printed bones for the distal, intermediate and proximal phalanx, connected by a leaf spring. The distal and intermediate phalanx are fused at an angle. The whole finger is then encased in soft silicone and actuated using a tendon. Compared to the hand by Hundhausen et al. (2020), in which each finger tip is equipped with a high resolution camera, we have adapted the mechanical structure of the finger to Printed Circuit Boards (PCBs) mounted on the distal and proximal bones of the finger. The plastic leaf spring in the original design has also been replaced by a steel leaf spring with 90 µm thickness, which also made it possible to attach the spring to the bones using screws instead of glue. Two Flat Flex Cables (FFCs) are taped to the spring, connecting the PCBs at the finger bones. An overview of the design of the fingers is depicted in Figure 3.25.

After the concept was explored using a non-scalable Computer Aided Design (CAD)-model, the model was extended to support scaling of the fingers in the same manner as presented in subsection 3.2.1.

3.3.2. Embedded Sensor System

The sensor system used in the fingers is based on work presented in section 3.2 originally developed for rigid fingers. The sensor system includes normal and shear force sensors, accelerometers, joint angle encoders and proximity sensing in each finger. Our approach toward the realization of sensorized humanoid hands relies on using commercially available off-the-shelf components and fabrication techniques to allow a reproduceable design. Hence, we use digital sensors on standard PCBs, which are connected to a central processing unit by a digital bus (Inter-Integrated Circuit (I^2C)). For the design of the sensor system for this soft hand in this work, we adapted all but two sensing modalities described in section 3.2. Unchanged are the accelerometers in the fingertip as well as the 3D hall effect sensors used for shear force measurement.

We replaced the time-of-flight based distance sensor by a proximity sensor as the sensor is covered by silicone and the silicone reflects some light and hence interferes with the time-of-flight measurement. Inspired by the results presented in (Yamaguchi et al., 2018), we integrated an infrared proximity sensor (VCNL4040, Vishay Semiconductors) at the base of the distal phalanx. Since the soft fingers have no clear axis of rotation in the joints and can also additionally

(a)

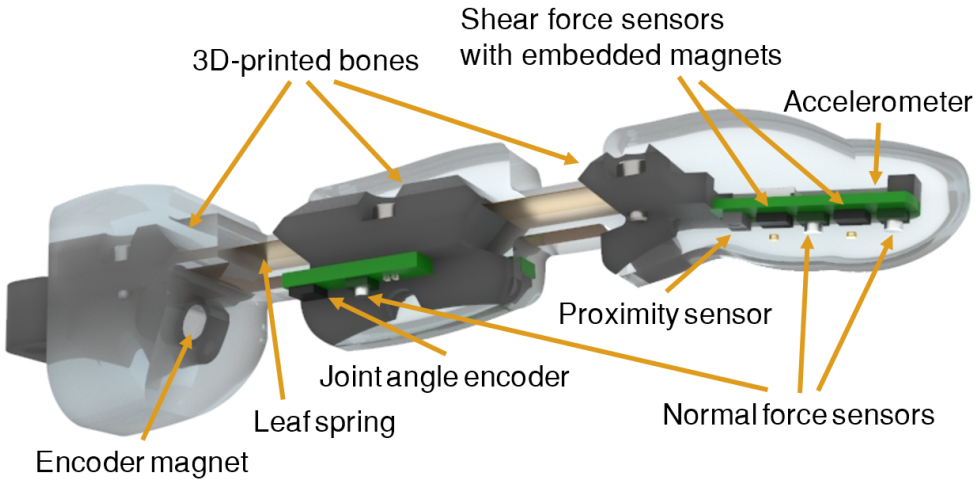

(b)

Figure 3.25.: (a) Palmar side of the soft finger. (b) Section view through the fingers silicone and distal bone exposing the internal structure and sensors visible from this side. The PCB with sensors on the intermediate phalanx covers both sides of the finger, as can be seen in (a). Reprinted from (Weiner et al., 2021), "Detecting grasp phases and adaption of object-hand interaction forces of a soft humanoid hand based on tactile feedback", IROS 2021, ©2021 IEEE.

twist, the joint angle measurement has also been adapted. Namely, we placed a magnet at the distal and proximal phalanx facing the respective joint and two 3D hall effect sensors at the intermediate phalanx facing these magnets. If the joint is actuated, the magnet moves closer to the sensor. This results in a nonlinear but monotonic signal that has been measured and fitted using a piecewise linear function.

Lastly, we adapted the barometer-based sensitive normal force sensors. The design we presented in section 3.2 uses barometers with a metal lid and a miniature hole for air, which made it necessary to encase them with small casted silicone covers. The cover ensured that an air pocket is formed above the sensor, transducing the pressure through the miniature hole in the lid to the sensor. Another work circumvented the problem by carefully removing the lid, drilling the hole open and gluing the lid back onto the sensor (Koiva et al., 2020). For

the soft fingers we now use barometers usually used for medical applications (LPS27HHW, ST Microelectronics), which feature an exposed sensor covered by soft gel. It is hence possible to directly cast the sensors into silicone without any prior modifications or additional covers, which greatly eases production. The barometer-based normal force sensors show a similar performance to the ones described in our previous work.

Similar to the rigid scalable fingers (see subsection 3.2.1), scalability of the electrical system is realized with small PCB modules that can be freely combined.

3.3.3. Discussion

In this section we described the design of a soft finger variant, that uses the same methods for mechanical and electrical scalability as the rigid counterparts (see section 3.2). In contrast to the rigid fingers, the soft fingers are completely encased in silicone, which enhances friction and compliance. The leaf spring in the joints provides stability and allows to fix the cables to the neutral phase of rotation. The soft fingers show how the three two core concepts introduced for rigid fingers – namely mechanical scalability based on a skeleton-based CAD-model, the electrical scalability based on PCB modules and the use of off-the-shelf digital sensors – can be transfered to different finger designs. As the underlying sensor system is very similar to one utilized in the rigid fingers, we evaluate these fingers directly as part of autonomous grasping described in chapter 5.

Grasping experiments with these fingers also revealed several shortcomings of the design. The metal leaf spring deforms plastically if bent below the minimum bending radius. The bending radius is proportional to the thickness of the spring, which puts a limit on the maximum thickness and hence the stability of the joint. Therefore, the stability of the joint is limited by the leaf spring and consequently the fingers exhibit a lower maximum load as their rigid counterparts. The leaf spring to a degree also allows torsion of the joint, which makes tracking of the joint position more difficult. As everything is covered in one piece of silicone, the silicone cover needs to be removed for repair of the finger and afterwards the finger needs to be cast into fresh silicone.

3.4. Intelligent Embedded System

To make use of the multimodal data from the sensors in fingers and palm, the data must be aggregated, fused and processed by a central system to enable intelligent behavior and control. Embedding this processing system directly into the hand has several advantages. Prostheses can remain as stand-alone devices, without the need to connect external computing recourses like smartphones or PCs to the hand. Robotic hands can implement a well-defined interface by aggregating all sensor data on the embedded processing system and sending the data via a bus interface. This strong modularization makes it possible to easily change hands on the robot using a quick-change adapter.

Such an embedded system has to provide numerous interfaces to read all individual sensors in real-time. Each finger is connected through one or two Inter-Integrated Circuit (I^2C) busses, and these busses should be read in parallel to ensure high sample rates for up to 150 sensors in the fingers. In addition, a camera is connected to the embedded system which needs high data throughput interfaces and requires both image processing capabilities and sufficient Random Access Memory (RAM) for image storage. The embedded system further needs to be as small as possible to leave room inside of the palm for actuation.

The following section presents two different approaches to the design of an embedded system that meets the above requirements. The first is based on a high-speed ARM microcontroller. The second embedded system is based on a System on Chip (SoC) combining an Field Programmable Gate Array (FPGA) with an ARM application processor. While the former is characterized by a low space requirement and energy consumption, the latter allows for truly parallel data readout and processing through the FPGA and application processor coupled with dedicated RAM at the expence of space and energy consumption.

3.4.1. Microcontroller-Based System

In recent years ARM-based microcontrollers with high clock frequencies as well as comparatively large RAM and flash became available. Due to their energy efficiency, ease of use, low price and feature-rich peripherals such a controller has been chosen as a base for the embedded system in the female prosthetic hand as described in subsection 3.1.1. The embedded system inside of the female prosthetic hand needs to interface to an Inertial Measurement

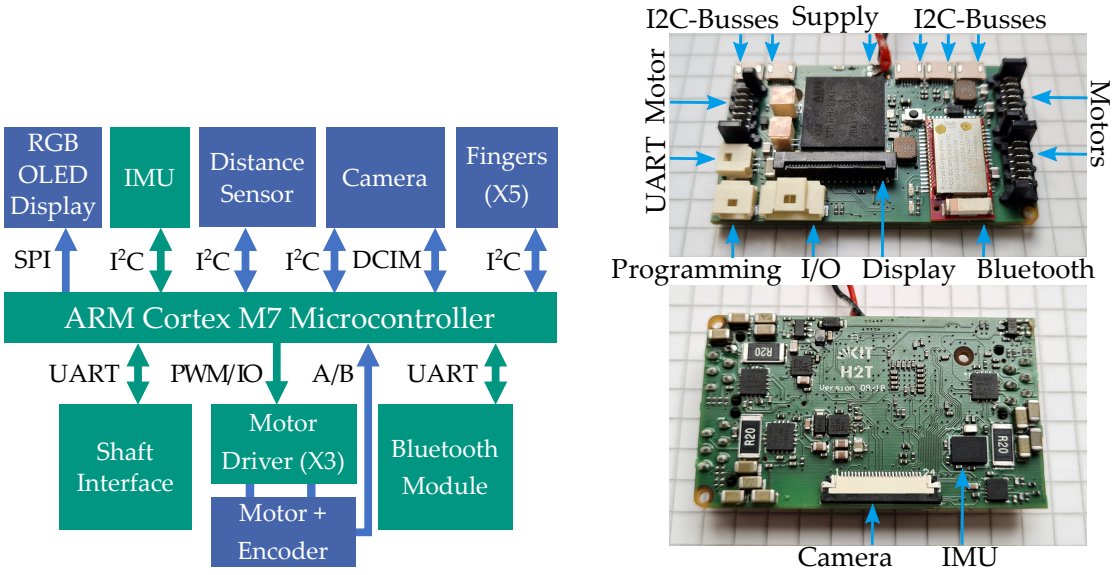

Figure 3.26.: a) Block diagram showing the functional units of the embedded system inside the female prosthetic hand. Parts in green are directly placed on the central Printed Circuit Board (PCB), the parts in blue are separate components distributed throughout the hand. b) Overview of the finished PCB

Unit (IMU), distance sensor and a camera, two motor relative encoders, two Electromyography (EMG) electrodes and a display. In addition, two motor controllers need to be included as well as an serial interface for communication with electronics in the prosthesis shaft and a Bluetooth connection. Furthermore, four I^2C busses for sensors in fingers should be included for future use. The microcontroller on the embedded system needs to be able to run a Convolutional Neural Network (CNN) used for object recognition on the camera images in less than 150 ms as this is estimated to be an acceptable delay in user interaction (Farrell and Weir, 2007).

Based on these requirements an ARM Cortex-M7 core (STM32H7, STMicroelectronics) with 2 MB flash, 1 MB of RAM and a clock frequency of 400 MHz is chosen. At the time of writing, STMicroelectronics provides ARM microcontrollers with the highest clock frequencies coupled large amounts of RAM and small housing footprints.

An overview of the complete embedded system is shown in Figure 3.26. The PCB measures 52 mm×30 mm×9.7 mm. Figure 3.3 in Subsection 3.1.2 shows the integration of the embedded system into the palm of the female prosthetic hand. The female prosthetic hand and hence this embedded system is utilized

for resource-aware image recognition in (Hundhausen et al., 2019) and semi-autonomous control of prostheses (see chapter 4).

While the microcontroller-based embedded system is very small, energy-efficient and has been successfully used in the female prosthesis, it exhibits several downsides. Scheduling of the readout of all sensors in the sensorized fingers via the five I^2C busses is time-consuming. Even though the controller possesses a capable Direct Memory Access (DMA) unit, only communications with individual can be outsourced. Hence the processor needs to interrupts its normal program execution for each new sensor on each bus to configure the DMA for the communication and retrieve the results of the last communication. This results in a considerable interrupt overhead considering the fingers include around 150 sensors. While in (Hundhausen et al., 2019) the feasability of implementing a CNN on the embedded system in the thesis has been shown, the small amount of RAM together with the amount of available processing power presents a challenge for resource-intensive tasks like CNN-based object recognition. This limits the amount of recognizable objects and hence the benefit of semi-autonomous control schemes which are dependent on visual information.

3.4.2. System-on-Chip-Based System

The limitations of the microcontroller-based embedded system discussed in subsection 3.4.1 arise mainly from the large amount of parallel tasks and operations. We hence explore the use of an FPGA for parallel communication on all I^2C busses of the sensorized fingers and its ability for massively parallel integer calculation. To keep the footprint small, we chose a SoC (Zynq 7020, Xilinx Inc.) that integrates both an FPGA with 85000 logic cells, 4.9 MB Block RAM and 220 compute units (DSP slices) as well as a dual-core ARM A9 application processor. In addition, 256 Gbit of dedicated DDR-3 RAM are installed to not be dependent on the small build-in memory. An overview of the components is provided in Figure 3.27a.

The physical system is depicted in Figure 3.27b. The embedded system is assembled from two individual PCBs, one for the processor and communication interfaces and one for power supply and motor controllers. Both PCBs are connected through two miniature connectors with 20 signals each. The physical separation of power and digital electronics aids signal integrity, especially for high speed signals. All 45 signals running between the processor and the RAM require impedance matching of the traces to 50 Ω, which made it necessary to

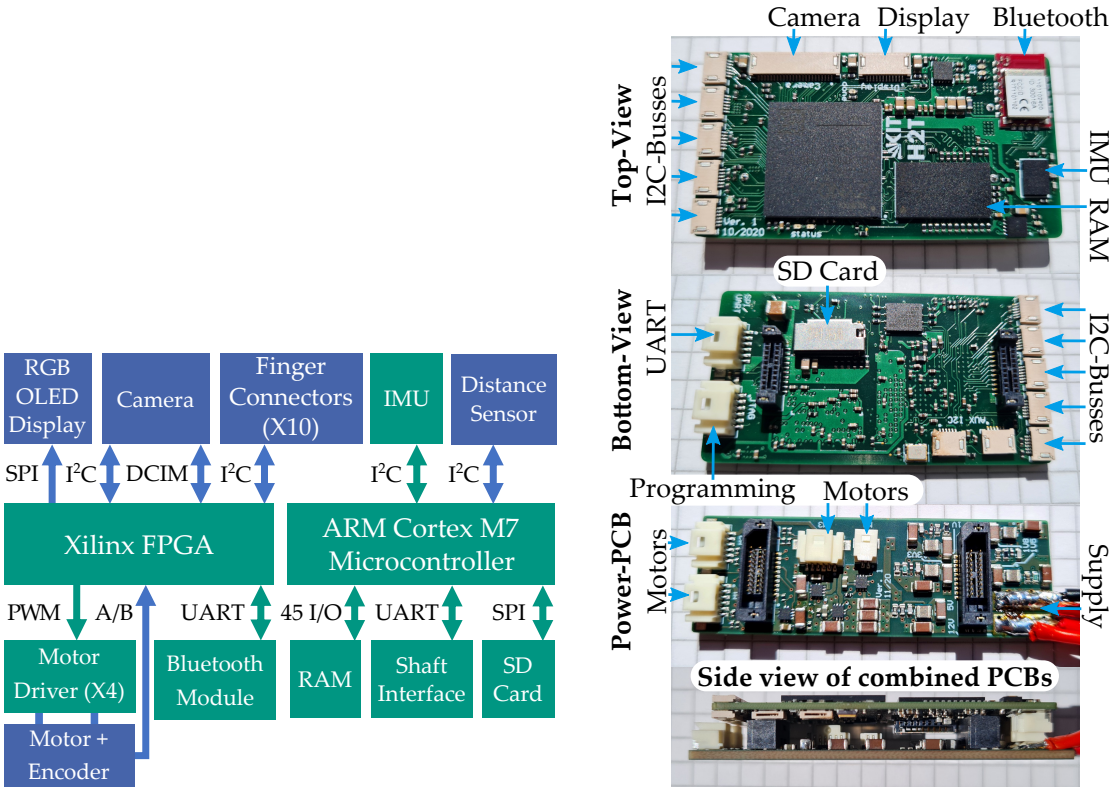

(a) (b)

Figure 3.27.: a) Block diagram showing the functional units of the SoC-based embedded system. Parts in green are directly placed on the central PCB, the parts in blue are separate components distributed throughout the hand. b) Overview of the finished PCB

route the PCB on eight layers. To match the impedance, signal and plane layers are furthermore separated by particularly thin dielectric layers with 110 µm, which also reduces the thickness of the PCB to just over 1 mm. The embedded system measures 64 mm×29 mm×9.93 mm.

3.4.3. Discussion

This section introduced two embedded systems suited for integration into prostheses and humanoid robotic hands. One is based on a microcontroller while the other is based on a SoC comprising a dual-core application processor and a FPGA. The microcontroller-based system has been successfully used for semi-autonomous control (see chapter 4) and for resource-aware object recognition in (Hundhausen et al., 2019). The SoC-based system is currently being integrated into the third generation of prosthetic and humanoid robotic hands, which will be used as the hands for the upcoming humanoid robot ARMAR-7. An early

prototype of the SoC-based system is used to read the sensor-streams of the soft sensorized fingersb utilized in the evaluation of the human-inspired grasp phases controller (see chapter 5).

3.5. Summary and Review

This chapter introduced the hardware necessary to implement intelligent behavior for anthropomorphic hands and thereby provides an answer to the first research question posed in this thesis:

How to perceive the environment as well as capture the prosthesis user state and intention to implement helpful autonomous behavior?

First, the KIT humanoid hands are introduced as the basis for both the hardware development and research into control strategies in this thesis. Second, rigid and soft finger designs were presented that combine mechanical scalability of the fingers with a multimodal haptic sensor system. Third, embedded systems for prostheses are developed, capable of reading the numerous sensors and computing Convolutional Neural Networks (CNNs) for object recognition. We evaluated both the developed prosthetic hand and the multimodal sensor system in the fingers functionally regarding key performance characteristics.

The KIT Humanoid Hands: The core idea of the KIT humanoid hands is to build human-sized, human-weight hands with integrated intelligence. On the one hand, an underactuated mechanism distributes the force of a single motor to all four fingers adaptively, meaning even if individual joints are blocked, the others can still close. This mechanical intelligence allows the hand to wrap its fingers around arbitrarily shaped objects without the need for explicit control. Sensors such as a camera, a distance sensor and an Inertial Measurement Unit (IMU) provide information about the hand's environment to an embedded system for control and intelligent behavior. The hand is evaluated regarding grasping forces and performance in Activity of Daily Livings (ADLs).

Rigid and Soft Scalable Sensorized Fingers: Two mechanical and electrical designs for prosthetic and robotic fingers are proposed. One design is based on soft silicone material enclosing an endoskeleton structure while the other is made of 3D-printed rigid parts. The mechanical model of both finger designs is

fully scalable according to a few high level parameters such as bone lengths and joint dimensions. Both fingers include a multimodal sensing system, comprising normal and shear force sensors, accelerometers, distance sensors, temperature sensors and joint angle encoders. The complete sensor system can be scaled with the fingers, such that larger fingers contain more sensors than smaller ones. The sensor system is split into small modules to enable this scalability.

Intelligent Embedded System: An embedded system positioned directly inside a prosthesis or humanoid robotic hand enables the execution of intelligent behavior based on multimodal sensor data. Therefore, two versions of the embedded system are developed, one with an microcontroller and one with a System on Chip (SoC). The embedded systems are able to read all sensor data from haptic sensors in the fingers and from environmental sensors like distance sensor and camera in the palm. The microcontroller or SoC allows the implementation of CNNs for object recognition and segmentation on images of the connected camera. Processing of all this sensor data enables the semi-autonomous pre-grasp behavior and human-inspired grasp phases controller introduced in the next two chapters.

4. Semi-Autonomous Grasping

Modern myoelectric prostheses provide a multitude of different grasping patterns as well as gestures. Classical control schemes utilizing Electromyography (EMG) signals for control reach their limit in these cases, as only a limited control signals can be distinguished. Switching between a large number of grasp types and control modes induces a high cognitive load on the user, as every command has to be issued consciously and control decision has to be made manually. In addition, EMG is prone to changes in sensor position or changes in conductance such as sweat. By automating parts of the grasping process such as the selection of the right grasping pattern, the number of required EMG inputs can be lowered.

The primary goal for the conception of the semi-autonomous controller is hence to reduce the number of EMG commands issued by the user to a minimum, thereby reducing the cognitive load required to operate the prosthesis. Two aspects are relevant to this goal. First, the resulting control should be intuitive to control, without reducing the grasping ability of the prosthesis available with classical control. Second, the user still needs to feel in control, despite the fact he is no longer directly controlling all parts of the grasping process. Not feeling in control of the prosthesis could lead to a lack of embodiment, meaning that the user does not perceive the prosthesis as part of the own body, which in turn could lead to poor acceptance of the prosthesis.

The main requirement for the development of the semi-autonomous control scheme is to only make use of the prosthesis-internal sensors and embedded systems. No external devices should be necessary to use the semi-autonomous control scheme in daily life. Hence, the control scheme can be used in any environment and situation without prior installation of sensors in the room or sensors attached to the user and without the need for external computational devices.

This chapter presents a novel semi-autonomous control scheme that infers the correct grasping pattern and approach direction using only two EMG signals. This is made possible by evaluating information from the multimodal sensor

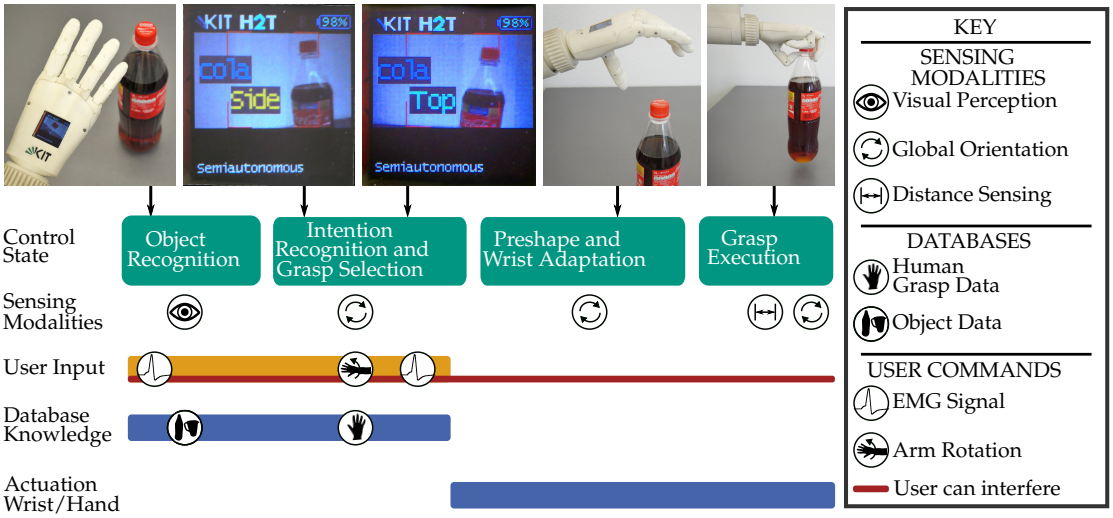

Figure 4.1.: Steps of the semi-autonomous controller, beginning with the first step on the left. User input is explicitly provided through an EMG signal and an arm rotation in the first two steps. Prior object knowledge in the object database is used for visual object recognition. Prior grasping knowledge in the grasp database is used for intention recognition and grasp selection. In the last two steps the grasp trajectory is performed on the prosthesis. User intervention is possible at any time. Reprinted from (Starke, Weiner et al., 2022) with changes (CC BY 4.0).

system embedded in the KIT female prosthetic hand (described in chapter 3). We first introduce the algorithm for the semi-autonomous control scheme in section 4.1. Second, section 4.3 details the experimental setup followed by the experimental results, presented in section 4.4. Lastly, the chapter is summarized and the results are discussed in section 4.5. This chapter, except for the conclusion, has been reprinted from (Starke, Weiner et al., 2022) with changes (CC BY 4.0). The contribution of this thesis is the design and implementation of the controller for semi-autonomous grasping that automatically selects and executes grasps based on multimodal sensor data.

4.1. The Semi-Autonomous Grasping Controller

The semi-autonomous control scheme automates parts of the grasping process to reduce the cognitive burden of the user. Simultaneously, the user can influence or stop the grasping process at any time to keep in control of their prosthetic hand. The control flow of the semi-autonomous control scheme, including the usage of sensor information, object and grasp databases as well as user

commands is depicted in Figure 4.1. An architectural diagram of the semi-autonomous control scheme is also depicted in Figure 4.2 and the finite state machine implementing the control scheme is shown in Figure 4.3. The user triggers actions of the prosthesis via muscle activations measured by a single EMG channel. Status information is presented to the user on the display at the back of the hand. Once the object to be grasped is identified based on visual information and object knowledge in the object database, the user's intention to grasp the object of interest is recognized and an appropriate grasp from the grasp database is selected. The recognized object and selected grasp type (top or side grasp) are suggested to the user on the hand display. Both the object and the selected grasp can be changed by the user. The hand and wrist motion is triggered by the user via an EMG signal to bring the hand in a suitable preshape for the selected object and grasp. The wrist orientation with respect to the object is actively maintained based on Inertial Measurement Unit (IMU) sensor data to compensate for unwanted orientation changes due to the reaching motion. Once the prosthesis is close enough to the object, it automatically closes the fingers based on the distance sensor information to firmly grasp the object.

4.1.1. Visual Object Recognition for Prosthetic Hands

To endow prosthetic hands with the ability to autonomously perform parts of grasping tasks, we utilize a vision-based approach to grasping. Given an object of interest that can be recognized with computer vision methods and an object database of daily objects, the prosthesis should be able to autonomously determine grasps and select the most appropriate one. A fundamental requirement to successfully recognize objects, plan and select grasps is that all computations should be performed in real-time on the in-hand integrated embedded system.

To achieve this ability, we use a resource-aware visual recognition system, which is based on a Convolutional Neural Network (CNN) running on the in-hand embedded system. This visual object recognition system used in this work is developed and described in detail by Hundhausen et al. (2019). Here, we give a very brief overview for completeness as the recognition of objects in the scene is key and the first step of the semi-autonomous control scheme. Within the presented controller, the object recognition is triggered by the user via a single EMG signal. A camera image is captured and processed by the recognition system to identify the object in the field of view of the prosthesis. The CNN outputs the recognition probability of all 13 pre-trained objects from a household environment and the object with the highest recognition probability is chosen.

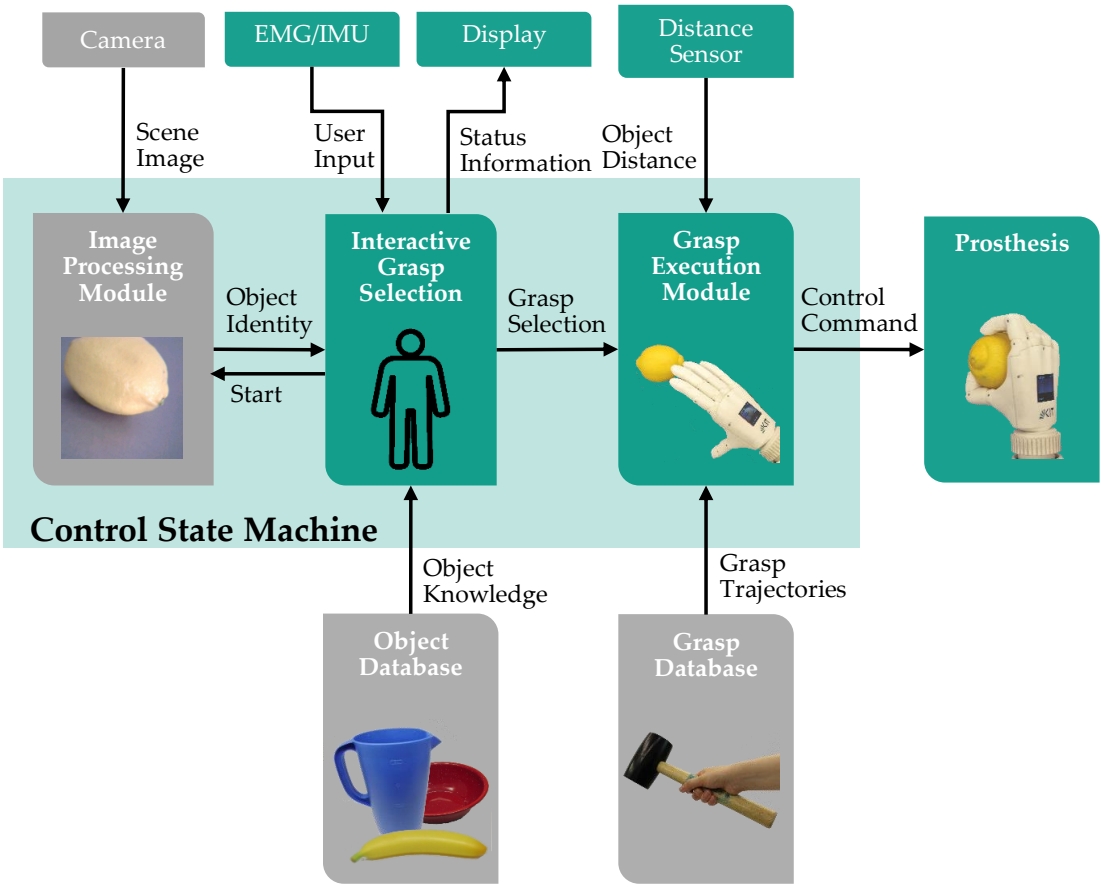

Figure 4.2.: Architectural diagram of the semi-autonomous control including the control state machine, sensor and feedback interfaces, knowledge databases and the prosthetic hand. This thesis contributes to the parts in green, gray parts are not part of this thesis. Reprinted from (Starke, Weiner et al., 2022) with changes (CC BY 4.0).

The focus of the visual object recognition as well as our semi-autonomous control scheme is set on free-standing single objects. While the CNN is capable of recognizing objects in front of varying multicolored backgrounds to some extent, the grasping of objects in cluttered environments is out of the scope of our work.

4.1.2. Grasp Database

In prosthetics, grasping is required to be stable, predictable and optically unobtrusive. Humans achieve these goals intuitively in their everyday grasping activities. Human-like grasps of the prosthesis should align with human expectations of hand behavior and therefore enhance the predictability of a prosthetic hand. Hence, the grasp trajectories in our semi-autonomous grasp control are

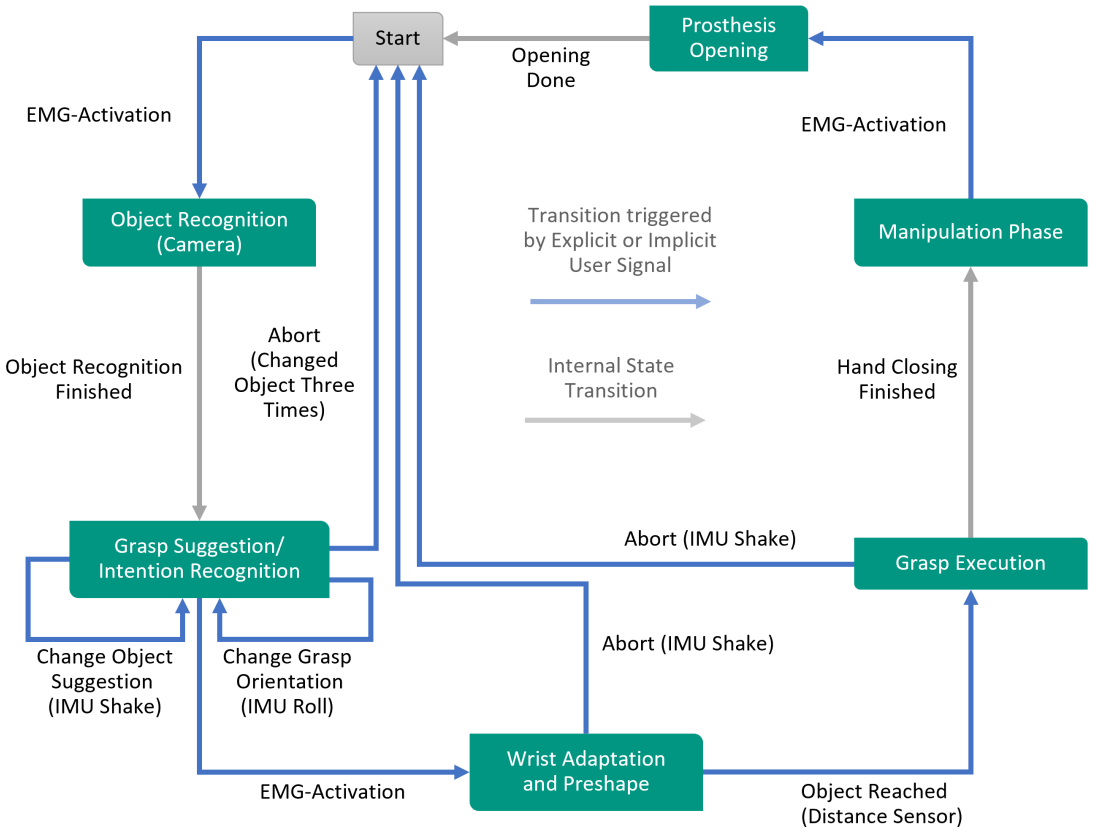

Figure 4.3.: Procedure of the semi-autonomous controller; throughout all grasp phases two explicit user signals are required and enhanced by implicit user input using the exteroceptive sensor information; the user can interfere at any time. Reprinted from (Starke, Weiner et al., 2022) with changes (CC BY 4.0).

learned from human demonstration. To this end, a grasp database with predefined human grasps on 29 objects from a household and workshop environment for the top and side grasps was created. While the grasp database is not part of the thesis, it is briefly explained here as is a vital part of the control scheme.

The human grasp demonstrations are taken from the Whole Body Human Motion Database (Mandery et al., 2016)[1]. The grasping motions consider hand orientation and finger joint angle trajectories of opposition grasps and are mapped to the prosthesis kinematics. Design and implementation of the grasp database are described by Starke (2022).

Each grasp in the database is denoted by three individual trajectories for thumb and finger closing motion as well as wrist orientation. The important characteristics of the grasps in the database is their continuous representation as they are

[1] https://motion-database.humanoids.kit.edu/

not defined by a fixed wrist orientation, static preshaping aperture and grasp pose, but instead, all degrees of freedom are controlled by continuous trajectories describing the entire motion throughout both preshaping and grasp acquisition. In contrast to a fixed hand closing with predefined preshape aperture, these continuous trajectories allow for different timing and closing order as well as interactions of the fingers and the thumb with varying, synchronized closing velocities. The third degree of freedom, namely the wrist orientation, is also described by a trajectory executed simultaneously to the finger and thumb closing motions. While the global reorientation of the hand according to the grasp orientation is performed early in the preshaping phase, IMU-based position control over all grasp phases enables further adjustment in orientation to ease the final grasp acquisition.

4.1.3. User Intention Recognition and Grasp Selection

To start the grasping process, the user takes an image of the desired object by a single muscle activation measured with the EMG electrodes, as shown in the leftmost image of Figure 4.1. The in-hand object recognition is run on this image which is recorded by the camera in the palm of the hand. Using the object information provided by the object recognition module, the object database is queried to retrieve detailed information about the given object including *object properties* and *associated grasps*. For each object, the following object properties are stored in the database: the three object dimensions, the weight of the object and its fragility. Grasps associated with the objects are stored in the human grasp database (see subsection 4.1.2). Here, a top and a side grasp are associated with most objects except flat objects and spheres that only permit a top grasp.

Once the object is identified, the user is informed about the result of the recognition by showing the object's name on the display. Based on the relation of the hand to the object, which is estimated based on IMU data, a top or side grasp is automatically proposed by the hand controller. These grasp proposals are continuously updated by the user by rotating the prosthesis. In the current implementation, a top grasp is selected if the prosthesis is held horizontally, and a side grasp is selected if the prosthesis is held at an angle of more than $\pm 15°$. The proposed grasp and orientation are shown in different colors on the display to ease the selection process for the user, as shown in Figure 4.1. The user intention, i. e. the target object to be grasped and the way to grasp it (top or side grasp), together with the object properties, is used to select, parametrize

and execute the grasp using the corresponding trajectories from the human grasp database.

It is important to emphasize that the user is able to interact with the hand during the entire process by confirming or rejecting alternatives proposed by the control scheme. If the user is satisfied with the proposed grasp, she/he can confirm and trigger the execution using one single EMG channel, which is the same as used for triggering the object recognition as described in subsection 4.1.1. Otherwise, the user is able to change the grasp direction by re-positioning their arm relative to the object.

In case of a wrong object classification, the user can reject the proposed grasp by shaking the hand. Such movement is recognized using the IMU. In case of rejection, the control scheme selects the object with the next highest recognition probability. If the first three proposed grasps are rejected by the user, the controller can be restarted by taking a new camera image for the object recognition.

4.1.4. Preshape Motion and Grasp Execution

Once a grasp is confirmed by the user, both hand and wrist pregrasp trajectories are selected from the human grasp database and executed as shown in Figure 4.3. The pregrasp trajectory is executed while approaching the object to ensure feasible hand orientation and finger aperture. The hand preshape motion and wrist orientation are performed simultaneously. At the end of the pregrasp trajectory, the wrist motion is nearly finished. The pregrasp and grasp poses are pictured in Figure 4.1 on the right.

Once the pregrasp motion is finished, the wrist is controlled to maintain the preshape orientation relative to the gravity vector using IMU sensor data, compensating rotations caused by the user's arm movements. Thereby, a correct hand orientation is ensured regardless of arm reconfiguration which might be required to reach the object, adjust grasping distance or avoid obstacles. This way, compensatory motions of the shoulder should be prevented as the user does not have to take the influence of their approach movement into account.

With the distance sensor in the palm of the prosthesis, the distance to the object is continuously measured. As soon as the distance between prosthesis and object falls below a predefined threshold and the prosthesis has reached the final posture of the pregrasp, the grasp motion is triggered and the grasp trajectory is executed. Finally, a closing force is applied. The amount of this force depends

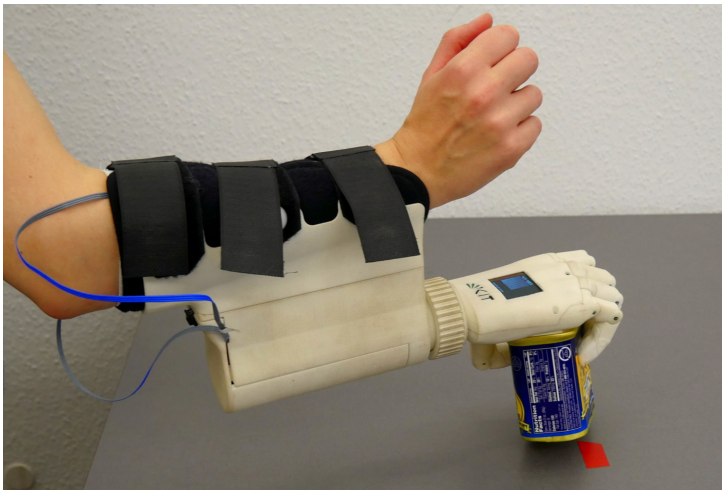

Figure 4.4.: A subject wearing the self experience shaft and prosthesis. Reprinted from (Starke, Weiner et al., 2022) with changes (CC BY 4.0).

on the fragility and weight defined by the object's properties stored for each object in the object database. Once the final grasp is completed, the object can be lifted.

At any time, the grasping process can be stopped and aborted by a shaking movement of the prosthesis detected by the IMU as described in subsection 4.1.3. The semi-autonomous control scheme focuses on the acquisition of a stable grasp. After the grasp is completed, the user can lift, use the object as needed and release the object when such action is triggered by another muscle activation signal measured by the EMG electrodes.

4.2. The Prosthetic Hand and Self Experience Shaft

The semi-autonomous control scheme developed in this work is implemented on the female KIT Prosthetic Hand presented in section 3.1 (Weiner, Starke, Rader et al., 2022). To allow the inclusion of able-bodied subjects into the experimental evaluation of the semi-autonomous control strategy developed in this work, a self-experience shaft was designed. It is used to attach the prosthesis below the arm at the palmar side of the human hand as depicted in Figure 4.4. This setup allows the execution of grasping actions by able-bodied subjects under conditions comparable to amputated users. The self-experience shaft is connected to the prosthesis by a quick release fastener. The wrist is actuated by a motor providing a pronation motion of 90° and a supination motion of 180°. Thereby it is spanning the human range of motion of forearm

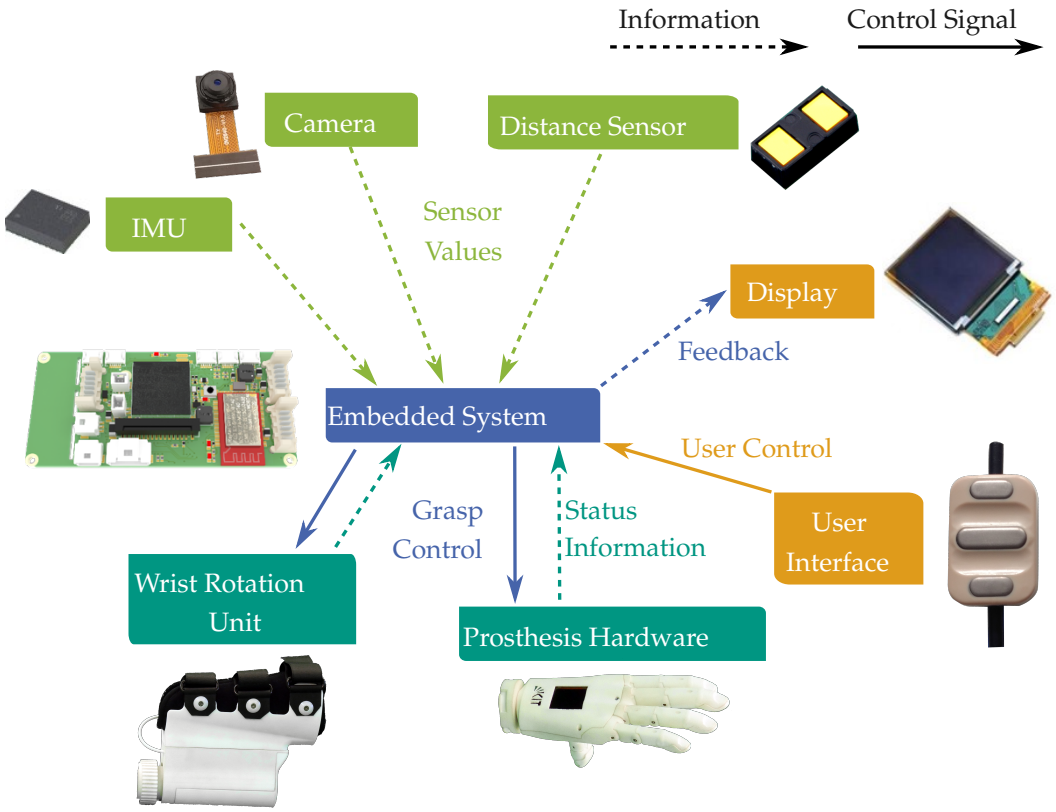

Figure 4.5.: Components of the system. Underactuated hand with two motors and ten Degree of Freedom (DoF); a sensor system consisting of camera, distance sensor and IMU; a color display and an embedded system for sensor data processing and control. In addition, the wrist rotation unit and user interface are shown, which are integrated in a self-experience shaft. Reprinted from (Starke, Weiner et al., 2022) with changes (CC BY 4.0).

pronation and supination combined with passive shoulder rotation (Wagner, 1977; Soubeyrand et al., 2017). The wrist rotation is also directly controlled by the on-board embedded system of the prosthesis. The shaft further contains the battery, powering the hand-wrist system as well as the two EMG electrodes (13E200, ottobock), which are used to measure the excitation of wrist flexor and extensor muscles.

The system components of the prosthetic hand and shaft are shown in Figure 4.5.

The developed algorithms for sensor data processing and control are running on an on-board embedded system integrated into the prosthesis as described in subsection 3.4.1. This integration allows using the prosthesis in standalone mode without the need for any external computing power, sensors or internet connection.

4.3. Experiment Design

To assess the functionality, intuitiveness and complexity of the proposed semi-autonomous control, a user study is performed comparing it to a conventional sequential control approach. A third control strategy with reduced autonomous functionality is additionally included to assess the influence of increasing autonomy of the hand on user experience and find the optimal trade-off between supporting functionality and user control. Hence, we compare three control strategies, which are all operated by the user via a standard two channel EMG input.

- **Conventional Sequential Control (CSC)** This sequential control approach allows either the wrist rotation or the opening and closing of thumb and fingers simultaneously with a fixed coordination. The two available electrode signals are thereby mapped to the two rotation directions or the opening and closing of the hand respectively. To switch between wrist rotation and hand control, both EMG electrodes have to be addressed simultaneously by a co-contraction of both muscles. This control approach is common in commercial hand prosthetics (see (Farina et al., 2014; Purushothaman, 2016; GmbH, 2014, 2016)) and represents the baseline for the comparison of our method.
- **Semi-Autonomous Control (SAC)** The semi-autonomous control applies our approach described in section 4.1, including object recognition based on the visual information, predefined grasp trajectories learned from human demonstrations and automatic hand closing based on a distance sensor located at the base of the thumb. All user commands, namely the start of the object recognition and the confirmation of a grasp proposed by the control scheme of the hand, can be generated by contracting either one or both of the muscles to which EMG electrodes are attached. Therefore, the user can issue control commands with the EMG signals that are easiest to generate for them. Aborting the current action is always possible by a fast and short shake of the prosthesis.
- **Semi-Autonomous Preshape (SAP)** Since the final hand closing is crucial for grasp success, this third control strategy allows an individual timing of the hand closing motion by the user. The preshape of the hand and the preparing wrist orientation are executed similar to the SAC strategy. However, hand closing is not triggered automatically based on the hand-object distance, but instead actively controlled by the user. While the first two control inputs similar to the SAC strategy can be triggered by any muscle

activation, hand closing is controlled by contracting the flexor muscles as in the CSC strategy. During this process, the finger and thumb trajectories are still derived from the human demonstrations and are therefore adapted according to the chosen grasp.

4.3.1. Setup and Procedure

The user study is performed with 20 able-bodied subjects wearing the prosthesis connected via the self-experience shaft on their right arm as depicted in Figure 4.4. From the nine female and eleven male subjects, ten had a background in robotics, five had no technical background. None of the subjects had experience with hand prosthetics or EMG control. The study was carried out in accordance with the recommendations of the ethical committee of the Karlsruhe Institute of Technology. The protocol was approved by this ethical committee and all subjects gave written informed consent.

The EMG electrodes are positioned for each subject individually and the electrode sensitivity is adjusted to maximize the signal quality. Electrode configurations are then kept fixed over the entire study session. During the experiment, the subject is positioned in a comfortable standing position in front of a table. A subset of the objects contained in the human grasp database is used for this user study. Ten different objects, chosen from a household environment, are successively placed on the table in front of the subject in a randomized order. The objects are depicted in Figure 4.6.

All three control strategies are evaluated consecutively in randomized order. Each control strategy is explained to the subjects by the experimenters. Subjects are given one minute prior to the evaluation to familiarize with the control and practice with an eleventh object not included in the evaluation. To begin each grasp, the prosthesis is positioned 13 cm to the front right of the object. An example for this experimental setup is depicted in Figure 4.4. For each control strategy the subject is asked to grasp all objects from the top first, then from the side if the object allows a side grasp, resulting in 16 grasps in total. If a grasp fails in the first grasp attempt, it can be repeated once. Each subject performs all three control strategies. The study is conducted with a counterbalanced crossover design of the control strategies. This means that the order of control strategies in the experiments is randomized with a similar number of participants starting with each control strategy. Additionally, the order of objects is randomized in between subjects but kept constant for all three control strategies in one subject.

Figure 4.6.: The objects used in the user study. Reprinted from (Starke, Weiner et al., 2022) with changes (CC BY 4.0).

4.3.2. Data Acquisition

To assess the performance of the semi-autonomous control scheme, several metrics are acquired in the user study. The grasp execution time is applied as metric for the grasp efficiency. Therefore, the time starting at the beginning of the grasp until lifting the object is recorded. As the quality of the object recognition is not a central part of the presented semi-autonomous control, the time required to discard wrong object recognitions is assessed individually. To quantify the required amount of physical effort, the EMG activation signal over the duration of the grasping process is recorded as a quantitative metric.

To assess complexity, success and user impression of each control strategy, a subjective questionnaire is collected. It provides the workload as measured by the NASA task load index (NASA TLX) as described in (Hart and Staveland, 1988). In our evaluation we aim to compare the workload of the different control schemes in each subject. Therefore, we apply the metric of the raw TLX and directly calculate the unweighted average of the sub-scale ratings provided by the subjects. Compared to the individual weighting of sub-scales this method has been found to be more sensitive (Hendy et al., 1993). The questionnaire is extended by several questions to quantify intuitiveness of the control, feeling of control and perception of feedback in the same style as the questions of the workload index. Furthermore, open questions on the subject's impression and preferences are asked.

4.4. Evaluation

Of all participants, 65.2 % preferred the SAC control, 25 % SAP and 12.5 % CSC. The results of the evaluating questionnaire and the recorded EMG signals are depicted in Figure 4.7. The reported preference of the SAC control strategy is also visible in the control intuitiveness as shown in Figure 4.7 a). All plots show the shape of the kernel density function around the data points. The mean is marked as a white dot, while the grey line denotes the range between the 25^{th} and 75^{th} percentile of the data. The colored points denote the answers/measurements of individual subjects. The horizontal distribution of data points is merely for visualization purposes.

4.4.1. Workload and Control Intuitiveness

The workload index of both SAP and SAC is significantly lower than for CSC, as depicted in Figure 4.7 b). The NASA Task Load Index (Hart and Staveland, 1988) ranges between 1 and 20 with higher numbers representing an increasing overall task load. With 11.8, the workload index of CSC is almost twice as high as for SAC with 6.5 and more than one third higher than for SAP with 8.5. In the following all results except the NASA TLX from the subjective questionnaire are converted from the scale between 0 and 20 to percent.

The high workload index of CSC is mainly caused by a high physical demand of 81.5 % and a high required effort of 74.4 %. A significant reduction (Friedman's Anova < 0.05) is achieved with the SAC for both the physical demand to 30.5 % and the effort to 38.3 %. Also for SAP the physical demand is notably decreased by 46.8 % compared to the common baseline of CSC. The amount of required effort and physical demand is visualized in Figure 4.7 c) and d).

The observed physical demand is clearly reflected in the use of EMG control signals. The EMG electrodes supply a filtered output voltage correlated to the muscle activation signal. Figure 4.7 e) shows the average EMG activation calculated by integrating the EMG voltage of both electrodes over the grasp trial and normalizing it according to the grasp execution time. While grasping with CSC requires an average electrode activation of 213.0 mV, in SAC only 83.5 mV is recorded. This clearly shows the lower muscle contraction due to the introduced autonomous functionality. In CSC, an EMG electrode activation is recognized three times more frequently than in SAC, proving that the reduction of muscle contraction is mainly caused by reducing the number and length of

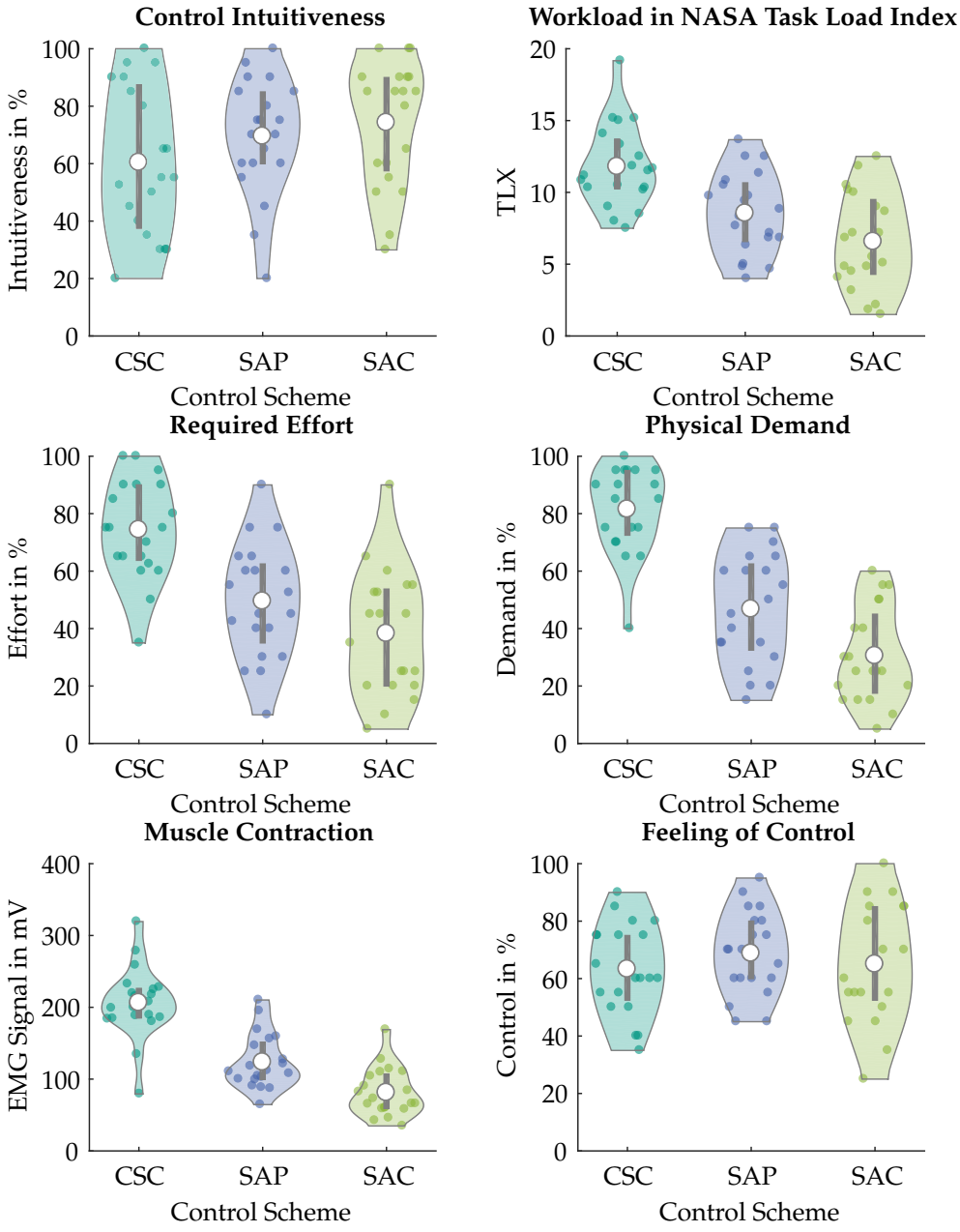

Figure 4.7.: Outcomes of the user study: (a) intuitiveness of the control reported by the subjects, (b) workload according to the NASA Task Load Index (Hart and Staveland, 1988), (c) effort put into the grasp execution, (d) physical demand of the control strategy, (e) mean muscle contraction signal over the entire recording and both EMG electrodes and (f) feeling of control reported by the subjects; all graphs show the data points together with the kernel density function, the mean is marked by a white dot and the grey line marks the section between the first and third quartile. Reprinted from (Starke, Weiner et al., 2022) with changes (CC BY 4.0).

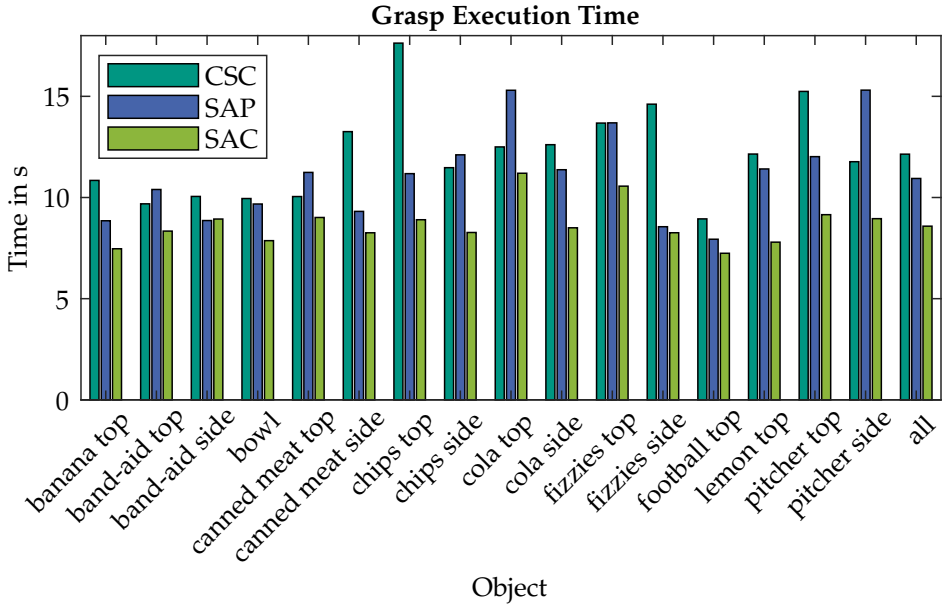

Figure 4.8.: Time required to execute the grasps on all ten objects and the overall grasp execution time in the three evaluated control strategies. Reprinted from (Starke, Weiner et al., 2022) with changes (CC BY 4.0).

necessary user inputs. As the reported intuitiveness shows, this input reduction can be achieved without a loss of trust into the device. Besides, subjects did not report any statistically significant difference in their feeling of control between CSC with 63.3 % and SAC with 65.0 % as shown in Figure 4.7 f). As expected, SAP has a higher average electrode activation than SAC. Nevertheless SAP still results in a significantly lower muscle activity of 126.6 mV compared to CSC with 213.0 mV.

The mean intuitiveness for SAC increased by 13.9 % compared to CSC. As shown in Figure 4.7 a), all three control strategies have an intuitiveness average of more than 50 %, with SAC being most intuitive with a mean of 74.3 %. In addition, a quarter of participants reported the SAC to be very intuitive when asked to describe their impression of the presented control in their own words in the questionnaire.

4.4.2. Grasp Execution Time

The grasp execution time was measured as the time needed to reach the object, grasp and lift it off the table surface. The average execution time over all subjects and objects is 12.14 s for CSC, 12.39 s for SAP and 9.64 s for SAC. For

the remainder of the evaluation, the time spent on wrong classifications by the object recognition will not be considered as the quality of the object recognition is not a central part of this work. Excluding this leads to a reduction of the average execution time to 8.7 s for SAC and 10.94 s for SAP.

A significant difference in the overall time required for a grasp is only notable between SAC and the other two control strategies SAP and CSC, respectively. The grasp execution time in SAC is 29.3 % faster compared to CSC. A quarter of the subjects specifically mentioned the SAC to be perceived as very fast. This was mainly ascribed to the automatic hand closing which was perceived as very helpful. The average grasp execution time for all individual grasps is depicted in Figure 4.8. Large and bulky objects like the football, the bowl or the canned meat are grasped from the top at a similar speed with all three control strategies. The merit of the autonomous coordination of all degrees of freedom of the hand becomes mainly apparent in objects which need a precise grasping strategy like the top grasps on the pitcher and chips. This is also evident for grasps that demand a large wrist rotation compared to the starting pose like the side grasps on the fizzies and the canned meat.

Looking at the grasp success for the 16 different grasps reveals that subjects were overall more effective in grasping objects with SAC and SAP. In total four of the 16 grasps in the conducted experiment could be executed successfully in the first trial by all participants in CSC while there were five grasps without failure in SAC and eight in SAP. Although SAP proves to be the most effective control strategy on this basis, participants preferred SAC. In addition, half of them commented on SAC being easy to control. A reason for this discrepancy might be found in the difficulties of SAP for specific cases, especially the top grasp on a package of fizzy tablets. As these have a small diameter, an accurate hand positioning is important. Keeping the exact hand position while performing a muscle contraction to close the hand was difficult for many subjects. Due to this reason, this specific grasp failed statistically once per subject.

4.5. Summary and Review

In this chapter a semi-autonomous control scheme for hand prosthesis is detailed. The scheme thereby provides an answer to the second research question posed in Chapter 1 of the thesis:

How to choose a hand preshape and wrist orientation prior to prehension?

The presented semi-autonomous control scheme exploits sensor information directly acquired on the hand to deduce context and user intention and proposes suitable grasps to the user. The control scheme is then evaluated in a user study, collecting both quantitative data and subjective feedback.

Semi-Autonomous Control: Based on sensor information directly acquired on the prosthetic hand, context and user intention are deduced and exploited to propose suitable grasps to the user. With a single EMG channel, the user is able to start the semi-autonomous grasping process and choose the desired trajectory. Grasp trajectories and object properties from an object database are selected by an image-based object recognition. The approach direction is deduced from the user's forearm orientation measured by an EMG within the prosthetic hand. Once the user has started the grasping motion via a single EMG command, a preshape is performed resulting in an appropriate hand orientation and finger aperture to approach the object. The final grasp is triggered based on a distance sensor as soon as it has reached the object. In contrast to existing control schemes, in this thesis all sensors and computations are contained in the prosthesis itself.

Evaluation: Compared to a conventional sequential EMG control, our semi-autonomous control requires less than half the amount in average EMG activation and the physical demand is rated 62.7 % lower. Together with an increase of the intuitiveness by 13.9 %, this causes a significant reduction of the workload by 26.1 %. As a consequence, the prosthesis user has to concentrate less on the performance of a stable grasp. In addition, this reduced workload allows for faster grasping especially for thin and delicate objects. At the same time, the feeling of control is comparable to the conventional sequential control as the user is able to intervene at any moment.

5. Human-Inspired Grasp Phases Controller

Robust grasping of unknown objects is a challenging task both in the field of hand prosthetics as well as humanoid robotics. In the case of prostheses, the user usually gets only visual feedback on the force the prosthesis applies to the object, so the user can only react after a observation of a slip event for heavy objects or visible singns of damage for fragile objects. The same problem exists for humanoid robot, but since robots are usually lacking an understanding of the properties of grasped objects, visual clues can in a majority of cases not be incorporated to adapt grasping forces. Both scenarios can heavily benefit from the use of multimodal haptic information to estimate grasp state and control grasping forces in a fully autonomous manner.

As neuroscientific studies have shown, humans employ a sophisticated control strategy when grasping and lifting objects (Johansson and Flanagan, 2009b). Employing this strategy in a robotic context allows to divide the difficult task of reliably grasping unknown objects into individual action phases with clear goals and transitions. This chapter, except for Section 5.1 and Section 5.4 has been reprinted from (Weiner et al., 2021), "Detecting grasp phases and adaption of object-hand interaction forces of a soft humanoid hand based on tactile feedback", IROS 2021, ©2021 IEEE. In the following the design, implementation and evaluation of this human-inspired grasp controller is detailed. First, we introduce neuroscientific findings on human grasp control in Section 5.1 as the source of inspiration for the presented grasp phases controller, followed by a detailed description of the controller itself in Section 5.2. Section 5.3 describes the evaluation and presents the experimental results. Lastly, Section 5.4 summarizes the chapter and discusses the results.

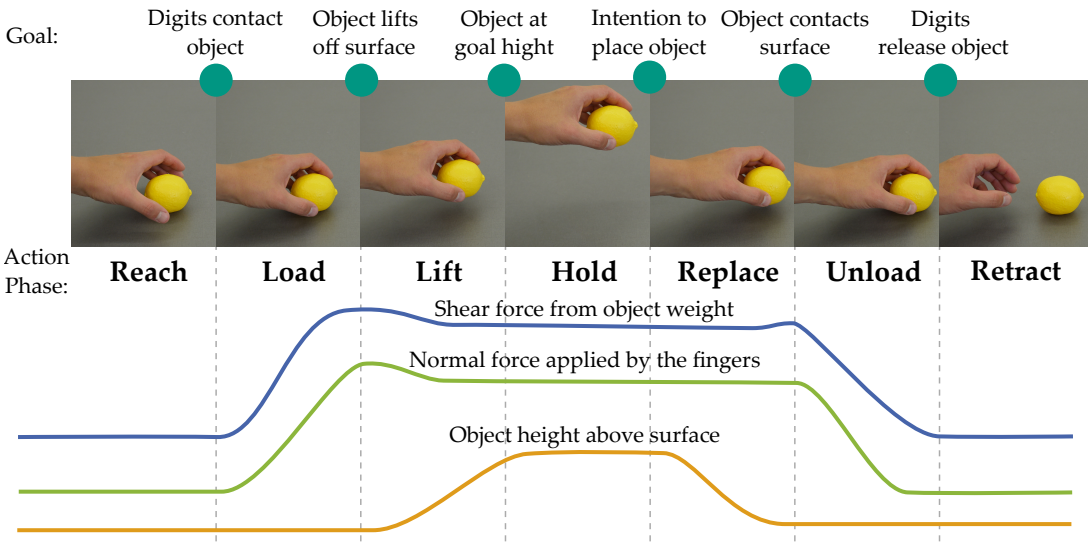

Figure 5.1.: Grasp phases and their respective task subgoals as observed in human grasping. The schematic curves show normal and shear forces acting between object and fingers as well as object height above a support surface. As can be seen, the applied normal force closely correlates with perceived shear forces and shows no disturbances or corrective actions. Control of normal forces in humans relies heavily on semantic knowledge of the lifted object as well as past lifting experiences. (Adopted from Box 3 in (Johansson and Flanagan, 2009a))

5.1. Grasp Control in Humans

Understanding of human grasp control can greatly aid development of robotic controllers. It offers a proven method that can be used as a guideline for a technical implementation. Humans are able to effortlessly grasp arbitrary objects utilizing multimodal haptic feedback and sophisticated feedforward control based on a rich body of past experiences. Roughly a decade of grasping experience is needed for children to perfect adult-like refined grasping force patterns (Forssberg et al., 1991, 1992). Rich haptic feedback is similarly important for successful grasping in humans. If the sense of touch is missing, otherwise trivial manipulation tasks are difficult or impossible to achieve for adults despite visual feedback (Johansson and Westling, 1984). Due to the high number of involved sensor signals, muscles and joints, large parts of the brain are engaged during both power and precision grasps (Ehrsson et al., 2000).

As detailed in (Johansson and Flanagan, 2009a), the human approach to grasping is to subconsciously subdivide the grasping task into a sequence of *action phases*. Each action phase has a specific subgoal and reaching this subgoal marks the

end of the phase and the start of the next phase. The subgoals are characterized by distinct sensory signals that describe a contact event or transient event. To reach this subgoal, in each action phase a specific *action-phase controller* is executed. Most of the control is based on feedforward terms while simultaneously predicted sensory signals are continuously compared to the actual signals. Any mismatch between expected and actual signals triggers corrective actions that depend on the specific nature of the mismatch, the current action-phase controller and the state of the environment. An schematic overview of the individual action phases, control goals of the action-phase controllers and grasping forces is given in Figure 5.1.

In the first phase, the *reach* phase, the fingers close around the object. The subgoal of the corresponding action-phase controller is to bring the fingers of the hand into contact with the object. In the sub-sequent *load* phase, its controller is tasked with applying normal force to the object and lifting the objects until contact with the support surface breaks. During the *lift* phase, the grasping force is further adjusted. The phase ends when the goal height of the object is reached. In the following *hold* phase, task specific manipulation of the object can take place and the phase is ended with the intent to place the object back down. The action-phase controller of the *replace* phase lowers the object down with the goal to contact the support surface. As soon as contact with a support surface is detected, the controller of the *unload* phase gradually lowers the normal force applied by the fingers to the object. When all fingers are unloaded, the fingers can open and the hand retracts.

The way that grasping is partitioned into individual phases with their own subgoal and set of corrective actions allows to subdivide the complex problem of grasping into much simpler individual control problems. (Johansson and Flanagan, 2009a) note that "*The context-dependent nature of corrective responses is reminiscent of finite-state control systems that operate by implementing rules based on IF, AND and THEN arguments*". This observation hints at a suitable implementation strategy for such grasp controllers in technical systems, which, as the authors note, has also already been successfully employed to model human walking.

5.2. Grasp-Phases Controller

Our goal is to realize a human-inspired grasping controller that is able to (i) detect the different phases of a grasping and manipulation task, (ii) adapt inter-

action forces with the manipulated object and (iii) balance the force distribution in both precision and power grasps based on multimodal haptic feedback.

The grasp-phases controller should be able to stabilize unknown objects during the whole grasping process, while minimizing the force exerted on the object based on tactile feedback. Using this grasp-phases controller, the hand should be able to grasp and lift fragile objects like a plastic cup or toast without crushing it, while it also should be able to stabilize heavy objects such as water bottles. Inspired by sensorimotor control in humans, grasping and manipulation (see Section 5.1), we consider all phases of a grasping and manipulation task, i. e. , closing the fingers to establish contact with the object, lifting, holding, manipulating and placing the object.

5.2.1. Overview of the Controller

The proposed grasp-phases controller is designed to grasp and manipulate unknown objects, without prior knowledge about object size, weight or shape is available to the controller. Hence, the controller has to infer the necessary grasping force purely based on sensor information at run-time and adapt forces at contact points in a reactive way. Figure 5.2 depicts the structure of the grasp-phases controller and employed control laws. The controller is implemented for a Hand, depicted in Figure 5.4a with three motors and five finger prototypes of the presented soft sensorized fingers (see Section 3.3)

Each of the three motors in the hand is controlled separately by its own motor controller based on the sensors in the fingers associated with the motor. The thumb motor is controlled based on the sensors inside the thumb, the index motor based on the sensors in the index finger and the third motor based on the signals from the remaining three fingers. As (Veiga et al., 2020) have shown, such an approach can reduce control complexity while ensuring the overall grasp stability based on the interaction between decentralized controllers through the object. The three motor controllers are synchronized after each grasp phase so that they start the new phase only if all fingers and motors are ready.

The code of the controller is publicly available[1]. The design of the grasp-phases controller follows two main principles: a) taking inspiration from human grasping and b) minimizing the number of necessary control parameters.

[1]Code available Online at: https://gitlab.com/ArmarX/Armar6RT/-/tree/master/source/armar6/rt/libraries/KITSensorizedSoftFingerHandV1NJointControllers

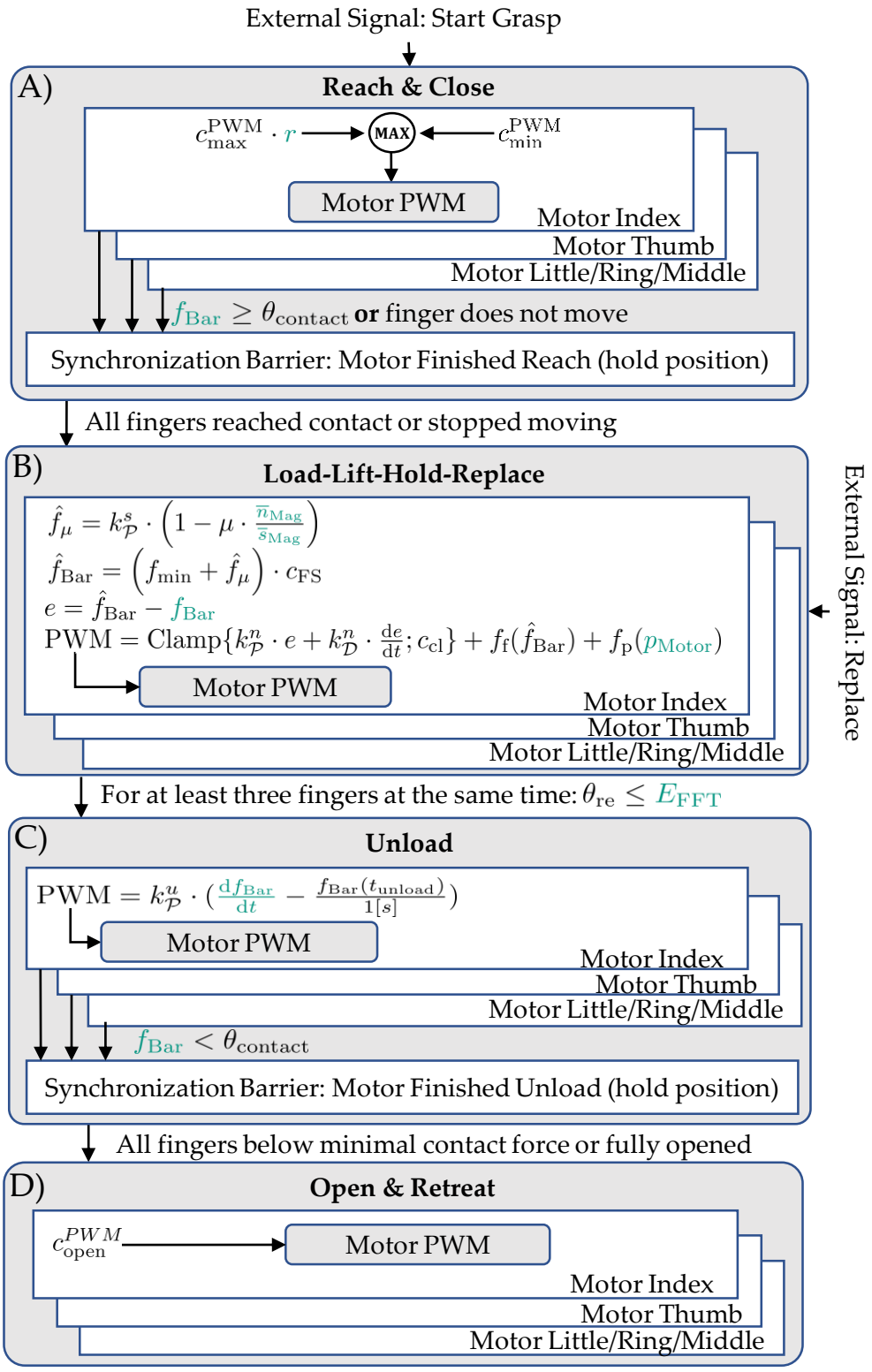

Figure 5.2.: State machine of the proposed grasp-phases controller; Values in green are continuously calculated based on sensor signals. Reprinted from (Weiner et al., 2021), "Detecting grasp phases and adaption of object-hand interaction forces of a soft humanoid hand based on tactile feedback", IROS 2021, ©2021 IEEE.

a) Human-inspired Phases of grasping and manipulation tasks The soft humanoid hand with its human-like shape and sensing modalities is predestined for the implementation of a human-inspired approach to grasping. Therefore, we divided the grasp-phases controller following the concept presented in (Johansson and Flanagan, 2009b) into the four grasping phases *reach & close*, *load-lift-hold-replace*, *unload* and *open & retreat*. Transitions between these phases are defined by contact events or sudden changes in interaction forces. Compared to the grasping phases in (Johansson and Flanagan, 2009b), our grasp-phases controller maps the four grasping phases load, lift, hold and replace to one single phase (*load-lift-hold-replace*) with one single sub-controller. We consider this assumption reasonable as, except the load phase, the lift, hold and replace phases are mainly concerned with arm motion and share similar goals in terms of object stabilization and force control. So, the goal of the grasp-phases controller, with its four sub-controllers for the four phases in a grasping and manipulation task, is to robustly grasp objects with different properties such as size, weight and shape while ensuring the right amount of forces to avoid squashing the object in the hand.

The grasp-phases controller generates Pulse Width Modulation (PWM) targets for each motor based on only two external control signals: 1) The command to start object grasping and 2) a signal indicating that the object will soon be replaced. As the controller does not rely on additional external information, it is easy to also use it in contexts such as grasping with as prosthetic hands, where only information from hand sensors is available.

b) Design of the sub-controllers For the sub-controllers, the number of control parameters can drastically influence the amount of time needed to tune the controller. Hence, we aim – wherever possible – to reduce the number of engineered control parameters. Furthermore, we selected parameters that are intuitively explainable, either in the context of the human grasping process or based on physical laws. Due to sensor offsets in the measurement of normal and shear force that depends on several changing conditions such as room temperature and atmospheric pressure, the controller automatically determines such offsets by continuously averaging these sensor values when the controller is inactive.

In the following we describe the different grasp phases and the implementation of their sub-controllers.

5.2.2. Reach & Close Sub-Controller

We assume a pre-defined grasping pose for the hand, as finding a suitable grasping pose for unknown objects goes beyond the scope of this work. The grasp-phases controller is started by an external signal at which the *reach & close* sub-controller is started for each motor. As the grasp should be executed as fast as possible, the fingers initially close with the maximum PWM PWM_{max}. To avoid hitting the object at maximum speed, the finger velocity is then scaled based on the sensor data of the proximity sensor. The values of proximity sensor $Proximity$ are normalized to the interval $[0, 1]$ where 1 indicates that no object is in the range of the sensor, i. e. , no reflected light is detected, and 0 indicates that the finger has contact with the object, i. e. , a maximum amount of light is reflected. Hence, the maximum PWM is scaled by the proximity sensor data $Proximity \cdot PWM_{max}$ to reduce the speed and gently establish contact with the object (see Figure 5.2-A). Due to this normalization, the fingers proportionally slow down as they reach a distance of around 2 to 3 cm. To make sure that the fingers establish contact with the object, the maximum value of $Proximity \cdot PWM_{max}$ and PWM_{min_cl} is used, where PWM_{min_cl} is the minimum PWM required to slowly close the fingers. Such slow closing of the fingers is also important to prevent damage of the object.

Contact with the object is detected by the contact threshold $ContactThres_{Baro}$ on signals from the sensitive barometer based normal force sensors. As soon as any finger sensor detects contact, the motor switches to position control mode to hold the position at which the contact occurred. When grasping an object with protruding edges, the finger may make contact with the object that is not detected by any normal force sensor because the sensors do not cover the entire finger. As a fallback for this case, we use the relative motor encoder to detect if the finger has stopped moving. This also covers the case where the finger misses the object and closes completely. The contact position is then held until the other two motors also bring their fingers into contact with the object or close the corresponding finger(s) completely. When all three motors are either in hold position mode or stopped moving, the sub-controllers of all three motors trigger the next phase. As described in (Jentoft et al., 2014), this contact sensing based closing behavior has advantages compared to closing the hand without sensor feedback, even in the presence of adaptive underactuation and passive compliance.

5.2.3. Load-Lift-Hold-Replace Sub-Controller

As soon as all fingers have detected contact with the object or have stopped moving, the motor controllers switch to force control mode for each motor and directly output PWM targets. Each motor acts based on the maximum over all barometer-based normal force sensor values $F_{Baro}^{FingerMax}$ measured in the fingers actuated by the motor. Specifically, the barometers are placed at the left and right of the proximal phalanx (B_{ProxL}, B_{ProxR}), at the distal phalanx next to the joint (B_{DistJ}) and next to the tip (B_{DistT}).

$$F_{Baro}^{FingerMax} = max\{B_{ProxL},\ B_{ProxR},\ B_{DistJ},\ B_{DistT}\}$$

For the motor actuating little, ring and middle finger, the maximum over all three fingers is taken.

The force controller consists of two feedforward terms as well as a PD-controller. The first feedforward term $FeedForward_{Position}^{PWM}(\cdot)$ takes the relative motor encoder position and calculates the PWM necessary to hold it. This term hence cancels the progressive spring force as a function of the motor relative encoder value. The term is realized as piece-wise linear function obtained by slowly increasing the PWM of the motor and recording the resulting finger position $CurMotorPos$. The second feedforward term $FeedForward_{Force}^{PWM}(\cdot)$ takes the target force F_{Target} as input and outputs a PWM value that produces this target. The piece-wise linear function representing this term was obtained by letting the index finger in a fully opened state press against a flat surface with increasing PWM while recording $F_{Baro}^{FingerMax}$. Lastly, a PD-controller reduces the error of the feedforward terms. This term is clamped to a value of $\pm C$, so that, if none of the barometers is in contact with the object, the controller outputs reasonable values based on the feedforward terms. The force controller can be expressed by (see Figure 5.2-B):

$$\begin{aligned} E &= F_{Target} - F_{Baro}^{FingerMax} \\ PWM &= clamp\{K_P^{Norm} \cdot E + K_D^{Norm} \cdot \frac{dE(t)}{dt},\ \pm C\} + \\ &\quad FeedForward_{Force}^{PWM}(F_{Target}) + \\ &\quad FeedForward_{Position}^{PWM}(CurMotorPos) \end{aligned}$$

The target F_{Target} is calculated by a P-controller acting on the normal to shear force ratio, with an offset defined by a fixed term of F_{min}. The fixed term ensures that the force controller always retains a small contact force with the object.

For the overlying friction control, we assume a fixed friction coefficient μ. The shear and normal forces $AvgShearForces_{Mag}$ and $AvgNormalForces_{Mag}$ are calculated over all fingers as an average over all *active* shear force sensors. A sensor is deemed *active* if the barometer between these two sensors indicates contact. The shear force controller is implemented as follows:

$$F_{Shear} = K_P^{Shear} \cdot (1 - \mu \cdot \frac{AvgNormalForces_{Mag}}{AvgShearForces_{Mag}})$$

The target forces are scaled by the factor $ForceScaling$ for all fingers other than the thumb so the four opposing fingers do not force the thumb open.

$$ForceScaling = \begin{cases} 1 & \text{if thumb} \\ \frac{1}{3} & \text{else.} \end{cases}$$

We used the factor $\frac{1}{3}$ instead of $\frac{1}{4}$ for balancing the four fingers opposing the thumb to compensate for friction in the mechanism and rope guides. Hence, the target for the normal force controller is calculated given as:

$$F_{Target} = (F_{Shear} + F_{min}) * ForceScaling.$$

5.2.4. Unload and Open & Retract Sub-Controllers

The *unload* sub-controller is triggered by an external signal from the robot control PC, indicating the intention to place the grasped object. This prevents triggering object unloading in the case of accidental contact events with the environment while performing a transfer motion. Once the external triggering signal is received and contact with a supporting surface is detected, the controller starts to reduce the forces applied to the object to replace it in a controlled manner. Contact is detected if at least three of the accelerometers embedded in each finger tip sense vibrations in the range of 400 to 800 Hz of the fast Fourier transform of the accelerator signals in a window with the last 32 measurements and a total energy over $ReplaceThres_{FFT}$. This indicates the start of the unloading phase. For each motor, the rate of change in pressure $MaxForce^{motor}_{pressure}dt$ is controlled by a P-controller with K_p^{unload}, setting a PWM target (see Figure 5.2-C). The target rate of change is calculated at the beginning of the phase such that unloading of the object is expected to finish within one second. As soon as all fingers driven by the motor reach a value below a contact threshold $MaxForce^{motor}_{Baro} < ContactThres_{Baro}$, the motor switches to position control

Table 5.1.: Parameters of the grasp phases controller. Reprinted from (Weiner et al., 2021), "Detecting grasp phases and adaption of object-hand interaction forces of a soft humanoid hand based on tactile feedback", IROS 2021, ©2021 IEEE.

Parameter	**Value**	**Parameter**	**Value**
PWM_{max}	100%	PWM_{min_cl}	30%
$ContactThres_{Baro}$	21 mBar	C	11%
K_P^{Norm}	1	K_D^{Norm}	0.2
F_{min}	120 mBar	μ	0.4
K_P^{Shear}	5000	$ForceScaling$	$\frac{1}{3}$ L/R/M/I, 1 T
$ReplaceThres_{FFT}$	40000	K_P^{unload}	-15

mode and holds the current position until all motors finished unloading, i. e. , all fingers are no longer in contact with the object.

The *unload* phase is considered completed when all fingers have either lost contact with the object or are completely opened. In the subsequent *Retreat* phase, see Figure 5.2-D, the fingers open with maximum motor speed to the maximum hand aperture.

5.3. Evaluation

The grasp-phases controller is evaluated experimentally by grasping everyday objects and food items using the humanoid robot ARMAR-6 (Asfour et al., 2019) and compared against the baseline approach of grasping with maximum force. The parameters used in all evaluation experiments are listed in Table 5.1. In our experiments, we use 31 different objects, see Figure 5.3. The objects include three drinking vessels that are grasped with two different liquid level, resulting in 31 grasps of objects with different properties. Object weight varies from 4.8 g for the paper cup to 1133.8 g for the plastic cola bottle. For the heavy objects, different materials are chosen (metal, plastic, glas) to assess the performance of grasping and lifting objects with different friction coefficients. The object set also contains rigid and soft objects like the elephant plushie, the capri sun bag and the sponge. The execution on the robot is completely decoupled from the grasp-phases controller since the controller only receives two commands from the robot in each grasping trial: the command to trigger grasping and the signal indicating that the object will soon be replaced.

Figure 5.3.: Set of objects used in the experiments. From left to right and back to front: chips, rectangular emptly bottle, cola glass, PET bottle, cola plastic, sponge, metal bottle, mustard bottle, potato starch, empty capri sun, empty can 333ml, empty can 500ml, full boxed juice, elephant plushie, full capri sun, boxed juice empty, peppermint tea, salt sticks apple, bell pepper, papercraft box, paper cup, plastic cup, orange, toast slices, jelly cup, yeast dumpling, ice cone, bananas, mie noodles. Reprinted from (Weiner et al., 2021), "Detecting grasp phases and adaption of object-hand interaction forces of a soft humanoid hand based on tactile feedback", IROS 2021, ©2021 IEEE.

5.3.1. Underactuated Hand and Embedded System

The haptic sensor data utilized in this work is provided by prototypes of the presented soft sensorized fingers (see Section 3.3).Five of these soft fingers are mounted on an underactuaded anthropomorphic hand. The hand design is based on a previous design presented in (Hundhausen et al., 2020) and described here briefly for completeness. The hand includes three identical Direct Current (DC) gear motors, where thumb and index fingers are driven by one motor each and the remaining fingers are driven by the third motor via an underactuated mechanism based on the mechanism presented in Subsection 3.1.2. This mechanism allows each of the three fingers to close even if others are blocked, hence the fingers can wrap around the object to conform to the object's shape. Through a block and tackle system, the force on the motor tendon is trippled and distributed to the three fingers at the cost of three times the closing time.

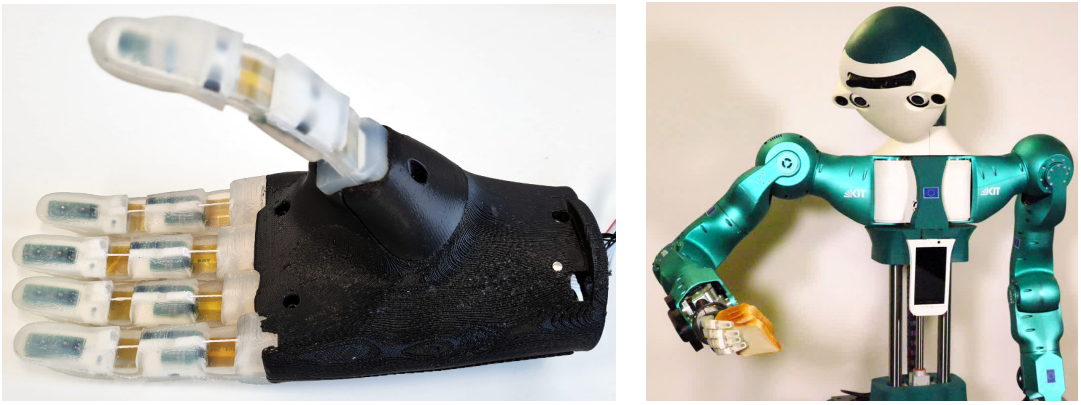

(a) (b)

Figure 5.4.: a) Soft humanoid hand with multimodal sensor system; b) Hand attached to the humanoid robot ARMAR-6. Reprinted from (Weiner et al., 2021), "Detecting grasp phases and adaption of object-hand interaction forces of a soft humanoid hand based on tactile feedback", IROS 2021, ©2021 IEEE.

Hence, the force acting on little, ring and middle finger is roughly the same as the force acting on the individually actuated index finger and thumb. This greatly eases the development of force control algorithms, as all fingers behave the same apart from closing speed. The completed hand with sensorized fingers is shown in Figure 5.4.

The hybrid embedded system for sensor data processing and control consisting of a microcontroller and FPGA integrated in the palm is the same as in (Hundhausen et al., 2020), which lead to the development of the System on Chip (SoC)-based system presented in Subsection 3.4.2. In this work, we use the Field Programmable Gate Array (FPGA) to read the ten buses to all sensor Printed Circuit Boards (PCBs) in the fingers in parallel with a sample rate of 140 to 160 Hz depending on processor timings. Multiple accelerometer values are transmitted in each frame since the accelerometer samples at 1.6 kHz. The aggregated sensor data is then passed to the microcontroller and from there to the EtherCAT bus of the humanoid robot ARMAR-6 we use in our experiments.

5.3.2. Experiment Protocol

The experiments are carried out on our humanoid robot ARMAR-6 (Asfour et al., 2019) with the hand attached to the right arm, see Figure 5.4. Each object is placed on the table at a pre-defined position. Each grasp trail is carried as follows:

1. We use kinesthetic teaching to guide the robot arm in zero-torque mode to a pre-grasp and grasp pose. We explicitly consider the reaching motion trough pre-grasp and grasp pose as we are in general interested in the whole grasping and manipulation task. The grasp pose is chosen so that the grasp is aligned with the longest object axis.
2. Trigger the grasp-phases controller with the arm in fixed starting position.
3. The arm moves to the pre-defined pre-grasp and grasp pose and starts closing the fingers (reach and close phase).
4. As soon as the controller has reached the load phase, the object is lifted and moved to the right of the table.
5. The hand is rotated approximately 45° using wrist pronation/supplination and flexion/extention to disturb the grasp.
6. The arm moves the object back to the pre-defined grasping position on the table and informs the grasp-phases controller that the object can now be replaced.
7. The hand moves down until the grasp-phases controller enters the unload phase.
8. The arm moves back to the fixed initial position.

For the baseline approach, the same protocol is used with the difference that the object is grasped with maximum force and lifted after a 3 s delay. Further, the object placement is realized by detecting contact with the table using the 6D-force/torque sensor in the wrist of the arm. Example grasps are depicted in Figure 5.5. For the evaluation, we consider several aspects that are important to assess the quality of grasps in the conducted experiments:

1. The generated grasping force,
2. the number of dropped objects and
3. the number of damaged objects.

5.3.3. Average Grasping Force

The amount of grasping force is quantified in terms of motor effort, i. e. the time of PWM modulation in percent. The baseline approach always utilizes 100 % motor effort. For the grasp-phases controller, this value is calculated by taking the average of the motor PWM at each time step during the execution, beginning with the closing of the fingers in the reach phase and ending with opening

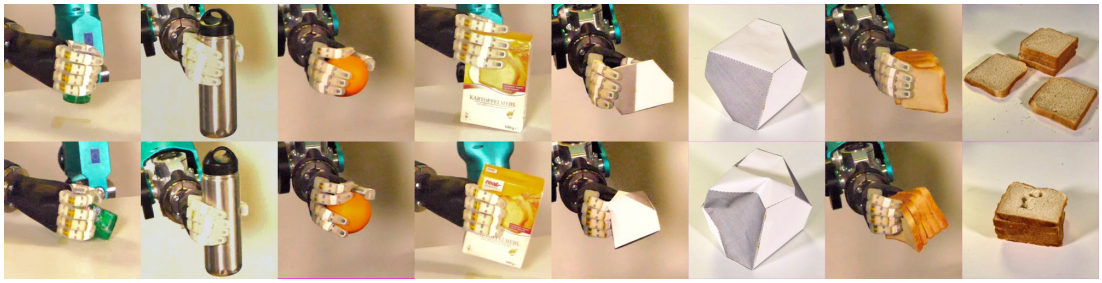

Figure 5.5.: Example grasps using our approach (top row images) and the baseline approach (bottom row images).

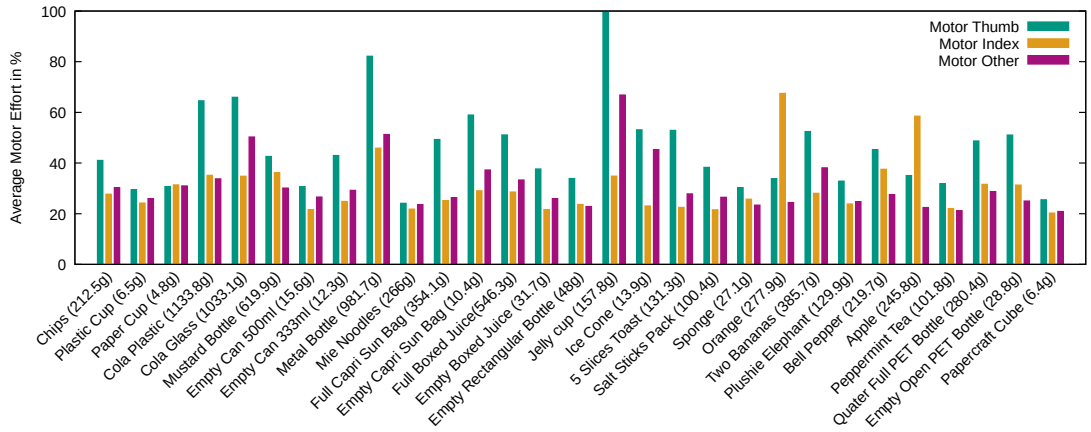

Figure 5.6.: Motor effort averages calculated over the duration of the experiments for the grasp-phases controller. While the baseline always requires 100 %, the grasp-phases controller uses averaged over all objects only 35.64 %. As a result, the grasp-phase controller transmits less force to the object and thus avoids damaging fragile objects. Reprinted from (Weiner et al., 2021), "Detecting grasp phases and adaption of object-hand interaction forces of a soft humanoid hand based on tactile feedback", IROS 2021, ©2021 IEEE.

the fingers in the *open & retreat* phase. Since each motor receives different targets, the values are calculated for each individual motor. Over all motors and grasping trials, the average motor effort is 35.64 %. The results for each motor and each grasping trial are shown in Figure 5.6. As can be seen, the grasp phases controller generates higher motor efforts for heavy objects without a form closure grasp as in the case of the metal bottle and the boxed juice. The controller also generates higher targets for deformable objects like the empty capri sun bag, the pet bottle and the toast. This is caused by high perceived shear forces, which are most likely induced by the fingers deforming the object, causing the fingers to drag along the surface. The jelly cup shows a clear anomaly, caused by its geometry. While grasping the cup, contact occurred at the protruding edge at

the top of the cup where the lid is glued to, resulting in excessive shear forces and low normal forces, probably since the silicone of the finger was distorted locally due to the sharp edge.

5.3.4. Dropped and Damaged Objects

The baseline approach was able to lift and hold all objects except the jelly cup in all experiments while the grasp-phases controller was not able to lift the yeast dumpling and the potato starch. In the case of the potato starch, the fingers formed a pinch grasp such that the sensors on the inside of the fingertip had no contact with the object. For the yeast dumpling, the shear force sensors were in contact with the object but did slide along the surface without sticking, most likely due to its crumbly surface. The baseline approach did lift the dumpling but damaged it and failed to lift the jelly cup because the quickly moving index and thumb pushed the object out of the hand.

During the 31 grasp attempts executed for each approach, the baseline approach damaged nine objects (plastic and paper cup, both cans, boxed juice empty, toast, bananas, empty open PET bottle, paper-craft cube). The grasp-phases controller slightly pushed in the toast with the thumb, otherwise all objects where grasped and replaced without noticeable damage.

5.3.5. Placing of Objects

When placing objects, the grasp-phases controller managed to replace 22 objects in the same pose they were picked up, while the baseline managed to replace 23 objects correctly. The primary failure of the grasp phases controller was due to missing the placing event especially for soft objects, while the baseline toppled over tall objects or flung away light objects. It has to be noted, that the baseline approach used an accurate force-torque sensor while the grasp-phases controller only relied on less accurate sensors of the finger tips. When used as the hand of a humanoid robot, the feedback of the force/torque sensor could of course be integrated into the controller, in a hand prostheses setting the additional information would not be available.

5.4. Summary and Review

This chapter detailed the design, implementation and evaluation of a fully autonomous, human-inspired grasp controller for unknown objects and thereby provides an answer to the third research question posed in this thesis:

How to grasp safely with the right amount of force?

The proposed controller takes inspiration from grasping strategies observed in humans to break down the difficult problem of grasp control into individual action-phases. Force targets are calculated based on sensors exclusively mounted inside of the hand. The controller is explicitly designed to work with incomplete sensor data caused by the non-sensorized palm contacting the object or individual fingers completely missing the objects. The controller has been evaluated in grasping trials with 31 objects regarding grasp success and damage to grasped objects.

Human-inspired Grasp Phases Control: We present a human-inspired grasp-phases controller that is able to detect different phases of a grasping and manipulation task and adapts object-hand interaction forces based on tactile feedback. The phases are motivated by neurophysiological findings in humans and mapped into the robotic context. Each phase and transition carries semantic meaning in the context of grasping. Like in the human role model, each finger or in this case motor controls the applied normal force independent of the other fingers (Edin et al., 1992). At the end of each phase, the controllers of all motors are synchronized before transitioning to the next phase.

Robust Control with In-Hand Sensors: All sensor data used by the controller stems from sensors directly embedded into the fingers of the used hand and is processed in real-time. The controller is explicitly designed to work with incomplete sensor data, for example if a finger misses the object completely, allowing the whole hand to engage in the grasp, not just the sensorized surfaces. While the current implementation of the controller is executed on a PC, all filters and calculations can also directly carried out in real-time on the embedded system due to the low computational complexity of the proposed controller.

Evaluation: We demonstrate the performance of the controller in several experiments with 31 objects and evaluate the ability to balance forces at the

contact points in precision and power grasps based on tactile feedback in the different phases of the task. The experimental evaluations also demonstrate the ability of the grasp-phases controller to adapt forces while grasping fragile objects preventing their damage as well as to heavy objects.

6. Conclusion

The goal of the thesis was to endow anthropomorphic hands such as prosthetic and humanoid robotic hands with advanced grasping abilities based on multimodal sensor information. Towards this goal, the thesis first presents the design of sensorized prosthetic hands and scalable fingers as well as embedded system for in-situ processing and control. Second, a semi-autonomous control scheme for the selection of grasp parameters and approach direction is proposed and evaluated in a user study. Third, a human-inspired autonomous grasp phases control for unknown objects is developed and evaluated in a grasping study with household objects.

6.1. Scientific Contributions of the Thesis

The scientific contributions of the thesis are:

Robotic Hands with a Multimodal Sensor System Chapter 3 presents the development of anthropomorphic hands. The hands include a novel design of the underactuated mechanism that allows to reduce installation space for actuation. Furthermore, in contrast to related work, the hand includes environmental sensors in the palm and accommodates a capable embedded system. These developments where published in (Weiner et al., 2018b) and (Weiner, Starke, Rader et al., 2022).

The chapter next introduces the design of scalable sensorized robot fingers. To the best of the authors knowledge, for the first time the problem of scaling these fingers according to anthropomorphic dimensions is tackled. This problem is furthermore solved in conjunction with a thorough concept for the sensorization of the fingers. Each finger is endowed with an array of multimodal haptic as well as distance or temperature sensors. Two variants of the fingers are described, one rigid and robust variant made out of laser-sintered nylon and one soft finger variant made out of an endoskeleton casted in silicone. This

thesis further contributes a simple fabrication technique for barometer-based normal force sensors. The fingers are described in (Weiner et al., 2019), and (Weiner et al., 2021). the haptic sensor system developed in this work has further been implemented in forcemyography sensors measuring muscle activity for exoskeleton control in Marquardt et al. (2022).

Lastly, the design of embedded systems for prosthetic and humanoid robotic hands is described. Two variants of the embedded systems are presented, one based on a low-power microcontroller and one based on a System on Chip (SoC) including an dual-core application processor and an Field Programmable Gate Array (FPGA) for higher computational loads. In contrast to the state of the art these systems are designed for in-situ processing of sensor data and real-time control, allowing the stand-alone use the hand.

Semi-autonomous Grasping In Chapter 4, a semi-autonomous grasping scheme for prosthetic hands is described. The control scheme allows the user to choose both an appropriate grasp type as well as an approach direction by issuing only Electromyography (EMG) control signals. While other control schemes rely heavily on sensors attached either to the user or to the user's environment, this work utilizes only sensors directly embedded into the prosthetic hand itself. In contrast to related work, all computations also take place on the embedded system inside the prosthetic hand. This makes the use of the control scheme in every-day scenarios viable.

The control scheme is employed on the embedded system of the KIT prosthetic hand and evaluated in a user study. In comparison to classical myoelectric control, the control scheme allowed faster grasp execution while users reported to experience less effort when using the presented scheme. The semi-autonomous control scheme is described in (Starke, Weiner et al., 2022).

Human-Inspired Grasp Phases Control Chapter 5 presents the implementation of a grasp force controller for the complete grasping process for unknown objects, starting from approaching and wrapping the fingers around an object to lifting, holding, replacing and letting go of the object. The controller takes inspiration from the grasping strategy employed by humans, effectively dividing the grasping process into a sequence discrete action phases with individual control goals, sequenced by distinct haptic events. Using the multimodal information provided by the sensors of the soft sensorized fingers, the controller is able to

detect the haptic events dividing the individual phases and control the finger motion and the grasping force for each phase with dedicated sub-controllers.

While this human-inspired approach has been successfully employed parallel grippers and a prosthesis by manually bringing individual fingers into contact with the object, the grasp-phases controller in the thesis controls all fingers of a five-fingered in all grasping phases fully autonomously. For each motor in the hand, an independent controller instance is executed and all instances are explicitly synchronized at the end of each phase.

Most grasping controllers presented in literature choose grasping patterns such that only sensorized parts of the gripper or hand are in contact with the object, so the controller has complete knowledge about the interaction forces. In this work, the complete hand is engaged in grasping, including surfaces that are not endowed with sensors. The controller is explicitly designed to be able to deal with incomplete sensor information while maintaining a stable grasp on the object. The grasp phases controller has been published in (Weiner et al., 2021).

6.2. Discussion and Future Work

The thesis described both hardware and algorithms to support grasp selection and robust grasp execution using multimodal sensor information. The presented algorithms have been successfully deployed in real-world scenarios both in user trails and experimental robot evaluations. However, further improvements and new applications for both the mechanical and sensor systems as well as the presented algorithms can be envisioned. This section points out possible future directions of research.

Feedback of Sensor Data to the User The thesis focuses on using the multimodal sensor system in the prosthetic hands to automate the grasping process with prostheses to reduce effort and cognitive burden for the user. Studies on providing tactile feedback from the prostheses to the user have shown great potential in increasing the usability of prostheses and allowing for more fine-grained manipulation. Tactile feedback is commonly provided by vibration or electrostimulation at the interface between stump and shaft. The addition of tactile feedback from the already available sensors inside the hand would enable the user to supervise the grasping force selected by the semi-autonomous grasping scheme and correct it if needed. Especially dynamic changes in object

weight could then be adapted by the user based on tactile feedback. This also opens up the possibility for the user to teach the grasping force for new objects added to the database in an intuitive manner.

Tactile feedback can also be used in demonstrating contact-rich actions to a robot. With the ability to provide tactile feedback to the operator in a tele-operating scenario, the interaction forces between the robot's fingers and an object could be demonstrated directly by the human.

Sensor-Based Control of Bimanual Actions The semi-autonomous control scheme and the grasp-phases controller in the thesis are concerned with grasping and placing tasks involving a single anthropomorphic hand. Large objects may be grasped with both hands, requiring different pre-shapes and grasp types as well as effectively coupling both hands and inducing interaction forces between both hands that need to be taken into account when calculating grasping forces. Furthermore, grasping is often just the first stage of manipulating the object with the second hand. The grasp-phases controller needs to take these interaction forces into account while the object is manipulated with the second hand to ensure stable grasping. Open research questions in this area include, among others, how to recognize the intention of the user and how to recognize the manipulation task that is carried out. Information about the manipulation task could be partially inferred from the grasped object through affordances associated with the objects or particular regions of the object using visual information. The intention recognition could be further informed by wearable devices like smart watches on the other arm of the user.

Learning and Model-Predictive Control The grasp-phases controller in the thesis utilizes classical control to compare sensor data to a desired goal signal. As shown in (Johansson and Flanagan, 2009b), humans rely heavily on sensory prediction for motor control during a manipulation task. A mismatch between predicted and actual sensory signals triggers situation-specific corrective actions. This predictive coding of sensory signals not only enables humans to learn sophisticated manipulation capabilities, but also to execute them in unparalleled speed due to the predictive nature of the learned model.

Transfer of these concepts to the control of anthropomorphic hands could likewise increase robustness and speed of humanoid robot and prosthetic grasping. For sensory prediction a model could be learned that predicts future sensory signals given the current system state and adapts corresponding motor commands

on top of the current classical controller. This would also enable prediction of failures due to events like slippage, especially if the model is able to link multiple sensor modalities to detect these incipient events. Open research questions include how to construct such a predictive model and link predictions to motor commands that maximize the likelihood of realizing these predictions.

Appendix

A. From Human Hand Anatomy to Robotic Hands

The following describes human hand anatomy aspects relevant to this work and the transfer of the kinematic structure as well as actuation to robotic hands. The introduction to human hand anatomy is based on the book in (Jones and Lederman, 2006), where a in-depth description of the topic can be found.

The human hand is a highly versatile system comprised of 27 bones, 29 muscles and 21 active Degree of Freedoms (DoFs). Figure 1 shows an overview of bones and joints of the human hand. Each finger has three joints: the Distal Interphalangeal (DIP) and Proximal Interphalangeal (PIP) joints are hinge joint only capable of flexion/extension while the metacarpophalangeal (MCP) joint is a condyloid joint additionally capable of adduction/abduction. In total these are 16 DoFs. The thumb, while missing the intermediate phalanx, also has three joints: the Interphalangeal (IP) and notably also the MCP joints are hinge joints while the Carpometacarpal (CMC) joint is a saddle joint allowing for flexion/extension, adduction/abduction and circumvention of the thumb. The joints between the metacarpals and carpals of the other fingers also allow for some motion, although this is very constraint and are depending on the definition not considered a true DoF.

The combined range of motion of all three flexion joints in each finger is 260° where the MCP joint contributes 85°, the PIP joint 110° and the DIP joint 65°. Due to the relative low range of motion of the DIP joint and small length of the distal phalanx, the DIP joint is often omitted in robotic hands to reduce the mechanical complexity of the fingers. In this case the distal and intermediate phalanx are fused together, usually at an angle.

The hand is actuated by 29 muscles, of which some divide into multiple parts actuating multiple tendons totaling to 38 actuated tendons overall. While 17 of these tendons are actuated by *intrinsic* muscles originating and inserting inside the hand, the bulk of muscle mass for hand actuation is situated *extrinsically*

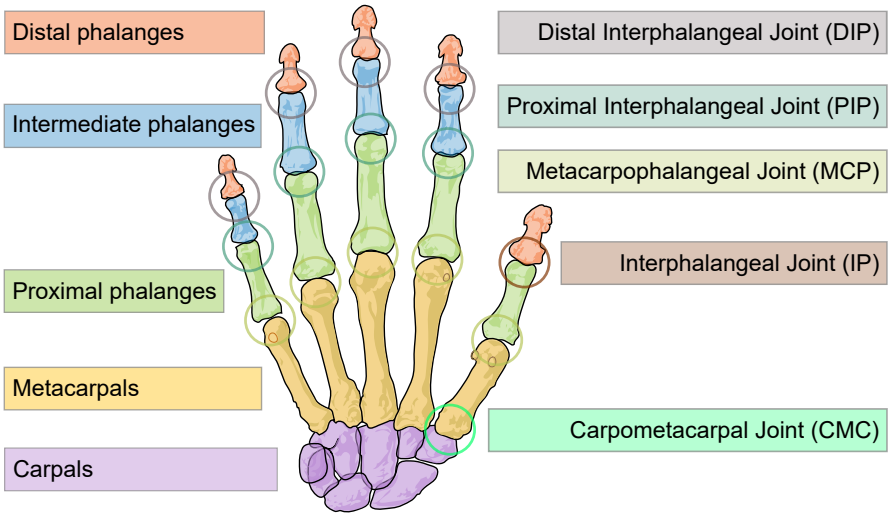

Figure 1.: Human hand bone and finger joint nomenclature (based on a graphic by Mariana Ruiz Villarreal)

in the forearm. This poses a huge challenge for artificial hand design as the forearm is usually still present in the case of prosthesis users and oftentimes completely occupied by actuation of forearm rotation and wrist actuation in case of humanoid robots. Hence the actuators for artificial hands often need to be placed inside of the hand, which – in a sense – poses an even harder problem than that evolution had to solve. Roboticists often simplify the hand kinematics to save on space otherwise needed for additional actuators, resulting in a difficult tradeoff between dexterity and size/weight of the hand.

Since some muscle actuate multiple tendons, not every joint in the human hand is actuated individually. These physiological couplings of joints already give insight in possible simplifications for artificial hand actuation. As evidence from Santello et al. (1998) suggests, there also exist patterns of higher level coordination and covariation between joints that allow to describe a grasp using low-dimensional representations called *synergies*.

The technical implementation of co-actuation of multiple joints is called *under-actuation* and is usually realized by a mechanism that distributes the torque or force of a single actuator to multiple joints and fingers. Consequent use of such a mechanism leads to hands with few as one motor (e. g. Fukaya et al., 2000; Bonilla et al., 2014). An underactuated mechanism is called *adaptive* if the actuated joints are not rigidly coupled, meaning that blockage of one joint does not hinder other joints from closing.

List of Figures

List of Tables

Acronyms

3D-MID Three-Dimensional Molded Interconnect Device

AC Alternating Current
ADC Analog to Digital Converter
ADL Activity of Daily Living

CAD Computer Aided Design
CDC Capacitance to Digital Converter
CMC Carpometacarpal
CNC Computer Numerical Control
CNN Convolutional Neural Network

DC Direct Current
DIP Distal Interphalangeal
DMA Direct Memory Access
DoF Degree of Freedom

EMG Electromyography

FFC Flat Flex Cable
FPGA Field Programmable Gate Array
FSR Force Sensing Resistor

I^2C Inter-Integrated Circuit
IMU Inertial Measurement Unit
IP Interphalangeal

LED Light Emitting Diode

MCP metacarpophalangeal
MEMS Micro-ElectroMechanical Systems

PCB Printed Circuit Board
PIP Proximal Interphalangeal
PWM Pulse Width Modulation

RAM Random Access Memory

ShA Shore A
SLA Stereolithography
SLS Selective Laser Sintering
SoC System on Chip
SPI Serial Peripheral Interface
STFT Short-Time Fourier Transform

ToF Time of Flight

UV ultraviolet

Bibliography

Abad, A. C., Ormazabal, M., Reid, D., and Ranasinghe, A. (2021a). Pilot study: A visuotactile haptic primary colors sensor. In *2021 IEEE Sensors*, pages 1–4. 20

Abad, A. C. and Ranasinghe, A. (2020a). Low-cost GelSight with UV markings: Feature extraction of objects using AlexNet and optical flow without 3D image reconstruction. In *2020 IEEE International Conference on Robotics and Automation (ICRA)*, pages 3680–3685. 20

Abad, A. C. and Ranasinghe, A. (2020b). Visuotactile sensors with emphasis on GelSight sensor: A review. *IEEE Sensors Journal*, 20(14):7628–7638. 19

Abad, A. C., Reid, D., and Ranasinghe, A. (2021b). HaptiTemp: A next-generation thermosensitive GelSight-like visuotactile sensor. *IEEE Sensors Journal*, pages 1–1. 20

Ajoudani, A., Hocaoglu, E., Altobelli, A., Rossi, M., Battaglia, E., Tsagarakis, N., and Bicchi, A. (2016). Reflex control of the Pisa/IIT softhand during object slippage. In *International Conference on Robotics and Automation*, pages 1972–1979. 43, 48

Al-Mohammed, M., Ding, Z., Liu, P., and Behal, A. (2018). An adaptive control based approach for gripping novel objects with minimal grasping force. In *International Conference on Control and Automation*, pages 1040–1045. 44, 48

Alagi, H., Navarro, S. E., Mende, M., and Hein, B. (2016). A versatile and modular capacitive tactile proximity sensor. In *2016 IEEE Haptics Symposium (HAPTICS)*, pages 290–296. 15, 16

Amsuess, S., Goebel, P., Graimann, B., and Farina, D. (2014). Extending mode switching to multiple degrees of freedom in hand prosthesis control is not efficient. In *International Conference of the IEEE Engineering in Medicine and Biology Society*, pages 658–661. 37

Asfour, T., Schill, J., Peters, H., Klas, C., Bücker, J., Sander, C., Schulz, S., Kargov, A., Werner, T., and Bartenbach, V. (2013). ARMAR-4: A 63 DOF torque controlled humanoid robot. In *IEEE/RAS International Conference on Humanoid Robots (Humanoids)*, pages 390–396, Atlanta, USA. 26, 34

Asfour, T., Wächter, M., Kaul, L., Rader, S., Weiner, P., Ottenhaus, S., Grimm, R., Zhou, Y., Grotz, M., and Paus, F. (2019). ARMAR-6: a high-performance humanoid for human-robot collaboration in real world scenarios. *IEEE Robotics & Automation Magazine*, 26(4):108–121. 67, 128, 130

Belter, J. T. and Dollar, A. M. (2013). Novel differential mechanism enabling two dof from a single actuator: Application to a prosthetic hand. In *IEEE International Conference on Rehabilitation Robotics (ICORR)*, pages 1–6. 24, 35, 50, 53, 66, 71

Belter, J. T., Segil, J. L., Dollar, A. M., and Weir, R. F. (2013). Mechanical design and performance specifications of anthropomorphic prosthetic hands: A review. *The Journal of Rehabilitation Research and Development*, 50(5):599–617. 37

Bennett, D. A., Dalley, S. A., Truex, D., and Goldfarb, M. (2015). A multigrasp hand prosthesis for providing precision and conformal grasps. *IEEE/ASME Transactions on Mechatronics*, 20(4). 28, 34, 35

Berstis, V. and Zimmerman, T. G. (2000). Trackpoint device. (United States Patent No. US6115030A). 17

Bhirangi, R., Hellebrekers, T., Majidi, C., and Gupta, A. (2021). ReSkin: versatile, replaceable, lasting tactile skins. In *5th Conference on Robot Learning*. 13

Billard, A. and Kragic, D. (2019). Trends and challenges in robot manipulation. *Science*, 364(6446). 42

Bonilla, M., Farnioli, E., Piazza, C., Catalano, M., Grioli, G., Garabini, M., Gabiccini, M., and Bicchi, A. (2014). Grasping with soft hands. In *2014 IEEE-RAS International Conference on Humanoid Robots*, pages 581–587. 144

Calli, B., Walsman, A., Singh, A., Srinivasa, S., Abbeel, P., and Dollar, A. M. (2015). Benchmarking in manipulation research: Using the Yale-CMU-Berkeley object and model set. *IEEE Robotics Automation Magazine*, 22(3):36–52. 58, 60, 73

Canbay, D., Ferrentino, P., Liu, H., Moccia, R., Pirozzi, S., Siciliano, B., and Ficuciello, F. (2021). Calibration of tactile/force sensors for grasping with the

PRISMA Hand II. In *2021 IEEE/ASME International Conference on Advanced Intelligent Mechatronics (AIM)*, pages 442–447. 28

Carrozza, M. C., Cappiello, G., Micera, S., Edin, B. B., Beccai, L., and Cipriani, C. (2006). Design of a cybernetic hand for perception and action. *Biological Cybernetics*, 95:629–644. 30, 35, 52

Catalano, M., Grioli, G., Farnioli, E., Serio, A., Piazza, C., and Bicchi, A. (2014). Adaptive synergies for the design and control of the Pisa/IIT softhand. *The International Journal of Robotics Research*, 33(5):768–782. 50

Chadwell, A., Kenney, L., Thies, S., Galpin, A., and Head, J. (2016). The reality of myoelectric prostheses: Understanding what makes these devices difficult for some users to control. *Frontiers in Neurorobotics*, 10:1–21. 37

Cheng, G., Dean-Leon, E., Bergner, F., Rogelio Guadarrama Olvera, J., Leboutet, Q., and Mittendorfer, P. (2019). A comprehensive realization of robot skin: Sensors, sensing, control, and applications. *Proceedings of the IEEE*, 107(10):2034–2051. 21, 68

Chorley, C., Melhuish, C., Pipe, T., and Rossiter, J. (2009). Development of a tactile sensor based on biologically inspired edge encoding. In *2009 International Conference on Advanced Robotics*, pages 1–6. 19

Ciancio, A. L., Cordella, F., Barone, R., Romeo, R. A., Bellingegni, A. D., Sacchetti, R., Davalli, A., Pino, G. D., Ranieri, F., Lazzaro, V. D., et al. (2016). Control of prosthetic hands via the peripheral nervous system. *Frontiers in Neuroscience*, 10:1–17. 37

Cipriani, C., Controzzi, M., and Carrozza, M. C. (2010). Objectives, criteria and methods for the design of the SmartHand transradial prosthesis. *Robotica*, 28(6). 30, 32

Cipriani, C., Controzzi, M., and Carrozza, M. C. (2011). The SmartHand transradial prosthesis. *Journal of NeuroEngineering and Rehabilitation*, 8(1):29. 30, 32, 34, 35

Cipriani, C., Zaccone, F., Micera, S., and Carrozza, M. (2008). On the shared control of an EMG-controlled prosthetic hand: Analysis of user-prosthesis interaction. *IEEE Transactions on Robotics*, 24(1):170–184. 38, 40

Controzzi, M., Clemente, F., Barone, D., Ghionzoli, A., and Cipriani, C. (2017). The SSSA-MyHand: A dexterous lightweight myoelectric hand prosthesis.

IEEE Transactions on Neural Systems and Rehabilitation Engineering, 25(5):459–468. 27, 34, 35, 66

Cordella, F., Ciancio, A. L., Sacchetti, R., Davalli, A., Cutti, A. G., Guglielmelli, E., and Zollo, L. (2016). Literature review on needs of upper limb prosthesis users. *Frontiers in Neuroscience*, 10:1–14. 1, 24, 33, 37, 51, 52, 53, 71

Dahiya, R. S., Metta, G., Valle, M., and Sandini, G. (2010). Tactile sensing - from humans to humanoids. *IEEE Transactions on Robotics*, 26(1). 10

Dalley, S. A., Wiste, T. E., Varol, H. A., and Goldfarb, M. (2010). A multigrasp hand prosthesis for transradial amputees. In *2010 Annual International Conference of the IEEE Engineering in Medicine and Biology*, pages 5062–5065. 27

De Maria, G., Falco, P., Natale, C., and Pirozzi, S. (2015). Integrated force/tactile sensing: The enabling technology for slipping detection and avoidance. In *Int. Conf. on Robotics and Automation*, pages 3883–3889. 18, 43, 48

De Maria, G., Natale, C., and Pirozzi, S. (2012). Force/tactile sensor for robotic applications. *Sensors and Actuators A: Physical*, 175:60 – 72. 18

Degol, J., Akhtar, A., Manja, B., and Bretl, T. (2016). Automatic grasp selection using a camera in a hand prosthesis. In *Int. Conference of the IEEE Engineering in Medicine and Biology Society*, pages 431–434. 40

Deimel, R. and Brock, O. (2016). A novel type of compliant and underactuated robotic hand for dexterous grasping. *Int. Journal of Robotics Research*, 35(1-3):161–185. 36

Deng, H., Zhong, G., Li, X., and Nie, W. (2017). Slippage and deformation preventive control of bionic prosthetic hands. *Trans. on Mechatronics*, 22(2):888–897. 44

Deng, Z., Jonetzko, Y., Zhang, L., and Zhang, J. (2020). Grasping force control of multi-fingered robotic hands through tactile sensing for object stabilization. *MDPI Sensors*, 20(4). 44

Dhillon, G. S. and Horch, K. W. (2005). Direct neural sensory feedback and control of a prosthetic arm. *IEEE TRansactions on Neural Systems and Rehabilitation Engineering*, 13:468–472. 37

Dong, S., Yuan, W., and Adelson, E. H. (2017). Improved GelSight tactile sensor for measuring geometry and slip. In *2017 IEEE/RSJ International Conference on Intelligent Robots and Systems (IROS)*, pages 137–144. 20

Donlon, E., Dong, S., Liu, M., Li, J., Adelson, E., and Rodriguez, A. (2018). GelSlim: A high-resolution, compact, robust, and calibrated tactile-sensing finger. In *2018 IEEE/RSJ International Conference on Intelligent Robots and Systems (IROS)*, pages 1927–1934. 20, 21

Došen, S., Cipriani, C., Kostić, M., Controzzi, M., Carrozza, M., and Popović, D. (2010). Cognitive vision system for control of dexterous prosthetic hands: Experimental evaluation. *Journal of NeuroEngineering and Rehabilitation*, 7(1):42. 38, 40, 50, 52

Došen, S. and Popović, D. B. (2011). Transradial prosthesis: Artificial vision for control of prehension. *Artificial Organs*, 35(1):37–48. 38, 40

Edin, B., Ascari, L., Beccai, L., Roccella, S., Cabibihan, J.-J., and Carrozza, M. (2008). Bio-inspired sensorization of a biomechatronic robot hand for the grasp-and-lift task. *Brain Research Bulletin*, 75(6):785–795. Special Issue: Robotics and Neuroscience. 30, 32

Edin, B. B., Westling, G., and Johansson, R. S. (1992). Independent control of human finger-tip forces at individual digits during precision lifting. *The Journal of Physiology*, 450(1):547–564. 134

Ehrsson, H. H., Fagergren, A., Jonsson, T., Westling, G., Johansson, R. S., and Forssberg, H. (2000). Cortical activity in precision- versus power-grip tasks: An fmri study. *Journal of Neurophysiology*, 83(1):528–536. 1, 120

Fajardo, J., Ferman, V., Cardona, D., Maldonado, G., Lemus, A., and Rohmer, E. (2020). Galileo hand: An anthropomorphic and affordable upper-limb prosthesis. *IEEE Access*, 8:81365–81377. 29, 33, 35

Farina, D., Jiang, N., Rehbaum, H., Holobar, A., Graimann, B., Dietl, H., and Aszmann, O. C. (2014). The extraction of neural information from the surface EMG for the control of upper-limb prostheses: emerging avenues and challenges. *IEEE Transactions on Neural Systems and Rehabilitation Engineering*, 22(4):797–809. 110

Farrell, T. R. and Weir, R. F. (2007). The optimal controller delay for myoelectric prostheses. *IEEE Transactions on Neural Systems and Rehabilitation Engineering*, 15(1):111–118. 95

Fiedler, N., Ruppel, P., Jonetzko, Y., Hendrich, N., and Zhang, J. (2021). A low-cost modular system of customizable, versatile, and flexible tactile sensor

arrays. In *2021 IEEE/RSJ International Conference on Intelligent Robots and Systems (IROS)*, pages 1771–1777. 17

Forssberg, H., Eliasson, A., Kinoshita, H., Johansson, R., and Westling, G. (1991). Development of human precision grip I: basic coordination of force. *Experimental brain research*, 85(2):451–457. 42, 120

Forssberg, H., Kinoshita, H., Eliasson, A., Johansson, R., Westling, G., and Gordon, A. (1992). Development of human precision grip. *Experimental Brain Research*, 90(2):393–398. 42, 120

Fras, J. and Althoefer, K. (2018). Soft biomimetic prosthetic hand: Design, manufacturing and preliminary examination. In *Int. Conf. on Intelligent Robots and Systems*, pages 1–6. 36

Friedl, W. A. and Roa, M. A. (2021). Experimental evaluation of tactile sensors for compliant robotic hands. *Frontiers in Robotics and AI*, 8:241. 32

Fukaya, N., Asfour, T., Dillmann, R., and Toyama, S. (2013). Development of a five-finger dexterous hand without feedback control: The TUAT/Karlsruhe humanoid hand. In *IEEE/RSJ International Conference on Intelligent Robots and Systems (IROS)*, pages 4533–4540, Tokyo, Japan. 36

Fukaya, N., Toyama, S., Asfour, T., and Dillmann, R. (2000). Design of the TUAT/Karlsruhe humanoid hand. In *IEEE/RSJ International Conference on Intelligent Robots and Systems (IROS)*, pages 1754–1759, Takamatsu, Japan. 36, 50, 144

Funabashi, S., Yan, G., Geier, A., Schmitz, A., Ogata, T., and Sugano, S. (2019). Morphology-specific convolutional neural networks for tactile object recognition with a multi-fingered hand. In *2019 International Conference on Robotics and Automation (ICRA)*, pages 57–63. 12

Gao, X., Jin, M., Jiang, L., Xie, Z., He, P., Yang, L., Liu, Y., Wei, R., Cai, H., Liu, H., Butterfass, J., Grebenstein, M., Seitz, N., and Hirzinger, G. (2003). The HIT/DLR dexterous hand: work in progress. In *2003 IEEE International Conference on Robotics and Automation (Cat. No.03CH37422)*, volume 3, pages 3164–3168 vol.3. 29

George, J. A., Davis, T. S., Brinton, M. R., and Clark, G. A. (2020). Intuitive neuromyoelectric control of a dexterous bionic arm using a modified kalman filter. *Journal of Neuroscience Methods*, 330:108462. 37

George Thuruthel, T., Bosman, A. W., Hughes, J., and Iida, F. (2021). Soft self-healing fluidic tactile sensors with damage detection and localization abilities. *Sensors*, 21(24). 15

Ghazaei, G., Alameer, A., Degenaar, P., Morgan, G., and Nazarpour, K. (2017). Deep learning-based artificial vision for grasp classification in myoelectric hands. *J. of Neural Engineering*, 14(3):aa6802. 40, 50, 52

GmbH, O. H. P. (2014). *13E205 MyoRotronic - Instructions for Use*. OttoBock Healthcare Products GmbH. 110

GmbH, T. B. (2016). *I-Limb Quantum User Manual*. Touch Bionics GmbH. 110

Gonzalez-Vargas, J., Dosen, S., Amsuess, S., Yu, W., and Farina, D. (2015). Human-machine interface for the control of multi-function systems based on electrocutaneous menu: Application to multi-grasp prosthetic hands. *PLOS ONE*, 10(6):1–26. 40

Göger, D., Alagi, H., and Wörn, H. (2013). Tactile proximity sensors for robotic applications. In *2013 IEEE International Conference on Industrial Technology (ICIT)*, pages 978–983. 15

Hahne, J. M., Bießmann, F., Jiang, N., Rehbaum, H., Farina, D., Meinecke, F. C., Müller, K. ., and Parra, L. C. (2014). Linear and nonlinear regression techniques for simultaneous and proportional myoelectric control. *IEEE Transactions on Neural Systems and Rehabilitation Engineering*, 22(2):269–279. 37

Hansen, T. C., Trout, M. A., Segil, J. L., Warren, D. J., and George, J. A. (2021). A bionic hand for semi-autonomous fragile object manipulation via proximity and pressure sensors. In *International Conference of the IEEE Engineering in Medicine and Biology Society*, pages 6465–6469. 40, 41

Hao, Y., Controzzi, M., Cipriani, C., Popović, D. B., Yang, X., Chen, W., Zheng, X., and Carrozza, M. C. (2013). Controlling hand-assistive devices. *IEEE Robotics & Automation Mag.*, 20(1):40–52. 38

Hart, S. G. and Staveland, L. E. (1988). Development of NASA-TLX (task load index): Results of empirical and theoretical research. *Advances in Psychology*, 52:139–183. 112, 113, 114

Hellebrekers, T., Chang, N., Chin, K., Ford, M. J., Kroemer, O., and Majidi, C. (2020). Soft magnetic tactile skin for continuous force and location estimation

using neural networks. *IEEE Robotics and Automation Letters*, 5(3):3892–3898. 13

Hellebrekers, T., Kroemer, O., and Majidi, C. (2019). Soft magnetic skin for continuous deformation sensing. *Advanced Intelligent Systems*, 1(4):1900025. 13

Hendy, K. C., Hamilton, K. M., and Landry, L. N. (1993). Measuring subjective workload: When is one scale better than many? *Human Factors*, 35(4):579–601. 112

Holgado, A. C., Alvarez Lopez, J. A., Schmitz, A., Tomo, T. P., Somlor, S., Jamone, L., and Sugano, S. (2018). An adjustable force sensitive sensor with an electromagnet for a soft, distributed, digital 3-axis skin sensor. In *2018 IEEE/RSJ International Conference on Intelligent Robots and Systems (IROS)*, pages 2582–2588. 12

Holgado, A. C., Alvarez Lopez, J. A., Tomo, T. P., Somlor, S., and Sugano, S. (2019a). A soft, distributed, digital 3-axis skin sensor employing a hybrid permanent-adjustable magnetic field. In *2019 IEEE International Conference on Robotics and Biomimetics (ROBIO)*, pages 241–246. 12, 30

Holgado, A. C., Alvarez Lopez, J. A., Tomo, T. P., Somlor, S., and Sugano, S. (2020a). Improvements on a sensitivity adjustable 3-axis soft skin sensor with an electromagnet. In *2020 IEEE/SICE International Symposium on System Integration (SII)*, pages 68–73. 12

Holgado, A. C., Piga, N., Tomo, T. P., Vezzani, G., Schmitz, A., Lorenzo, and Sugano, S. (2019b). Magnetic 3-axis soft and sensitive fingertip sensors integration for the iCub humanoid robot. In *2019 IEEE-RAS 19th International Conference on Humanoid Robots (Humanoids)*, pages 344–351. 12

Holgado, A. C., Tomo, T. P., Somlor, S., and Sugano, S. (2020b). A multimodal, adjustable sensitivity, digital 3-axis skin sensor module. *Sensors*, 20(11). 12

Huang, H., Jiang, L., Zhao, D., Zhao, J., Cai, H., Liu, H., Meusel, P., Willberg, B., and Hirzinger, G. (2006). The development on a new biomechatronic prosthetic hand based on under-actuated mechanism. In *2006 IEEE/RSJ International Conference on Intelligent Robots and Systems*, pages 3791–3796. 29, 35

Hundhausen, F., Grimm, R., Stieber, L., and Asfour, T. (2021). Fast reactive grasping with in-finger vision and in-hand FPGA-accelerated CNNs. In

IEEE/RSJ International Conference on Intelligent Robots and Systems (IROS), pages 6825–6832. 32

Hundhausen, F., Megerle, D., and Asfour, T. (2019). Resource-aware object classification and segmentation for semi-autonomous grasping with prosthetic hands. In *IEEE/RAS International Conference on Humanoid Robots (Humanoids)*, Toronto, Canada. 40, 50, 96, 97, 103

Hundhausen, F., Starke, J., and Asfour, T. (2020). A soft humanoid hand with in-finger visual perception. In *IEEE/RSJ International Conference on Intelligent Robots and Systems (IROS)*, pages 8722–8728, Las Vegas, USA. 31, 33, 36, 55, 67, 90, 91, 129, 130

Jamali, N., Maggiali, M., Giovannini, F., Metta, G., and Natale, L. (2015). A new design of a fingertip for the iCub hand. In *2015 IEEE/RSJ International Conference on Intelligent Robots and Systems (IROS)*, pages 2705–2710. 15, 16, 30, 32

Jentoft, L. P., Wan, Q., and Howe, R. D. (2014). Limits to compliance and the role of tactile sensing in grasping. In *Int. Conf. on Robotics and Automation*, pages 6394–6399. 125

Jeong, S. H., Kim, K., and Kim, S. (2017). Designing anthropomorphic robot hand with active dual-mode twisted string actuation mechanism and tiny tension sensors. *IEEE Robotics and Automation Letters*, 2(3):1571–1578. 27, 35

Ji, S.-Q., Huang, M.-B., and Huang, H.-P. (2019). Robot intelligent grasp of unknown objects based on multi-sensor information. *MDPI Sensors*, 19(7). 44

Johansson, R., Landström, U., and Lundström, R. (1982a). Responses of mechanoreceptive afferent units in the glabrous skin of the human hand to sinusoidal skin displacements. *Brain Research*, 244(1):17–25. 8

Johansson, R., Landström, U., and Lundström, R. (1982b). Sensitivity to edges of mechanoreceptive afferent units innervating the glabrous skin of the human hand. *Brain Research*, 244(1):27–32. 8

Johansson, R. S. and Flanagan, J. R. (2009a). Coding and use of tactile signals from the fingertips in object manipulation tasks. *Nature Reviews Neuroscience*, 10(5):345. 1, 42, 45, 90, 120, 121

Johansson, R. S. and Flanagan, J. R. (2009b). Coding and use of tactile signals from the fingertips in object manipulation tasks. *Nature Reviews Neuroscience*, 10(5):345–359. 119, 124, 140

Johansson, R. S. and Vallbo, A. B. (1979). Tactile sensibility in the human hand: relative and absolute densities of four types of mechanoreceptive units in glabrous skin. *The Journal of Physiology*, 286(1):283–300. 1, 9

Johansson, R. S. and Westling, G. (1984). Influences of cutaneous sensory input on the motor coordination during precision manipulation. In von Euler, C., Franzén, O., Lindblom, U., and Ottoson, D., editors, *Somatosensory Mechanisms: Proceedings of an International Symposium held at The Wenner-Gren Center, Stockholm, June 8–10, 1983*, pages 249–260. Springer US, Boston, MA. 120

Johansson, R. S. and Åke B. Vallbo (1983). Tactile sensory coding in the glabrous skin of the human hand. *Trends in Neurosciences*, 6:27–32. 8, 9

Johnson, M. K. and Adelson, E. H. (2009). Retrographic sensing for the measurement of surface texture and shape. In *2009 IEEE Conference on Computer Vision and Pattern Recognition*, pages 1070–1077. 20

Johnson, M. K., Cole, F., Raj, A., and Adelson, E. H. (2011). Microgeometry capture using an elastomeric sensor. *ACM Transactions on Graphics*, 30(4). 20

Jones, L. A. and Lederman, S. J. (2006). *Human hand function*. Oxford University Press, Oxford [u.a.]. 1, 143

Kaboli, M., Yao, K., and Cheng, G. (2016). Tactile-based manipulation of deformable objects with dynamic center of mass. In *Int. Conf. on Humanoid Robots*, pages 752–757. 43, 48

Kamper, D. G., Cruz, E. G., and Siegel, M. P. (2003). Stereotypical fingertip trajectories during grasp. *Journal of Neurophysiology*, 90(6):3702–3710. 56

Kappassov, Z., Corrales, J.-A., and Perdereau, V. (2015). Tactile sensing in dexterous robot hands — review. *Robotics and Autonomous Systems*, 74(1). 10

Kasper, A., Xue, Z., and Dillmann, R. (2012). The KIT object models database: An object model database for object recognition, localization and manipulation in service robotics. *International Journal of Robotics Research*, 31(8):927–934. 73

Kaye, R. and Konz, S. (1986). Volume and surface area of the hand. In *Human Factors Society Annual Meeting*, volume 30, pages 382–384. 53, 66

Knibestöl, M. and Vallbo, Å. B. (1970). Single unit analysis of mechanoreceptor activity from the human glabrous skin. *Acta Physiologica Scandinavica*, 80(2):178–195. 8

Koiva, R., Schwank, T., Walck, G., Meier, M., Haschke, R., and Ritter, H. (2020). Barometer-based tactile skin for anthropomorphic robot hand. In *International Conference on Intelligent Robots and Systems*, pages 1–9. 14, 15, 92

Kyberd, P. J. and Chappell, P. H. (1993). A force sensor for automatic manipulation based on the hall effect. *Measurement Science and Technology*, 4(3):281–287. 11

Kõiva, R., Schwank, T., Walck, G., Haschke, R., and Ritter, H. J. (2018). Mechatronic fingernail with static and dynamic force sensing. In *2018 IEEE/RSJ International Conference on Intelligent Robots and Systems (IROS)*, pages 2114–2119. 14, 25

Kõiva, R., Zenker, M., Schürmann, C., Haschke, R., and Ritter, H. J. (2013). A highly sensitive 3D-shaped tactile sensor. In *2013 IEEE/ASME International Conference on Advanced Intelligent Mechatronics*, pages 1084–1089. 14, 16, 17, 24

Lancaster, P. E., Smith, J. R., and Srinivasa, S. S. (2019). Improved proximity, contact, and force sensing via optimization of elastomer-air interface geometry. In *2019 International Conference on Robotics and Automation (ICRA)*, pages 3797–3803. 18

Li, Q., Kroemer, O., Su, Z., Veiga, F. F., Kaboli, M., and Ritter, H. J. (2020). A review of tactile information: Perception and action through touch. *Trans. on Robotics*, 36(6):1619–1634. 42

Li, R., Platt, R., Yuan, W., ten Pas, A., Roscup, N., Srinivasan, M. A., and Adelson, E. (2014). Localization and manipulation of small parts using GelSight tactile sensing. In *2014 IEEE/RSJ International Conference on Intelligent Robots and Systems*, pages 3988–3993. 20

Li, W., Konstantinova, J., Noh, Y., Alomainy, A., and Althoefer, K. (2018). Camera-based force and tactile sensor. In Giuliani, M., Assaf, T., and Giannaccini, M. E., editors, *Towards Autonomous Robotic Systems*, pages 438–450, Cham. Springer International Publishing. 20

Light, C. M., Chappell, P. H., and Kyberd, P. J. (2002). Establishing a standardized clinical assessment tool of pathologic and prosthetic hand function: Normative

data, reliability, and validity. *Archives of Physical Medicine and Rehabilitation*, 83(6):776–783. 61

Liu, H., Ferrentino, P., Pirozzi, S., Siciliano, B., and Ficuciello, F. (2019). The PRISMA Hand II: A sensorized robust hand for adaptive grasp and in-hand manipulation. In *2019 International Symposium on Robotics Research*. 18, 28, 32, 35

Ma, D., Donlon, E., Dong, S., and Rodriguez, A. (2019). Dense tactile force estimation using GelSlim and inverse FEM. In *2019 International Conference on Robotics and Automation (ICRA)*, pages 5418–5424. 21

Ma, X., Ye, Y., Meng, H., Wang, W., Wang, W., and Bao, G. (2021). Sensor embedded soft fingertip for precise manipulation and softness recognition. *IEEE Robotics and Automation Letters*, 6(4):8734–8741. 15

Maiolino, P., Maggiali, M., Cannata, G., Metta, G., and Natale, L. (2013). A flexible and robust large scale capacitive tactile system for robots. *IEEE Sensors Journal*, 13(10):3910–3917. 15

Mandery, C., Terlemez, O., Do, M., Vahrenkamp, N., and Asfour, T. (2016). Unifying representations and large-scale whole-body motion databases for studying human motion. *IEEE Transactions on Robotics*, 32(4):796–809. 105

Markovic, M., Došen, S., Cipriani, C., Popovic, D., and Farina, D. (2014). Stereovision and augmented reality for closed-loop control of grasping in hand prostheses. *Journal of Neural Engineering*, 11(4):046001. 39

Markovic, M., Došen, S., Popovic, D., Graimann, B., and Farina, D. (2015). Sensor fusion and computer vision for context-aware control of a multi degree-of-freedom prosthesis. *Journal of Neural Engineering*, 12(6):066022. 39, 40, 50, 52

Marquardt, C., Weiner, P., Dezman, M., and Asfour, T. (2022). Embedded barometric pressure sensor unit for force myography in exoskeletons. In *IEEE/RAS International Conference on Humanoid Robots (Humanoids)*, pages 0–0. 138

Matheus, K. and Dollar, A. M. (2010). Benchmarking grasping and manipulation: Properties of the objects of daily living. In *International Conference on Robotics and Automation*, pages 5020–5027. IEEE. 51, 61

Ming Cheng, Jiang, L., Fenglei Ni, Fan, S., Liu, Y., and Liu, H. (2017). Design of a highly integrated underactuated finger towards prosthetic hand. In *2017 IEEE International Conference on Advanced Intelligent Mechatronics (AIM)*, pages 1035–1040. 25

Mohammadi, A., Xu, Y., Tan, Y., Choong, P., and Oetomo, D. (2019). Magnetic-based soft tactile sensors with deformable continuous force transfer medium for resolving contact locations in robotic grasping and manipulation. *Sensors*, 19(22). 12

Nakagawa-Silva, A., Thakor, N. V., Cabibihan, J., and Soares, A. B. (2019). A bio-inspired slip detection and reflex-like suppression method for robotic manipulators. *IEEE Sensors*, 19(24):12443–12453. 44, 48

Negrello, F., Stuart, H. S., and Catalano, M. G. (2020). Hands in the real world. *Frontiers in Robotics and AI*, 6. 1

Ntagios, M., Nassar, H., Pullanchiyodan, A., Navaraj, W. T., and Dahiya, R. (2020). Robotic hands with intrinsic tactile sensing via 3D printed soft pressure sensors. *Advanced Intelligent Systems*, 2(6). 29

Odhner, L. U., Jentoft, L. P., Claffee, M. R., Corson, N., Tenzer, Y., Ma, R. R., Buehler, M., Kohout, R., D. Howe, R., and Dollar, A. M. (2014). A compliant, underactuated hand for robust manipulation. *The International Journal of Robotics Research*, 33(5). 13, 25

Or, K., Morikuni, S., Ogasa, S., Funabashi, S., Schmitz, A., and Sugano, S. (2016). A study on fingertip designs and their influences on performing stable prehension for robot hands. In *2016 IEEE-RAS 16th International Conference on Humanoid Robots (Humanoids)*, pages 772–777. 76

Ortiz-Catalan, M., Håkansson, B., and Brånemark, R. (2014). Real-time and simultaneous control of artificial limbs based on pattern recognition algorithms. *IEEE Transactions on Neural Systems and Rehabilitation Engineering*, 22(4):756–764. 37

Park, M., Bok, B.-G., Ahn, J.-H., and Kim, M.-S. (2018). Recent advances in tactile sensing technology. *Micromachines*, 9(7). 10

Paskett, M. D., Brinton, M. R., Hansen, T. C., George, J. A., Davis, T. S., Duncan, C. C., and Clark, G. A. (2021). Activities of daily living with bionic arm improved by combination training and latching filter in prosthesis control

comparison. *Journal of NeuroEngineering and Rehabilitation*, 18(45):1743–0003. 37

Patel, R., Cox, R., and Correll, N. (2018). Integrated proximity, contact and force sensing using elastomer-embedded commodity proximity sensors. *Autonomous Robots*, 42(7):1443–1458. 18

Peerdeman, B., Valori, M., Brouwer, D., Hekman, E., Misra, S., and Stramigioli, S. (2014). UT hand I: A lock-based underactuated hand prosthesis. *Mechanism and Machine Theory*, 78:307–323. 27, 32, 35

Pelliccia, L., Schumann, M., Dudczig, M., Lamonaca, M., Klimant, P., and Di Gironimo, G. (2018). Implementation of tactile sensors on a 3-fingers Robotiq® adaptive gripper and visualization in VR using Arduino controller. *Procedia CIRP*, 67:250–255. 11th CIRP Conference on Intelligent Computation in Manufacturing Engineering, 19-21 July 2017, Gulf of Naples, Italy. 14

Pfeifer, R. and Gómez, G. (2009). Morphological computation – connecting brain, body, and environment. In *Creating Brain-Like Intelligence: From Basic Principles to Complex Intelligent Systems*, pages 66–83. Springer Berlin Heidelberg. 52

Piacenza, P., Sherman, S., and Ciocarlie, M. (2018). Data-driven super-resolution on a tactile dome. *IEEE Robotics and Automation Letters*, 3(3):1434–1441. 14

Piazza, C., Grioli, G., Catalano, M., and Bicchi, A. (2019). A century of robotic hands. *Annual Review of Control, Robotics, and Autonomous Systems*, 2(1):1–32. 24, 37, 71

Piazza, C., Santina, C. D., Catalano, M., Grioli, G., Garabini, M., and Bicchi, A. (2016). SoftHand Pro-D: Matching dynamic content of natural user commands with hand embodiment for enhanced prosthesis control. In *Int. Conference on Robotics and Automation*, pages 3516–3523. 35, 37

Pons, J., Rocon, E., Ceres, R., Reynaerts, D., Saro, B., Levin, S., and Van Moorleghem, W. (2004). The manus-hand dextrous robotics upper limb prosthesis: Mechanical and manipulation aspects. *Autonomous Robots*, 16(2). 29, 34, 35

Purushothaman, G. (2016). Myoelectric control of prosthetic hands: State-of-the-art review. *Medical Devices: Evidence and Research*, 9:247–255. 110

Pylatiuk, C., Schulz, S., and Döderlein, L. (2007). Results of an internet survey of myoelectric prosthetic hand users. *Prosthetics and Orthotics International*, 31(4):362–370. 53

Quigley, M., Salisbury, C., Ng, A. Y., and Salisbury, J. K. (2014). Mechatronic design of an integrated robotic hand. *The Int. Journal of Robotics Research*, 33(5). 18, 31, 32

Romano, J. M., Hsiao, K., Niemeyer, G., Chitta, S., and Kuchenbecker, K. J. (2011). Human-inspired robotic grasp control with tactile sensing. *Trans. on Robotics*, 27(6):1067–1079. 44, 47, 48

Romero, B., Veiga, F., and Adelson, E. (2020). Soft, round, high resolution tactile fingertip sensors for dexterous robotic manipulation. In *2020 IEEE International Conference on Robotics and Automation (ICRA)*, pages 4796–4802. 21

Salminger, S., Stino, H., Pichler, L. H., Gstoettner, C., Sturma, A., Mayer, J. A., Szivak, M., and Aszmann, O. C. (2020). Current rates of prosthetic usage in upper-limb amputees – have innovations had an impact on device acceptance? *Disability and Rehabilitation*, 0(0):1–12. PMID: 33377803. 1, 33, 50

Santello, M., Flanders, M., and Soechting, J. F. (1998). Postural hand synergies for tool use. *Journal of Neuroscience*, 18(23):10105–10115. 144

Sato, K., Kamiyama, K., Kawakami, N., and Tachi, S. (2010). Finger-shaped GelForce: Sensor for measuring surface traction fields for robotic hand. *IEEE Transactions on Haptics*, 3(1):37–47. 19

Sato, K., Kamiyama, K., Nii, H., Kawakami, N., and Tachi, S. (2008). Measurement of force vector field of robotic finger using vision-based haptic sensor. In *2008 IEEE/RSJ International Conference on Intelligent Robots and Systems*, pages 488–493. 19

Saudabayev, A. and Varol, H. A. (2015). Sensors for robotic hands: A survey of state of the art. *IEEE Access*, 3(0). 10, 24

Schmitz, A., Maggiali, M., Natale, L., Bonino, B., and Metta, G. (2010). A tactile sensor for the fingertips of the humanoid robot iCub. In *2010 IEEE/RSJ International Conference on Intelligent Robots and Systems*, pages 2212–2217. 15, 30

Schmitz, A., Maiolino, P., Maggiali, M., Natale, L., Cannata, G., and Metta, G. (2011). Methods and technologies for the implementation of large-scale robot tactile sensors. *IEEE Transactions on Robotics*, 27(3):389–400. 15

Schweitzer, W., Thali, M. J., and Egger, D. (2018). Case-study of a user-driven prosthetic arm design: Bionic hand versus customized body-powered technology in a highly demanding work environment. *Journal of NeuroEngineering and Rehabilitation*, 15(1):1–27. 53

Segil, J., Patel, R., Klingner, J., Weir, R. F. f., and Correll, N. (2019). Multi-modal prosthetic fingertip sensor with proximity, contact, and force localization capabilities. *Advances in Mechanical Engineering*, 11(4):1687814019844643. 26

SensorHand (2020). *SensorHand Speed*. Otto Bock HealthCare Deutschland GmbH. https://www.ottobockus.com/media/local-media/prosthetics/upper-limb/speedhands/prosthesis_systems_information_for_practitioners.pdf, Accessed March 03, 2020. 35

She, Y., Li, C., Cleary, J., and Su, H.-J. (2015). Design and fabrication of a soft robotic hand with embedded actuators and sensors. *Journal of Mechanisms and Robotics*, 7(2). 36

Sonar, H. A., Yuen, M. C., Kramer-Bottiglio, R., and Paik, J. (2018). An any-resolution pressure localization scheme using a soft capacitive sensor skin. In *2018 IEEE International Conference on Soft Robotics (RoboSoft)*, pages 170–175. 16

Soubeyrand, M., Assabah, B., Bégin, M., Laemmel, E., Dos Santos, A., and Crézé, M. (2017). Pronation and supination of the hand: Anatomy and biomechanics. *Hand Surgery & Rehabilitation*, 36:2–11. 109

Starke, J. (2022). *Synergy-Based Human Grasp Representations and Semi-Autonomous Control of Prosthetic Hands*. PhD thesis, Karlsruhe Institute of Technology. 105

Starke, J., Weiner, P., Crell, M., and Asfour, T. (2022). Semi-autonomous control of prosthetic hands based on multimodal sensing, human grasp demonstration and user intention. *Robotics and Autonomous Systems*, 154:1–16. 35, 37, 102, 104, 105, 108, 109, 112, 114, 115, 138

Su, Z., Hausman, K., Chebotar, Y., Molchanov, A., Loeb, G. E., Sukhatme, G. S., and Schaal, S. (2015). Force estimation and slip detection/classification for grip control using a biomimetic tactile sensor. In *Int. Conf. on Humanoid Robots*, pages 297–303. 43, 48

Suzuki, Y. (2017). Multilayered center-of-pressure sensors for robot fingertips and adaptive feedback control. *IEEE Robotics and Automation Letters*, 2(4):2180–2187. 17

Swain, I. D. and Nightingale, J. M. (1980). An adaptive control system for a complete hand/arm prosthesis. *Journal of Biomedical Engineering*, 2(3):163–166. 38

Takahashi, T., Tsuboi, T., KishidaTakeo, Kawanami, Y., Shimizu, S., Iribe, M., Fukushima, T., and Masahiro, F. (2008). Adaptive grasping by multi fingered hand with tactile sensor based on robust force and position control. In *International Conference on Robotics and Automation*, pages 264–271. 44, 48

Taska (2020). *Specifications V1.1*. Taska TM. https://www.taskaprosthetics.com/en/support, Accessed August 14, 2020. 35

Tavakoli, M., Lopes, P., Lourenço, J., Rocha, R. P., Giliberto, L., de Almeida, A. T., and Majidi, C. (2017). Autonomous selection of closing posture of a robotic hand through embodied soft matter capacitive sensors. *IEEE Sensors Journal*, 17(17):5669–5677. 28, 32, 35, 39, 41

Tavakoli, M., Sayuk, A., Lourenço, J., and Neto, P. (2017). Anthropomorphic finger for grasping applications: 3D printed endoskeleton in a soft skin. *International Journal of Advanced Manufacturing Technology*, 91. 28

Tenzer, Y., Jentoft, L. P., and Howe, R. D. (2014). The feel of mems barometers: Inexpensive and easily customized tactile array sensors. *IEEE Robotics Automation Magazine*, 21(3). 13, 14, 69, 73, 79

Tomo, T. P., Regoli, M., Schmitz, A., Natale, L., Kristanto, H., Somlor, S., Jamone, L., Metta, G., and Sugano, S. (2018). A new silicone structure for uSkin—a soft, distributed, digital 3-axis skin sensor and its integration on the humanoid robot iCub. *IEEE Robotics and Automation Letters*, 3(3):2584–2591. 12

Tomo, T. P., Schmitz, A., Wong, W. K., Kristanto, H., Somlor, S., Hwang, J., Jamone, L., and Sugano, S. (2017). Covering a robot fingertip with uSkin: A soft electronic skin with distributed 3-axis force sensitive elements for robot hands. *IEEE Robotics and Automation Letters*, 3(1). 12

Tomo, T. P., Somlor, S., Schmitz, A., Jamone, L., Huang, W., Kristanto, H., and Sugano, S. (2016a). Design and characterization of a three-axis hall effect-based soft skin sensor. *Sensors*, 16(4). 11, 74, 79

Tomo, T. P., Wong, W. K., Schmitz, A., Kristanto, H., Sarazin, A., Jamone, L., Somlor, S., and Sugano, S. (2016b). A modular, distributed, soft, 3-axis sensor system for robot hands. In *2016 IEEE-RAS 16th International Conference on Humanoid Robots (Humanoids)*, pages 454–460. 11, 69, 74, 79

Torres-Jara, E., Vasilescu, I., and Coral, R. (2006). A soft touch: Compliant tactile sensors for sensitive manipulation. *CSAIL Technical Reports*, 0(0). 11, 18

Varol, H. A., Dalley, S. A., Wiste, T. E., and Goldfarb, M. (2014). *Biomimicry and the Design of Multigrasp Transradial Prostheses*, pages 431–451. Springer International Publishing, Cham. 27

Veiga, F., Edin, B., and Peters, J. (2020). Grip stabilization through independent finger tactile feedback control. *MDPI Sensors*, 20(6). 44, 48, 122

Vergara, M., Agost, M. J., and Gracia-Ibáñez, V. (2018). Dorsal and palmar aspect dimensions of hand anthropometry for designing hand tools and protections. *Human Factors and Ergonomics in Manufacturing & Service Industries*, 28(1):17–28. 70, 78

Vergara, M., Agost Torres, M.-J., and Gracia-Ibáñez, V. (2016). Comparison of dorsal and palmar aspect dimensions of hand anthropometry. *Human Factors and Ergonomics in Manufacturing & Service Industries*, 28(1):1–12. 55

Votta, A. M., Günay, S. Y., Erdoğmus, D., and Önal, c. (2019). Force-sensitive prosthetic hand with 3-axis magnetic force sensors. In *2019 IEEE International Conference on Cyborg and Bionic Systems*. 12

Wade, J., Bhattacharjee, T., Williams, R. D., and Kemp, C. C. (2017). A force and thermal sensing skin for robots in human environments. *Robotics and Autonomous Systems*, 96:1–14. 17

Wagner, C. (1977). Determination of the rotary flexibility of the elbow joint. *European Journal of Applied Physiology and Occupational Physiology*, 37(1):47–59. 109

Wall, V. and Brock, O. (2019). Multi-task sensorization of soft actuators using prior knowledge. In *Int. Conf. on Robotics and Automation*, pages 9416–9421. 36

Wang, H., De Boer, G., Kow, J., Alazmani, A., Ghajari, M., Hewson, R., and Culmer, P. (2016). Design methodology for magnetic field-based soft tri-axis tactile sensors. *Sensors*, 16(9). 11

Wang, H., Totaro, M., and Beccai, L. (2018). Toward perceptive soft robots: Progress and challenges. *Advanced Science*, 5(9):1800541. 10

Wang, L., DelPreto, J., Bhattacharyya, S., Weisz, J., and Allen, P. K. (2011). A highly-underactuated robotic hand with force and joint angle sensors. In *2011 IEEE/RSJ Int. Conf. on Intelligent Robots and Systems*, pages 1380–1385. 24

Wang, S., She, Y., Romero, B., and Adelson, E. (2021). GelSight wedge: Measuring high-resolution 3D contact geometry with a compact robot finger. 21

Weiner, P., Hundhausen, F., Grimm, R., and Asfour, T. (2021). Detecting grasp phases and adaption of object-hand interaction forces of a soft humanoid hand based on tactile feedback. In *IEEE/RSJ International Conference on Intelligent Robots and Systems (IROS)*, pages 3956–3963, Prague, Czech Republic. 15, 42, 67, 90, 92, 119, 123, 128, 129, 130, 132, 138, 139

Weiner, P., Neef, C., and Asfour, T. (2018a). A multimodal embedded sensor system for scalable robotic and prosthetic fingers. In *IEEE/RAS International Conference on Humanoid Robots (Humanoids)*, pages 286–292, Beijing, China. 15, 26, 68, 75, 79

Weiner, P., Neef, C., Shibata, Y., Nakamura, Y., and Asfour, T. (2019). An embedded, multi-modal sensor system for scalable robotic and prosthetic hand fingers. *Sensors*, 20(1):108–121. 11, 24, 68, 69, 70, 71, 72, 74, 76, 77, 78, 79, 80, 82, 83, 85, 86, 88, 138

Weiner, P., Starke, J., Hundhausen, F., Beil, J., and Asfour, T. (2018b). The KIT prosthetic hand: Design and control. In *IEEE/RSJ International Conference on Intelligent Robots and Systems (IROS)*, pages 3328–3334, Madrid, Spain. 50, 53, 59, 72, 137

Weiner, P., Starke, J., Rader, S., Hundhausen, F., and Asfour, T. (2022). Designing prosthetic hands with embodied intelligence: The KIT prosthetic hands. *Frontiers in Neurorobotics*, 16:1–14. 49, 51, 54, 56, 57, 59, 60, 62, 64, 66, 67, 108, 137

Weiss, K. and Wörn, H. (2005). The working principle of resistive tactile sensor cells. In *IEEE International Conference Mechatronics and Automation, 2005*, pages 471–476. 16

Wettels, N., Fishel, J. A., and Loeb, G. E. (2014). Multimodal tactile sensor. In Balasubramanian, R. and Santos, V. J., editors, *The Human Hand as an Inspiration for Robot Hand Development*, pages 405–429. Springer International Publishing, Cham. 25

Wettels, N., Parnandi, A. R., Moon, J.-H., Loeb, G. E., and Sukhatme, G. S. (2009). Grip control using biomimetic tactile sensing systems. *TRansactions On Mechatronics*, 14(6):718–723. 43, 48

Wijk, U. and Carlsson, I. (2015). Forearm amputees' views of prosthesis use and sensory feedback. *Journal of Hand Therapy*, 28(3):269 – 278. 53

Wilson, S. and Vaidyanathan, R. (2017). Upper-limb prosthetic control using wearable multichannel mechanomyography. In *International Conference on Rehabilitation Robotics*, pages 1293–1298. 37

Winstone, B., Griffiths, G., Melhuish, C., Pipe, T., and Rossiter, J. (2012). TACTIP — tactile fingertip device, challenges in reduction of size to ready for robot hand integration. In *2012 IEEE International Conference on Robotics and Biomimetics (ROBIO)*, pages 160–166. 19

Wiste, T. and Goldfarb, M. (2017). Design of a simplified compliant anthropomorphic robot hand. In *2017 IEEE International Conference on Robotics and Automation (ICRA)*, pages 3433–3438. 28, 35

Wiste, T. E., Dalley, S. A., Atakan Varol, H., and Goldfarb, M. (2011). Design of a Multigrasp Transradial Prosthesis. *Journal of Medical Devices*, 5(3). 27, 35

Yamaguchi, A. and Atkeson, C. G. (2016). Combining finger vision and optical tactile sensing: Reducing and handling errors while cutting vegetables. In *2016 IEEE-RAS 16th International Conference on Humanoid Robots (Humanoids)*, pages 1045–1051. 19

Yamaguchi, A. and Atkeson, C. G. (2017). Implementing tactile behaviors using fingervision. In *International Conference on Humanoid Robotics*, pages 241–248. 45, 47, 48

Yamaguchi, N., Hasegawa, S., Okada, K., and Inaba, M. (2018). A gripper for object search and grasp through proximity sensing. In *2018 IEEE/RSJ International Conference on Intelligent Robots and Systems (IROS)*, pages 1–9. 18, 47, 91

Yousef, H., Boukallel, M., and Althoefer, K. (2011). Tactile sensing for dexterous in-hand manipulation in robotics —- a review. *Sensors and Actuators A: Physical*, 167(2):171–187. Solid-State Sensors, Actuators and Microsystems Workshop. 10

Yuan, W., Dong, S., and Adelson, E. H. (2017). GelSight: High-resolution robot tactile sensors for estimating geometry and force. *Sensors*, 17(12). 20

Yuan, W., Li, R., Srinivasan, M. A., and Adelson, E. H. (2015). Measurement of shear and slip with a GelSight tactile sensor. In *2015 IEEE International Conference on Robotics and Automation (ICRA)*, pages 304–311. 20

Zhang, T. and Jiang, L. (2018). Biomimetic tactile data driven closed-loop control of myoelectric prosthetic hand. In *2018 IEEE International Conference on Robotics and Biomimetics (ROBIO)*, pages 1738–1742. 45, 47, 48

Zhang, T., Jiang, L., and Liu, H. (2018). Design and functional evaluation of a dexterous myoelectric hand prosthesis with biomimetic tactile sensor. *IEEE Transactions on Neural Systems and Rehabilitation Engineering*, 26(7):1391–1399. 31, 35, 45

Zhang, T., Jiang, L., Wu, X., Feng, W., Zhou, D., and Liu, H. (2015). Fingertip three-axis tactile sensor for multifingered grasping. *IEEE/ASME Transactions on Mechatronics*, 20(4):1875–1885. 17, 31, 43

Zhao, H., O'Brien, K., Li, S., and Shepherd, R. F. (2016). Optoelectronically innervated soft prosthetic hand via stretchable optical waveguides. *Science robotics*, 1(1). 36

Zhuang, K. Z., Sommer, N., Mendez, V., Aryan, S., Formento, E., D'Anna, E., Artoni, F., Petrini, F., Granata, G., Cannaviello, G., et al. (2019). Shared human–robot proportional control of a dexterous myoelectric prosthesis. *Nature Machine Intelligence*, 1(9):400–411. 37

Zou, L., Ge, C., Wang, Z. J., Cretu, E., and Li, X. (2017). Novel tactile sensor technology and smart tactile sensing systems: A review. *Sensors*, 17(11). 10